SYNAPTIC REQUIREMENTS FOR GLYCAN MODIFICATION

By

William Matthew Parkinson

Dissertation
Submitted to the Faculty of the
Graduate School of Vanderbilt University
in partial fulfillment of the requirements
for the degree of

DOCTOR OF PHILOSOPHY

In

Biological Sciences
May, 2016
Nashville, Tennessee

Approved:

Donna Webb, Ph.D.

Kendal Broadie, Ph.D.

Terry Page, Ph.D.

Todd Graham, Ph.D.

Aurelio Galli, Ph.D.

TABLE OF CONTENTS

Page

LIST OF FIGURES vi

LIST OF TABLES vii

CHAPTER

I. INTRODUCTION 1

Synaptic Glycosylation 1
The chemical synapse synaptomatrix 1
The Drosophila neuromuscular junction synapse model 2
Drosophila trans-synaptic signaling 8
Drosophila NMJ synaptic glycosylation 9
N-Linked Glycosylation 11
N-Linked Glycosylation Pathway 11
N-linked glycosylation at the synapse 14
Congenital Disorders of Glycosylation 14
Clinical diagnosis and symptoms 14
Synaptic CDG disease models 19
Thesis Outline 21
MGAT1 21
PMM2 22
References 25

II. N-GLYCOSYLATION REQUIREMENTS IN NEUROMUSCULAR SYNAPTOGENESIS 39

Summary 40
Introduction 41
Materials and Methods 43
Drosophila Genetics 43
Immunocytochemistry 43
Western Blotting 44
Electrophysiology 45
FM1-43 Dye Imaging 45
Statistics 46

Results 46
Mgat1 shapes the glycosylated synaptomatrix of the neuromuscular junction 46
Development of NMJ structural overgrowth in the mgat1 null condition 52
Pre- and postsynaptic mgat1 roles restrict synaptic functional differentiation 55
Mgat1 regulates development of synaptic vesicle cycling properties 58
Selective loss of pre-and postsynaptic components in mgat1 null mutants 61
Multiple trans-synaptic signaling pathways altered in mgat1 null mutants 64
Loss of key synaptic scaffolds driving synaptogenesis in mgat1 null mutants 67
Discussion 70
References 74

III. NEUROLOGICAL ROLES FOR PHOSPHOMANNOMUTASE TYPE 2 IN A NEW DROSOPHILA CONGENITAL DISORDER OF GLYCOSYLATION DISEASE MODEL 85

Translational Impact 86
Abstract 88
Introduction 89
Results 91
Degree of Drosophila PMM2 loss determines lifespan duration 91
Neuronal PMM2 maintains normal posture and coordinated movement 95
PMM2 loss suppresses N-glycosylation and enhances glycan turnover 96
PMM2 maintains the normal glycan environment in the NMJ synaptomatrix 102
PMM2 restricts NMJ structural growth and synaptic bouton differentiation 102
Coupled pre- and postsynaptic PMM2 function limits NMJ transmission strength 108
PMM2 positively regulates the synaptic extracellular matrix proteinase pathway 111
PMM2 positively regulates the Wnt Wingless trans-synaptic signaling pathway 114
Discussion 117
Materials and Methods 122
Drosophila Genetics 122
PCR Methods 122
Behavioral Assays 123
Glycomic Analyses 124
Immunocytochemistry Imaging 124
Western Blot analyses 125
Electrophysiology 126
Statistics 126
References 127

IV. CONCLUSIONS AND FUTURE DIRECTIONS 139

Mgat1 Conclusion 139
Mgat1 Future Directions 141
PMM2 Conclusions 145
PMM2 Future Directions 150
References 153

LIST OF FIGURES

Figures Page

1. Ultrastructure of *Drosophila* Neuromuscular Junction 3

2. Larva Muscular Anatomy 6

3. N-Glycosylation Pathway 12

4. Loss of mgat1 activity dramatically alters the NMJ synaptomatrix 47

5. Fasciclin 2 and Dystroglycan are normally expressed in mgat1 nulls 50

6. Drosophila NMJ is structurally overgrown in mgat1 null mutants 53

7. Strengthened synaptic functional differentiation in mgat1 null mutants 56

8. Altered NMJ synaptic vesicle cycling in the mgat1 null mutants 59

9. Pre- and postsynaptic component recruitment reduced at mgat1 NMJs 62

10. Multiple trans-synaptic signaling pathways altered in mgat1 null mutant 65

11. Synaptic scaffolds DLG and LGL reduced in the mgat1 null mutants 68

12. Drosophila PMM2 levels determine lifespan and coordinated movement ability 92

13. PMM2 loss dramatically alters N-linked glycoprotein glycosylation 97

14. PMM2 loss increases FOS and reduces NMJ N-linked glycoprotein glycosylation 100

15. PMM2 loss results in striking NMJ synaptic structural overgrowth 103

16. Early lethal pmm2 null mutants exhibit NMJ overgrowth and loss of N-glycans 106

17. Coupled pre- and postsynaptic PMM2 removal increases neurotransmission 109

18. Loss of PMM2 down-regulates the synaptic matrix proteinase pathway 112

19. Loss of PMM2 down-regulates the trans-synaptic Wnt signaling pathway 115

20. Ultrastructural Analysis of *mgat1* Mutant Boutons 142

21. Tracheal Maintenance Requires pmm2 Activity..... 147

LIST OF TABLES

Table Page

1. Congenital Disorders of Glycosylation with *Drosophila* Homologs 16

CHAPTER I

INTRODUCTION

Glycosylation is the most common post-translational protein modification, involving the addition of chained sugars to modulate folding, localization and protein-protein interactions. Glycosylated proteins are most heavily concentrated on the extracellular side of the cell membrane, and most secreted proteins are glycosylated. Both of these glycoprotein classes are critical for cell-cell interactions, particularly during development. The nervous system appears selectively enriched for glycans and neurons appear particularly dependent on glycosylation in the regulation of synapse morphology and function. This thesis work probes the intersection between protein glycosylation and synaptic neuroscience, focusing on how loss of glycosylation results in neurological disease states.

Synaptic Glycosylation

The chemical synapse synaptomatrix

A chemical synapse involves 1) a presynaptic signaling cell, 2) a postsynaptic receptive cell and 3) the extracellular space between (the synaptic cleft). The presynaptic axon terminates in swollen varicosities (synaptic boutons) that store the necessary machinery for transmission (Slater, 2015). A bouton can contain one to several specialized fusion sites (active zones) that contain the machinery for synaptic vesicles (SV) exocytosis. SVs are both localized in close proximity to each active zone (readily-releasable pool) and at a distance from the plasma membrane in a larger internal collection (reserve pool). SV fusion with the membrane releases neurotransmitter into the synaptic cleft, which is a highly organized, heavily-glycosylated cellular interface microenvironment (the synaptomatrix; Scott and Panin, 2014a,b). Glycosylated scaffolding proteins, signaling ligands, receptors, proteinases and many other glycans occupy this extracellular space and modulate the neurotransmission traveling to the postsynaptic cell. Unlike the general space between two cells, the synaptomatrix membranes

are held in rigid, close proximity, both restricting the extracellular proteins capable of occupying this space and also limiting the space that the neurotransmitter must travel (Rohrbough et al., 2007). The neurotransmitter passes through the synaptomatrix to bind its appropriate receptor and elicit the postsynaptic response. Neurotransmitter ligand-gated ion channels allow passage of specific ions to change the voltage of the postsynaptic cell. The complex nature of synaptic communication as well as the multitude of components involved, reveal the myriad levels at which aberrant synaptic development and function can lead to neurological disease states.

The *Drosophila* neuromuscular junction synapse model

The neuromuscular junction (NMJ) is a specialized synapse formed by the connection of a presynaptic motoneuron on a postsynaptic muscle (Deshpande and Rodal, 2015; Menon et al., 2013). The motoneuron axon terminates on the muscle surface and forms NMJ boutons, which are engulfed throughout development by folds of muscle membrane, the subsynaptic reticulum (SSR; Slater, 2015). The SSR is important for amplifying the synaptic signal throughout the muscle. SSR structural integrity is dependent on scaffolding molecules that aid in forming and holding the membrane in place. Mammalian extracellular components within the SSR membrane and synaptomatrix include neurotransmitter receptors, agrin, Dystroglycan, laminin and matrix metalloproteinases; all components that direct function, stabilization and development of the NMJ (Bloch-Gallego, 2015; Muntoni et al., 2008; Sanes and Lichtman, 1999). The vertebrate NMJ is cholinergic with presynaptic release of acetylcholine neurotransmitter directed to postsynaptic acetylcholine receptors. Neurotransmitter passage thought the synaptic cleft is dependent on cell adhesion molecules that hold the pre and postsynaptic membrane in close proximity and maintain the stabilization of active zone components. Dystroglycan structurally connects intracellular cytoskeleton with extracellular laminin to support muscle strength and acetylcholine receptor clustering at the synapse. Presynaptically released agrin binds laminin and dystoglycan to direct and maintain acetylcholine receptors clustering (Bloch-Gallego, 2015). Matrix metalloproteinases cleave agrin to regulate its ability to bind laminin resulting in loss of the agrin-laminin complex and resultant acetylcholine receptor clustering (Patel et al., 2012). Laminin also stabilizes presynaptic calcium

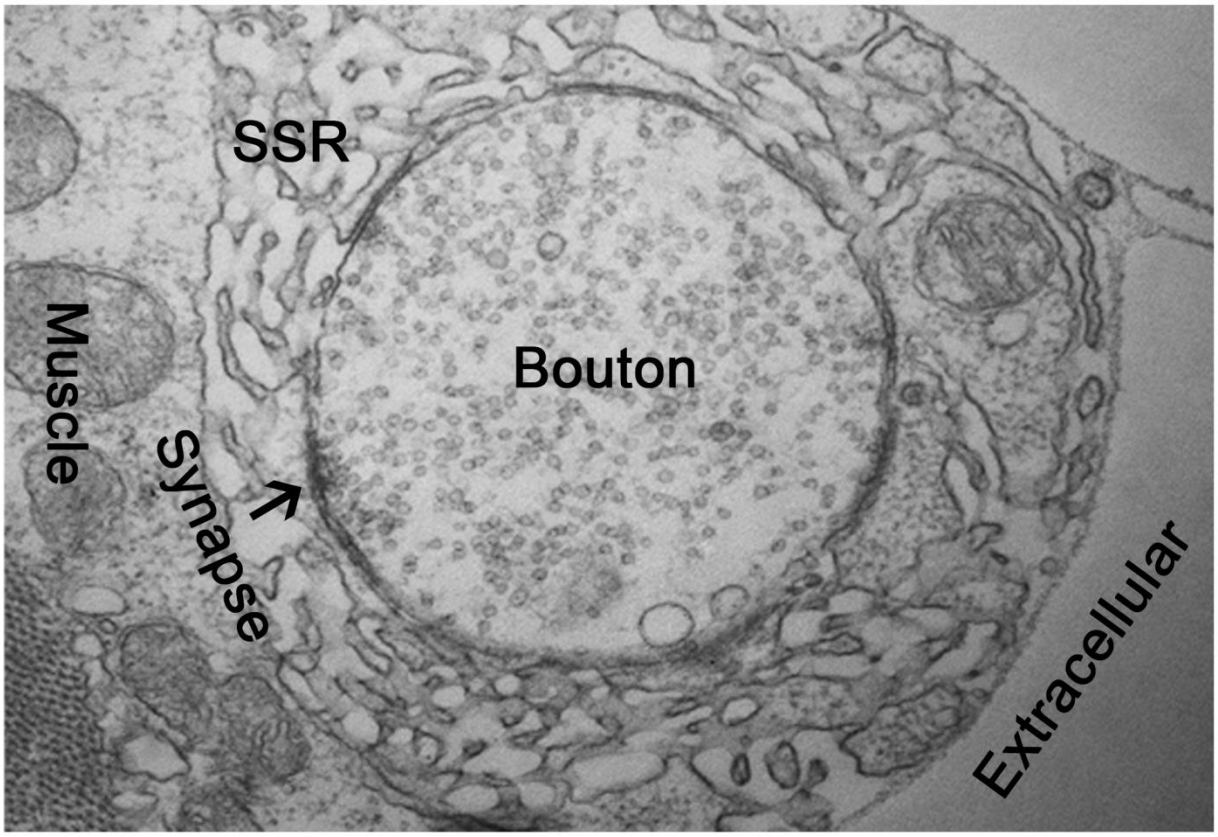

Figure 1

Figure 1: Ultrastructure of *Drosophila* Neuromuscular Junction

The neuromuscular junction is composed of the presynaptic bouton, postsynaptic muscle and the extracellular synaptomatrix between both cells. The nerve's axon terminates on the muscle in the form of boutons. The bouton stores all the necessary components for presynaptic release of neurotransmitter which is stored in hundreds of synaptic vesicles that appear like small circles with ultrastructural imaging. Along the edge of the bouton, dark regions can be seen where an increased number of synaptic vesicles congregate around machinery that facilitates synaptic vesicle fusion with the membrane, this is the location of the synapse. Several layers of membrane folds surround the bouton forming the subsynaptic reticulum (SSR), this region is important for amplifying the signal throughout the muscle.

channel clustering surrounding active zones which in turn recruit other presynaptic elements (Bloch-Gallego, 2015; Wu et al., 2010). These proteins are required to form a functionally active synapse, but likewise require glycan modification to carry out their function. After a synapse is formed it must be actively maintained or it will be degraded, active maintenance requires continued protein recruitment that is initiated through bidirectional trans-synaptic signals that drive synaptic protein translation.

Studies using the *Drosophila* NMJ have greatly influenced our understanding of synaptic structural and functional development. Neuroligins, members of the cell adhesion molecules family, bind to neurexins forming a trans-synaptic connection between the pre and postsynaptic membrane (Chen et al., 2012; Xing et al., 2014). Loss of the neuroligin-neurexin complex results in aberrant bouton formation and synaptic transmission strength likely in part to disorganization of the SSR (Chen et al., 2012). The SSR is largely dependent on intracellular scaffolds to maintain the number and density of membrane folds. Loss of one particular scaffold, Discs Large (DLG), reduces the number and size of membrane folds in the SSR as well as reducing synaptic function (Blunk et al., 2014; Budnik et al., 1996; Lahey et al., 1994). Ultrastructural analysis of boutons reveals a similar synaptic structure seen in mammalian boutons with SSR surrounding a bouton that contains synaptic vesicles and active zones (Fig. 1). However, in *Drosophila* active zones are decorated by "T-bars" that serve to facilitate synaptic vesicle membrane fusion. Also in contrast to mammals, the *Drosophila* NMJ synapse is glutamatergic. The ease of physical access to *Drosophila's* NMJ makes it a powerful synapse to study structural development and function. The larval body wall is lined with 30 muscles per hemisegment stereotypically arranged making identification of each muscle simple for experiment standardization (Fig. 2; Brent et al., 2009). Corresponding motoneurons within the neuropil project their axon through the cytoplasm to each target muscle. A simple dissection exposes the innervating axons and musculature allowing functional and structural assays. Synaptic transmission is assayed by clamping the muscle's voltage, stimulating the axon and recording the resultant current that enters the muscle (Parkinson et al., 2013). Structural parameters are imaged and quantified to assay bouton number, branch number and overall

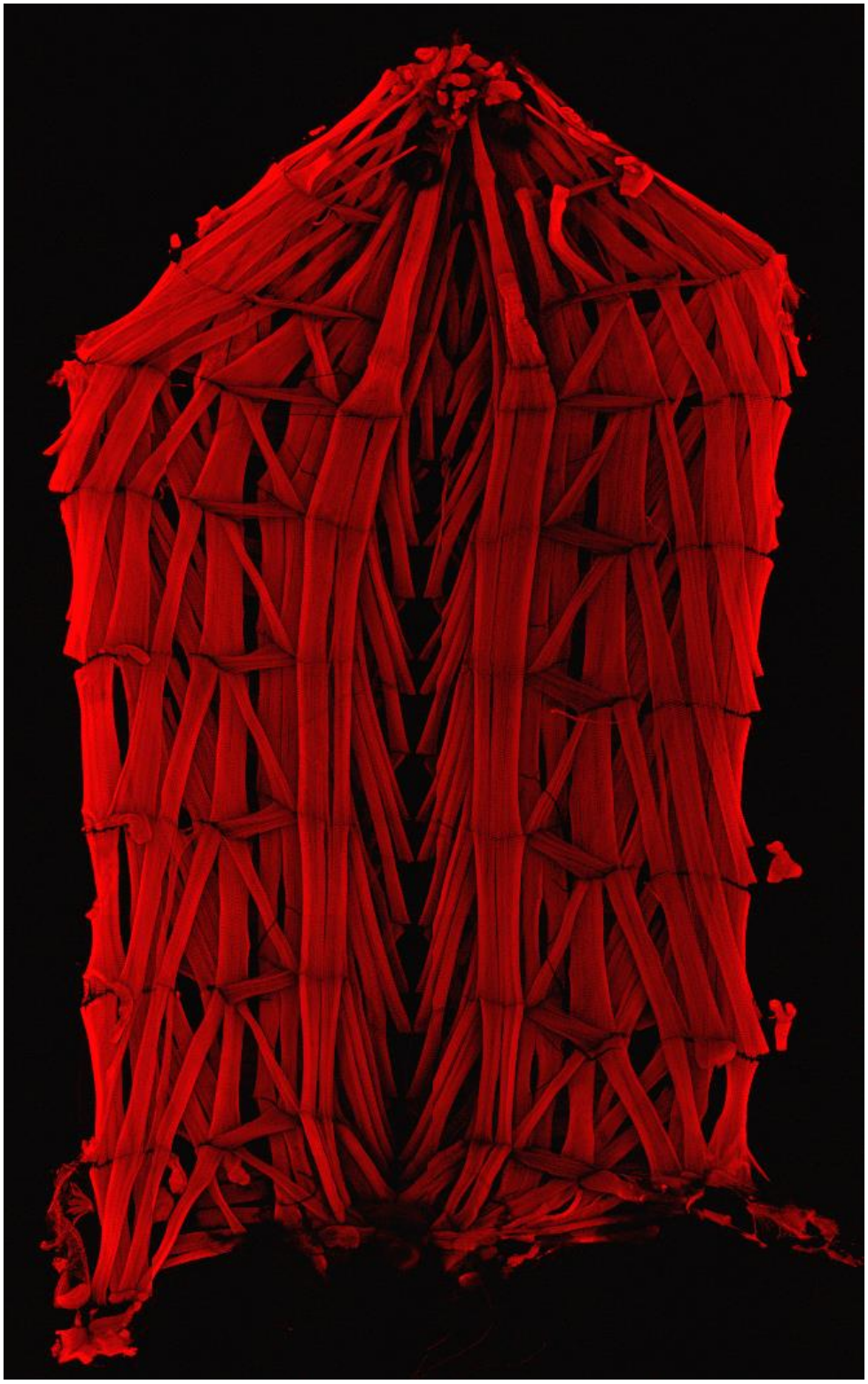

Figure 2

Figure 2: The Drosophila 3rd instar larval musculature

The larval body wall is beautifully lined with a repeated muscle pattern containing 30 muscles in each segment. This pattern allows quick identification of each muscle providing a system to identify and study precise muscles and neuromuscular junctions for repeatability of experiments. The image was produced by cutting the dorsal side of the larval, removing all organs, pinning sides down, fixing and labeling all muscle tissue.

NMJ area. In addition to structure, protein scaffolds, active zones, trans-synaptic signals and glycans are easily labeled with antibodies and lectins at the NMJ to visualize quantity and localization.

Drosophila *trans*-synaptic signaling

Synaptogenic recruitment of presynaptic and extracellular scaffolds as well as active zone components requires bidirectional trans-synaptic signaling between the muscle and neuron in order to assure synaptic specificity and transmission integrity (Dani and Broadie, 2012). During larval development the muscle grows 100 fold which requires corresponding NMJ development to maintain stimulation strength. If the NMJ does not expand with muscle growth, neural stimulation will become weak and unable to elicit a muscle contraction. However conversely, if neural stimulation is too great then the muscle will be unable to repolarize in a timely manner, this is particularly important for fast acting muscles. Thus, throughout muscle development neural size needs to correspond to maintain proper muscle stimulation. To maintain synaptic transmission that is "just right", the neuron and muscle constantly send trans-synaptic signals back and forth in order to increase or decrease synaptic strength, fine-tuning the developing synapse. Trans-synaptic signals drive the translation and recruitment of synaptic building blocks for transmission, but also cell adhesion molecules such as neurexin, neuroligin and fasciclin 2 that are required to maintain synapse integrity. Neurexin forms a complex with neuroligin to modulate synapse development. Loss of *Drosophila* neuroligin 2 causes a reduction of bouton number, aberrant SSR development and impaired synaptic transmission (Chen et al., 2012). Fasciclin 2 is expressed both pre and postsynaptically and forms a homodimer across the synapse (Schuster et al., 1996; Spring et al., 2016). This trans-synaptic complex is not required to form the synapse but is required to maintain the synaptic connection, loss of Fas2 either pre or postsynaptically drives bouton retraction. These cell adhesion molecules communicate through direct physical trans-synaptic interactions. In addition to physical complex formation, the NMJ communicates through trans-synaptic signals that drive the recruitment of these synaptic proteins required to expand and maintain the developing NMJ.

Three particularly well-characterized *trans*-synaptic signals at the *Drosophila* NMJ are Wnt Wingless (Wg), BMP Glass Bottom Boat (Gbb), and Jelly Belly (Jeb) (Grosso et al., 2011; Kamimura et al., 2013; Rohrbough and Broadie, 2010; Tanaka et al., 2002). The Wnt signal, Wg, drives the development of pre and postsynapse active zones, boutons and SSR formation (Mosca and Schwarz, 2010). Wg is secreted presynaptically and binds postsynaptic Frizzled 2 receptors that are then internalized, cleaved and transported to the nucleus to initiate synaptic protein translation (Ataman et al., 2008; Korkut and Budnik, 2009). The integrity of Wg signaling on Frz2 receptors requires the co-receptor Dally-like-protein (Dlp), a GPI anchored glycoprotein that is proposed to temporarily bind Wg causing its accumulation near Frz2 receptors (Dear et al., 2016; Yan et al., 2009). The BMP signal, Gbb, is postsynaptically released and binds its presynaptic receptors that include wishful thinking (Wit), thick veins (Tkv) and saxophone (Sax) to drive transcription of neural proteins (Haghighi et al., 2003; Kim and Marques, 2010; McCabe et al., 2003; Nahm et al., 2010). Loss of Gbb signaling at the NMJs causes reduced boutons, active zone t-bars and synaptic transmission. Jeb is released presynaptically and binds postsynaptic anaplastic lymphoma kinase (Alk) receptors (Rohrbough et al., 2013). Activation of the Alk receptor reduces the muscles response to neural transmission, revealing a trans-synaptic pathway that negatively regulates synaptic activity. Loss and overexpression of these trans-synaptic signals and cell adhesion molecules alter the development of the NMJ synapse causing altered synaptic function and structure (Dani and Broadie, 2012). Synaptogenic events are regulated by bidirectional trans-synaptic signals that traverse the synaptomatrix, and glycosylation of both ligands and receptors alters localization and binding (Henriquez and Salinas, 2012; Patton, 2003).

Drosophila NMJ synaptic glycosylation

Most cells are coated with a glycocalyx (Abu-Qarn et al., 2008), with carbohydrate chains on proteins and lipids heavily decorating the plasma membrane's outter leaflet. At the synapse, the heavily-glycosylated synaptomatrix is composed of secreted and membrane-bound molecules residing at the interface between presynaptic active zone and postsynaptic receptor field. In *Drosophila,* genetic analyses show synaptomatrix glycan modification/binding has core roles in both structural and functional NMJ development (Broadie et al., 2011; Dani

and Broadie, 2012). Known glycan-dependent synaptogenic events include presynaptic active zone (AZ) differentiation, postsynaptic glutamate receptor (GluR) localization and ECM organization within the synaptic cleft, driven by the secreted endogenous lectin Mind-the-Gap (MTG) (Dani et al., 2012; Long et al., 2008; Rushton et al., 2012). The majority of extracellular synaptic proteins are glycosylated, which can be visualized by lectins that bind specific glycan branches or chains (Jumbo-Lucioni et al., 2014). For example, *Vicia villosa* (VVA) labels n-acetylgalactosamine glycans; antibody against Horse Radish Peroxidase (HRP) labels bifucosylated N-glycans; Erythrina cristagalli (ECL) binds to D-galactose glycans; all are particularly highly enriched at the *Drosophila* NMJ (Parkinson et al., 2013). Several other lectins have been used to visualize glycan composition revealing a heavy contribution of glycosylation at the NMJ (Dani et al., 2014; Jumbo-Lucioni et al., 2014). Lectins bind specific glycans but are not specific for proteins, so loss of lectin labeling does not necessarily mean loss of proteins. An antibody against Horse Radish Peroxidase (HRP) labels N-glycans that are bi-fucosylated, and this label has been classically used to visualize the *Drosophila* NMJ. The extensive lectin binding at the NMJ highlights the multitude of glycoproteins that both form the synapse and regulate its activity.

The majority of extracellular proteins at the synapse are glycosylation (Schachter and Boulianne, 2011; Scott and Panin, 2014). Proteins are glycosylated with a highly varied level of necessity, some proteins require glycosylation to fold properly or function whereas others seemingly receive glycan modifications without purpose or benefit. At the *Drosophila NMJ* there are several examples of glycoproteins that require their glycan modification for structural and functional integrity of the synapse while the role for other N-glycan modifications has not been identified. The Wg trans-synaptic pathway is a good example of N-glycosylation modification. Wg signaling molecule itself is N-glycosylated but its removal has not shown any effects on signal transmission to the muscle. The co-receptor DLP is highly glycosylated and it is these glycan chains that enhance its binding to Wg (Yan et al., 2009). Additionally, DLP is GPI anchored which requires three mannose residues that have been modified by glycosylation enzymes. Dystroglycan is heavily glycosylated in vertebrates and loss of these glycan modifications cause congenital muscular dystrophies. Likewise, *Drosophila* Dystroglycan is

glycosylated and its loss causes a reduction in Dystroglycan at the NMJ, reduced quantal content (strength of neurotransmitter in an individual SV) and postsynaptic glutamate receptor composition (Wairkar et al., 2008). Loss of glycosylation on specific glycoproteins often leads to loss of protein function as seen above, but with loss of the enzymes responsible for glycosylation the impact is more widespread impacting proteins in several pathways.

N-Linked Glycosylation

N-Linked Glycosylation Pathway

The major focus of this thesis is the intersection of N-linked glycosylation and NMJ synaptic development. Most extracellular secreted and transmembrane proteins are N-glycosylated in the ER (Schachter and Boulianne, 2011; Scott and Panin, 2014). The addition occurs on one or more asparagines per protein within the three amino acid consensus sequence (asparagine-X-serine/threonine), with X being any amino acid other than proline. All N-linked glycans begin with the same 14-oligosaccharide transferred from a modified lipid (dolichol) by the oligosaccharide transferase complex (OST, Fig. 3). The process begins in the cytosol with the addition of N-acetyl-glucosamine (GlcNac) to dolichol phosphate, followed by the addition of a second GlcNac and then 5 mannose sugars. This 7-oligosaccharide is then flipped into the ER lumen by RFT1 flippase (Ondruskova et al., 2012), after which 4 mannose and 3 glucose sugars are added in sequential order. The 14-oligosaccharide is then transferred by the OST onto the asparagine in the co-translational protein transport mechanism (Fig. 3). Soon after addition, the oligossacharide is trimmed by glycanases to a 12-oligosaccharide recognized by chaperone proteins (calnexin and calreticulin) that aid folding (Lannoo and Damme, 2015; Wang et al., 2015). Improper folding results in trimming to a 9-oligosaccharide structure, which targets the protein for ERAD pathway degradation (Julio and Parodi, 2015; Lannoo and Damme, 2015). A properly folded protein is sent along the ER to Golgi pathway as the glycan is further trimmed to a 7-oligosaccharide and an N-acetyl-glucosamine is added by *mgat1* (Fig. 3). From this step foward, the N-glycosylation pathway differs between organisms, but involves the addition and cleavage of more sugars to generate a myriad of differentially

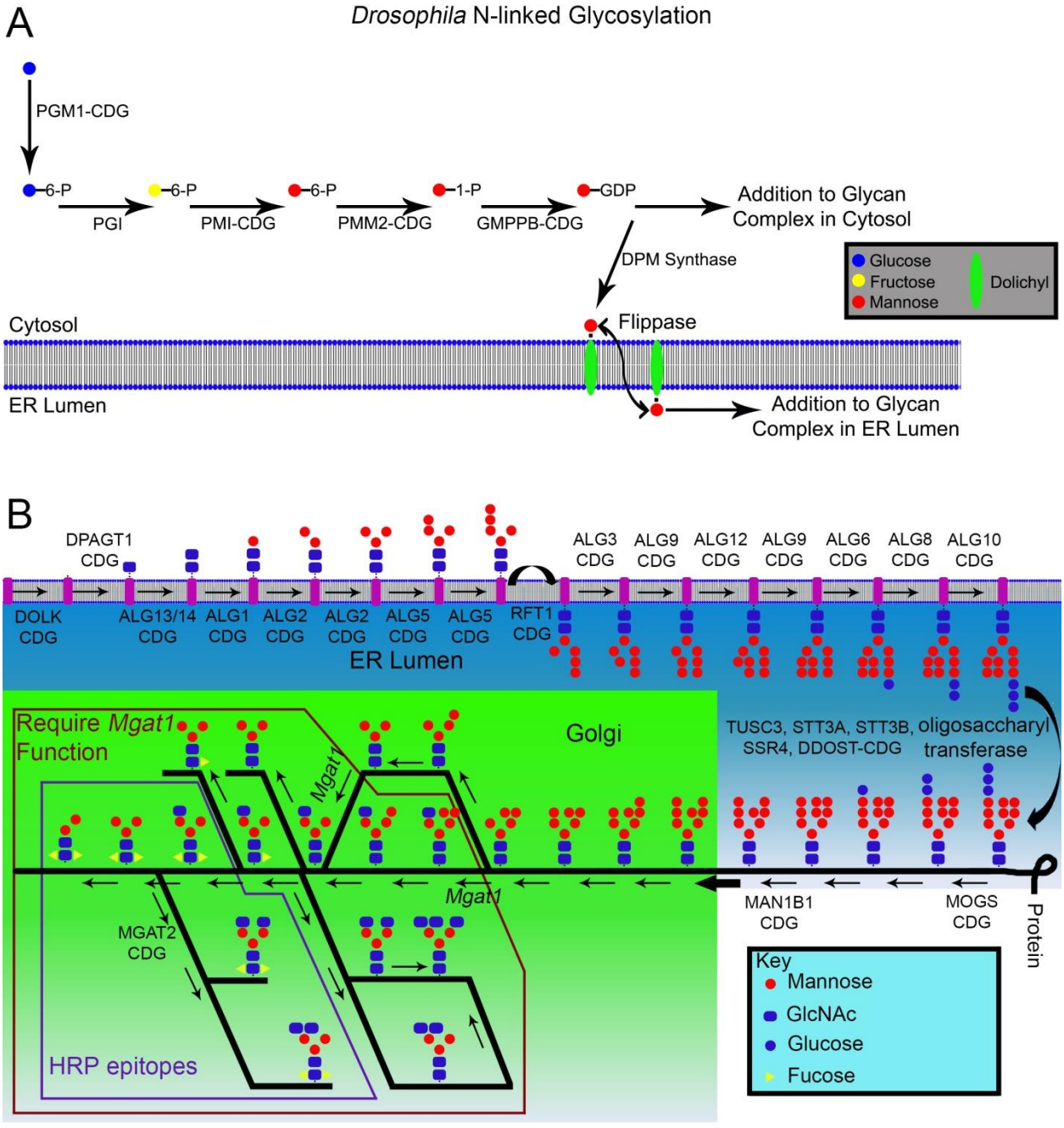
A
Drosophila N-linked Glycosylation
PGM1-CDG
6-P
PGI
6-P
PMI-CDG
6-P
PMM2-CDG
1-P
GMPPB-CDG
GDP
Addition to Glycan Complex in Cytosol
DPM Synthase
Glucose
Fructose
Mannose
Dolichyl
Cytosol
Flippase
ER Lumen
Addition to Glycan Complex in ER Lumen
B
DPAGT1 CDG
ALG3 CDG
ALG9 CDG
ALG12 CDG
ALG9 CDG
ALG6 CDG
ALG8 CDG
ALG10 CDG
DOLK CDG
ALG13/14 CDG
ALG1 CDG
ALG2 CDG
ALG2 CDG
ALG5 CDG
ALG5 CDG
RFT1 CDG
ER Lumen
Require Mgat1 Function
Golgi
Mgat1
TUSC3, STT3A, STT3B, SSR4, DDOST-CDG
oligosaccharyl transferase
Mgat1
MGAT2 CDG
MAN1B1 CDG
MOGS CDG
Protein
HRP epitopes
Key
Mannose
GlcNAc
Glucose
Fucose

Figure 3

Figure 3: Drosophila N-Linked Glycosylation Pathway with CDGs

A) GDP-Mannose and Dolichol-Mannose are derived from glucose and required for the assembly of the N-glycan oligosaccharide. Each step of glucose's conversion requires enzymatic activity that if mutated results in a Congenital Disorder of Glycosylation. GDP-mannose is required building the oligosaccharide in the cytosol and dolichol-mannose is required for addition of mannose in the ER and Golgi lumen. B) Building the N-glycan oligosaccharide is a linear process up to the addition of GlcNAc by Mgat1 and highly conserved in *Drosophila*. Post Mgat1's function the pathway of glycan modification splits into several directions and can be modified by different glycans and branching patterns. Glycan patterns that require Mgat1 function are depicted in the outlined section labeled "Required Mgat1 Function" and are absent in the *mgat1* mutant. Congenital Disorders of Glycosylation (CDG) result from mutation of glycosylation enzymes that reduce enzymatic activity and are shown.

glycosylated structures. For further details regarding the glycosylation pathway please see *Essentials of Glycobiology* (Varki et al., 2009).

N-linked glycosylation at the synapse

Hundreds of synaptic proteins are glycosylated, spanning multiple aspects of synapse structure and function development, as well as transmission modulation (Koles et al., 2007). On the presynaptic side, glycan dependent proteins includes synaptic vesicle protein 2 (SV2) and synaptophysin (Kwon and Chapman, 2012). SV2 has three N-glycan binding sites that are required for transport of SV2 to synaptic vesicles and its role in synaptic vesicle priming and recycling. Synaptophysin has only one N-glycan attachment but it is required for trafficking to synaptic vesicles and its loss results in reduced recycling. Within the synaptic cleft, extracellular glycoproteins include Dystroglycan, agrin and laminin (Broadie et al., 2011; Martin, 2003). Loss of these extracellular glycoproteins or their glycosylation can results in weakened membrane integrity and cell-cell connectivity. The glycans that modify Dystroglycan bind to laminin, loss of these glycans results in severe muscular dystrophies characterized by muscle weakness. Loss of the enzyme O-fucosyltransferase I that adds fucose to agrin results in an increase in acetylcholine receptors caused by the loss of agrin glycosylation; revealing a negative regulatory mechanism for glycosylation (Kim et al., 2008). On the postsynaptic side both acetylcholine and glutamate receptors are glycosylated. Acetylcholine receptor glycosylation regulates channel gating, whereas the glutamate receptors require glycosylation for trafficking to the synaptic membrane (Engel et al., 2015; Scott and Panin, 2014). Reduced glycosylation on acetylcholine receptors causes loss of synaptic transmission and results in congenital myasthenia syndrome in humans. See the following reviews on N-glycosylation of the nervous system (Dani et al., 2012; Scott and Panin, 2014 a, b).

Congenital Disorders of Glycosylation

Clinical diagnosis and symptoms

Congenital Disorders of Glycosylation (CDGs) occur when the glycosylation pathway is impaired via mutations reducing enzymatic activity (Scott et al 2014). Table 1 outlines the known N-linked CDGs, and Figure 3 depicts the enzyme location of CDGs within the N-linked

glycosylation pathway. CDGs typically manifest in hypomorphic heteroallelic conditions (two different partial loss of function mutations), in which patients maintain partial function of the mutated enzyme allowing some glycosylation to continue through the bottleneck but still hampers further glycan modifications resulting in disease conditions based on the amount of remaining enzymatic activity. Although CDGs are individually rare disease states, more CDG patients are being revealed due to advances in medical technology and a greater understanding of glycan related disorders (Hennet, 2012). Previously unidentified diseases are being defined as CDGs, with many more predicted but still unidentified due to a lack of routine testing. Altered blood serum glycosylation levels point to a potential CDG, and direct sequencing is required to identify the specific CDG, which is very important for treatment. CDG patients present with multi-system symptoms ranging from neurological, liver, intestinal and hepatic (Paragon et al., 2014), with blood defects, metabolic impairments, hypothyroidism and disorders with facial cranial development, skin, hypotonia, immune systems and general failure to thrive. In many cases, there are striking neurological problems (Paragon et al., 2014). The nervous system is particularly affected by glycan loss, as is evident by the high percentage of CDG patients presenting with neurological impairment.

Greater than 80% of CDGs cause a neurological deficiency, which can affect both the central and peripheral nervous system (Barone et al., 2014). In the central nervous system, reduced cerebral development, microcephaly, epilepsy, ataxia and mental retardation are all common in CDG patients. The peripheral nervous system can present with motor ataxia, muscle weakness and reduced limb control with a wide range of severity. Some CDGs primarily cause peripheral impairment, such as movement control at the neuromuscular junction, while others cause severe selective brain impairment, such as intellectual disability. The most common CDG (PMM2-CDG, >1000 patients) presents with neurological impairments including cerebellar atrophy causing ataxia and locomotion deficiencies, forcing many PMM2-CDG patients to be wheelchair-bound (Barone et al., 2014). Many CDG patients have intellectual disability caused by CNS involvement but some are mentally fully capable with only slight ataxia. The wide range of disease presentation is caused in part by the hypomorphic nature of most CDG disease states, with partial function of the causative enzyme allowing some level of glycosylation but

CDG Name	Enzyme Name/ function	Gene Symbol	CG number
	Glycan Precursors		
PGM1-CDG	phosphoglucomutase activity	PGM1	5165
	phosphoglucoisomerase	PGI	8251
MPI-CDG	phosphomannose isomerase	MPI	8417
PMM2-CDG	phosphomannomutase 2	PMM2	10688
GMPPA-CDG	mannose-1-phosphate guanylyltransferase activity	GMPPA	8207
GMPPB-CDG	GDP-mannose pyrophosphorylase B	GMPPB	1129
MPDU1-CDG	Mannose-P-dolichol utilization defect 1 protein	MPDU1	3792
Dolk-CDG	dolichol phosphokinase	Dolk	8311
	Sugar Transporters		
SLC35C1-CDG	GDP-fucose transmembrane transporter activity	SLC35C1	9620
SLC35CA2-CDG	UDP-galactose transmembrane transporter activity	SLC35A2	2675
	ER Oligosaccharide Building		
DPAGT1-CDG	UDP-N-acetylglucosamine—dolichyl-phosphate N-acetylglucosaminephosphotransferase	DPAGT1 or Alg7	5287
ALG13-CDG	UDP-N-acetylglucosaminyltransferase subunit	ALG13	14512
ALG14-CDG	N-acetylglucosaminyldiphosphodolichol N-acetylglucosaminyltransferase anchoring subunit	ALG14	6308
ALG1-CDG	Chitobiosyldiphosphodolichol beta-mannosyltransferase	ALG1	18012
ALG2-CDG	Alpha-1,3-mannosyltransferase	ALG2	1291
ALG11-CDG	Asparagine-linked glycosylation protein 11	ALG11	11306
RFT1-CDG	Man5GlcNAc2-PP-Dol flippase	RFT1	3149
ALG3-CDG	Dolichyl-P-Man:Man(5)GlcNAc(2)-PP-dolichyl mannosyltransferase	ALG3	4084
ALG12-CDG	Dolichyl-P-Man:Man(7)GlcNAc(2)-PP-dolichyl-alpha-1,6-mannosyltransferase	ALG12	8412
ALG9-CDG	Alpha-1,2-mannosyltransferase	ALG9	11851
ALG6-CDG	Dolichyl pyrophosphate Man9GlcNAc2 alpha-1,3-glucosyltransferase	ALG6	5091
ALG8-CDG	dolichyl pyrophosphate Glc1Man9GlcNAc2 alpha-1,3-glucosyltransferase	ALG8	4542

	Alpha 3-glucosyltransferase	ALG10	32076
DPM1-CDG	Dolichol-phosphate mannosyltransferase	Dpm1	10166
DPM3-CDG	Dolichol-phosphate mannosyltransferase subunit 3	DPM3	33977
DPM2-CDG	Dolichol phosphate-mannose biosynthesis regulatory	DPM2	42456
	Oligosaccharide Complex		
TUSC3-CDG	Oligosaccharyl transferase complex, subunit OST3/OST6		7830
	Dolichyl-diphosphooligosaccharide--protein glycosyltransferase subunit Swp1		6370
STT3A-CDG	Oligosaccharyl transferase, STT3 subunit		7748
STT3B-CDG	Oligosaccharyl transferase, STT3 subunit		1518
SSR4-CDG	Translocon-associated protein δ or Signal Sequence Receptor 4 (SSR4)		9035
DDOST-CDG	Dolichyl-diphosphooligosaccharide--protein glycosyltransferase 48 kDa subunit		9022
	dolichyl-diphosphooligosaccharide-protein glycotransferase activity		13393
	Glycan Cleaving Enzymes		
MOGS-CDG OR GCS1-CDG	Mannosyl-oligosaccharide glucosidase	MOGS or GCS1	1597
	alpha-1,4-glucosidase activity	ganab	14476
	mannosyl-oligosaccharide 1,2-alpha-mannosidase activity		32684
MAN1B1-CDG	Endoplasmic reticulum mannosyl-oligosaccharide 1,2-alpha-mannosidase	MAN1B1	11874
	mannosyl-oligosaccharide 1,2-alpha-mannosidase activity	alpha-Man-1c	31202
	Golgi Glycan Modifications		
	mannosyl (alpha-1,3-)-glycoprotein beta-1,2-N-acetylglucosaminyltransferase	mgat1	13431
	mannosyl-oligosaccharide 1,3-1,6-alpha-mannosidase activity	α Mannosidase II a	18802
	mannosyl-oligosaccharide 1,3-1,6-alpha-mannosidase activity	α-Man-IIb	4606
Mgat2-CDG	Alpha-1,6-mannosyl-glycoprotein 2-beta-N-acetylglucosaminyltransferase	mgat2	7921

	alpha(1,6)-fucosyltransferase	FucT6	2448
	beta-N-acetylglucosaminidase activity		8824
	alpha(1,3)-fucosyltransferase		6869
	alpha-(1->3)-fucosyltransferase activity		4435
	UDP-glucose:Glycoprotein Glucosyltransferase		6850
	dolichyl-phosphate beta-glucosyltransferase activity		7870

Table 1: Congenital Disorders of Glycosylation with Drosophila homologs

N-Linked Congenital Disorders of Glysolation (CDG) are listed in column 1 with N-glycosylation pathway enzymes in column 2. Commonly used abbreviations are listed in column 3 and all known *Drosophila* homologs are shown in column 4. This table will need to be exapanded as new enzymes, genes and CDGs are identified.

not full activity. This disease range is further broadened by unknown factors. Siblings with identical mutants have been shown to present very differently due to unknown genetic background and/or environmental factors. Given our current level of understanding, CDG treatment strategies are primarily limited to alleviating symptoms.

To date there are only three somewhat treatable CDGs: DPAGT1-CDG, MPI-CDG and PGMI-CDG. DPAGT1-CDG blocks the first step in building the dolichol-oligosaccharide, and results in a congenital myasthenic syndrome (CMS), a condition with muscle weakness caused by loss of glycosylation of NMJ acetylcholine receptors (Scott et al., 2014). Cholinesterase inhibitors increase available neurotransmitter to activate the reduced acetylcholine receptor number and restore some muscle strength, but most DPAGT1-CDG patients die before 1 year old due to additional disabilities (Belaya et al., 2012). MPI-CDG patients have severe multisystem impairment caused by a reduction in available mannose-6-phosphate, a glycan precursor required to build the N-oligosaccharide. High doses of mannose and heparin treatments can restore mannose levels, however developmental abnormalities that occur prior to mannose supplementation can still be severe and can require organ transplantation (Pagon et al., 2014; Scott et al., 2014). PGMI-CDG patients present with reduced galactosylation resulting in multisystem impairments caused by defects in the bidirectional interconversion of glucose-1-phosphate and glucose-6-phosphate. Galactose supplements improve liver function, hypoglycemia and abnormal coagulation (Scott et al., 2014; Tegtmeyer et al., 2014). Overall, CDG treatments are very limited and in no case completely correct disease states. The greatest barrier to developing treatments is the lack of understanding of the disease conditions on a cellular and molecular level. Future studies using animal models are required to gain a better understanding of the affected glycoprotein pathways, especially for neurological symptoms.

Synaptic CDG disease models

Synaptic defects are the leading hypothesized cause for neurological CDG disease states. For example, loss of dystroglycan glycosylation results in dystroglycanopathies, a form of muscular dystrophy caused by the inability of dystroglycan to bind its extracellular partners: laminin, neurexin and agrin (Kirschner, 2013). Muscular dystrophies present with severe muscle

failure and associated movement impairments, with intracellular NMJ components (dystrophin) unable to bind extracellular partners resulting in muscle weakness and failure to illicit strong movement. Mammailian models reveal strong requirement for glycosylation on a protein to protein basis, but models for CDGs that impact potentially dozens or hundreds of proteins are limited. Mouse CDG models have been somewhat useful for understanding glycosylation defects in multiple organ systems but have only been generated for 9 CDG conditions: PMI-CDG, PMM2-CDG, SRD5A3-CDG, DPAGT1-CDG, MGAT2-CDG, SLC35C1-CDG, B4GALT1-CDG, GNE-CDG and GALNT3-CDG (Schwarzkopf et al., 2002; Thiel and Korner, 2010; Yoshida et al., 2014). However, of these nine mouse models, none have resulted in synaptic characterization of any neural implications (Asano et al., 1997; Cantagrel et al., 2010; Malicdan et al., 2009; Malicdan et al., 2007; Hellbusch et al., 2007; Lu et al., 1997; Marek et al., 1999; Schneider et al., 2011; Schwarzkopf et al., 2002; Sharma et al., 2014; Ye and Marth, 2004; Yoshida et al., 2014). The lack of synaptic characterization in many of these models is causes by early lethality in null mutants or the lack of phenotypes with hypomorphic conditions that do not reduce activity adequately. The need still remains to study loss of function mutants but in a model system that can tightly regulate the degree of reduction in order to produce a disease state but not embryonic lethality.

Drosophila has been used extensively to model human disease states, but to date only a few CDG-causing genes have been extensively studied. *Drosophila* neurally altered carbohydrate gene (nac) encodes a Golgi fucose transporter required for the production of the HRP epitope, a bifucosylated N-glycan (Geisler et al., 2012; Katz et al., 1988; Whitlock, 1993). Loss of nac in wing neurons results in axonal misrouting. The role for the HRP epitope is largely unknown but expected to play a role in axonal projections. A transgenic RNAi screen of glycosylation related gene function at the *Drosophila* NMJ (Dani et al., 2012) uncovered a common role for glycosylation restricting both structure and function. Follow-up work on two hits from this screen, heparan sulfate proteoglycan (HSPG) sulfotransferase (hs6st) and sulfatase (sulf1), revealed a bidirectional disruption of both the WNT (Wingless, Wg) and BMP (Glass Bottom Boat, Gbb) trans-synaptic signaling pathways. Both hs6st and sulf1 mutants had overabundant NMJ structure whereas synaptic transmission strength was increased in the sulf1

mutant but decreased in the hs6st mutant. Subsequent studies on other screen hits, two N-acetyl-galactosamine transferases (pgant), showed regulation of synaptic development via trans-synaptic integrin signaling (Dani et al., 2014). Reduction of either pgant caused increased neural transmission and structural overelaboration at the NMJ. Pre and postsynaptic active zone components were more abundant and ultrastructural investigation revealed increased synaptic vesicle number around the presynaptic active zone T-bars. A specific CDG synaptic disease model that came out of this screen, Classic Galactosemia (Galt), identified aberrant components of Wingless trans-synaptic signaling (Jumbo-Lucioni et al., 2014). Similar to the general trend for glycosylation mutants, both NMJ structure and function were elevated in the Galt mutants. In addition to the above genes, several N-glycosylation CDG causing genes have yet to be studied further that were identified in the initial screen: Mgat2, PMM2, MOGS, MAN1B1, ALG10, ALG8, SLC35C1 and GMPPA. Each of these studies identified disruption of trans-synaptic signaling to be a common root causing compromised NMJ synaptogenesis underlying movement impairments. Ongoing *Drosophila* work aims at understanding these impairments in these disease states for the ultimate goal of improving CDG patient treatment and care.

Thesis Outline

MGAT1

The focus of the first half of this thesis is on the role of the *mgat1* gene encoding Mannosyl (α-1,3-)-glycoprotein β-1,2-N-acetylglucosaminyltransferase (GlcNAcT1). This enzymatic function is a prerequisite for producing all hybrid and complex N-glycosylation (Pownall et al., 1992; Ye and Marth, 2004), and without *mgat1* function all hybrid and complex N-glycan production is restricted (Fig. 3) (Puthalakath et al., 1996; Schachter, 2010). Importantly, this represents the most severe truncation of the N-glycosylation pathway that permits *Drosophila* viability, and therefore allows study of the consequences at the NMJ synapse. Proteins are glycosylated in the *mgat1* mutant and are decorated with high mannose structures, which permits protein folding, but provides a model to study the impact of hybrid and complex glycans on synapse development. Mgat1-dependent N-glycosylation modifies

many synaptic proteins including neurotransmitter receptors, Fasciclins, Neuroglians, Neurexins and Dystroglycans (Koles et al., 2007; Muntoni et al., 2008; Sun and Xie, 2012). Mouse mgat1 knockouts are lethal at E9.5, but conditional mutants show movement defects, tremors, paralysis and early death characteristic of neurodevelopmental impairments (Campbell et al., 1995; Grasa et al., 2012; Shi et al., 2004; Ye and Marth, 2004). *Drosophila mgat1* mutants are adult viable, but have reduced lifespan due to a specific neural requirement (Sarkar et al., 2006; Sarkar et al., 2010; Schachter and Boulianne, 2011). Neurally reduced *mgat1* reveals a striking locomotion deficiency and loss of the HRP glycan labeling that characterizes neuronal tissue (Desai et al., 1994; Paschinger et al., 2009; Sarkar et al., 2006). Interestingly, *mgat1* overexpression in neurons rescues the *mgat1* null mutant and even extends lifespan, implicating a neuronal role for complex and hydrid glycosylation in increasing the conditioning of the animal, although through unknown mechanisms.

Our work focused on characterizing hybrid and complex N-glycosylation roles at the *Drosophila* NMJ. We identify overabundant structural morphology and elevated synaptic transmission in the *mgat1* mutants. Synaptic vesicle number within the bouton is increased and likely accounts in part for the elevated neurotransmission. Trans-synaptic signaling molecules that drive the recruitment of synaptic proteins are also altered with an increase in Wg but decrease in both Gbb and Jeb within the synapse. Likely results of aberrant trans-synaptic signaling, two intracellular scaffolds are reduced resulting in presynaptic SSR distribution and folding errors. We conclude that Mgat1-dependent N-glycosylation shapes the synaptomatrix glycan environment to facilitate transmission of trans-synaptic signaling ligands driving synaptic scaffold recruitment during synaptogenesis.

PMM2

The focus of the second half of this thesis is on the PMM2-CDG disease gene phosphomannomutase 2 (*pmm2*), the enzyme responsible for converting mannose-6-phosphate into mannose-1-phosphate, an obligatory precursory required in building the N-glycan oligosaccharide (Andreotti et al., 2014; Freeze et al., 2014; Freeze et al., 2015). PMM2 functions very early in the N-glycosylation pathway prior to the building of the oligosaccharide

on dolichol so loss of pmm2 results in the complete loss of all N-glycosylation. Since the first patient in 1980, >100 different mutations in >1000 PMM2-CDG patients have been characterized (Freeze et al., 2014; Haeuptle and Hennet, 2009; Jaeken, 2013; Jaeken et al., 1980; Yuste-Checa et al., 2015). PMM2-CDG infant mortality is ~20% in the first year, with patients manifesting subsequent increased susceptibility to organ failure, infection and injury (Grunewald, 2009). PMM2-CDG patients present with a spectrum of neurological symptoms (Jaeken, 2013), ranging from severe neurological impairments with early death, to mild defects with slight psychomotor delay (Grunewald, 2009; Marquardt and Denecke, 2003). The first PMM2-CDG mouse model showed early embryonic lethal, which limited its usefulness (Thiel et al., 2006). Heteroallelic combination of two PMM2 mutations allows partial enzymatic activity, protracted embryonic survival and has demonstrated potential maternal dietary intervention in treatment (Schneider et al., 2011). In this study, feeding mannose to mothers during gestation further increased offspring lifespan. These results gave hope for PMM2-CDG patients, but mannose treatments for patients have showed no benefit (Kjaergaard et al., 1998; Mayatepek and Kohlmuller, 1998). However, patients with PMI-CDG (phosphomannoisomerase, converts fructose-6-phosphate into mannose-6-phosphate) respond favorably to mannose supplementation, and hepato-intenstinal conditions are strongly improved (Jenssen et al., 2014). Recently, a PMI-CDG mouse model showed a detrimental response to mannose supplementation (Sharma et al., 2014). Hypomorphic PMI-CDG mice with PMI loss similar to human patients did not present with any noticeable disease conditions. However, mannose supplementation early in development resulted in eye defects revealing a potential disease causing role for increase mannsose-6-phosphate. A subsequent zebrafish model via PMM2 morpholino knockdown revealed altered development, reduced motility and altered glycan profiles (Cline et al., 2012). Most recently, a similar *Xenopus* morpholino knockdown model demonstrated strong reduction in Wnt signaling, revealing a PMM2 requirement in intercellular communication (Himmelreich et al., 2015). For this thesis work, I produced and characterized *Drosophila pmm2* mutants, showing the characteristic failure to thrive, loss of coordinated movement and reduced N-glycosylation, with severity corresponding to the degree of *pmm2* reduction. We therefore set out to develop a *Drosophila* PMM2-CDG disease model.

Here, we report the generation and characterization of the first *Drosophila* PMM2-CDG model. CRISPR-generated *Drosophila pmm2* null mutants display severely disrupted glycosylation and early lethality. Partial loss of function mutants display incoordination and later lethality corresponding to the reduction of *pmm2*. Analyses of the well-characterized *Drosophila* neuromuscular junction (NMJ) reveal synaptic glycosylation loss accompanied by structural architecture and functional neurotransmission defects. Matrix metalloproteinase 2 (MMP2) is identified as one of the extracellular enzymes with restricted glycosylation resulting in reduced expression of MMP2 at the NMJ. Wnt Wingless (Wg) trans-synaptic signaling is likewise affected with a loss of synaptic Wg ligand, its co-receptor Dlp and downstream transcriptional regulator Frizzled 2 at the muscle nuclei. Taken together, we propose a model for *pmm2* dependent glycosylation of synaptic proteins, enzymes and trans-synaptic signaling that drive synaptic development and maturation.

References

Abu-Qarn, M., Eichler, J., Sharon, N. (2008). Not just for Eukarya anymore: protein glycosylation in Bacteria and Archaea. *Curr Opin Struct Biol*. 18(5):544-50.

Andreotti, G., Cabeza de Vaca, I., Poziello, A., Monti, M.C., Guallar, V., Cubellis, M.V. (2014). Conformational response to ligand binding in phosphomannomutase2: insights into inborn **glycosylation** disorder. *J Biol Chem.* 289(50), 34900-10.

Asano, M., Furukawa, K., Kido, M., Matsumoto, S., Umesaki, Y., Kochibe, N., Iwakura, Y. (1997). Growth retardation and early death of beta-1,4-galactosyltransferase knockout mice with augmented proliferation and abnormal differentiation of epithelial cells. *EMBO J*. 16(8), 1850-7.

Ataman, B., Ashley, J., Gorczyca, M., Ramachandran, P., Fouquet, W., Sigrist, S.J. and Budnik, V. (2008). Rapid activity-dependent modifications in synaptic structure and function require bidirectional Wnt signaling. Neuron. 57(5), 705-18.

Barone, R., Fiumara, A., Jaeken, J. (2014). Congenital disorders of glycosylation with emphasis on cerebellar involvement. *Semin Neurol*. 34(3), 357-66.

Belaya, K., Finlayson, S., Cossins, J., Liu, W.W., Maxwell, S., Palace, J., Beeson, D. (2012). Identification of DPAGT1 as a new gene in which mutations cause a congenital myasthenic syndrome. *Ann N Y Acad Sci.* 1275, 29-35.

Bloch-Gallego, E. (2015). Mechanisms controlling neuromuscular junction stability. *Cell Mol Life Sci.* 72(6), 1029-43.

Blunk, A.D., Akbergenova, Y., Cho, R.W., Lee, J., Walldorf, U., Xu, K., Zhong, G., Zhuang, X., Littleton, J.T. (2014). Postsynaptic actin regulates active zone spacing and glutamate receptor apposition at the Drosophila neuromuscular junction. *Mol Cell Neurosci*. 61:241-54.

Brent, J.R., Werner, K.M., McCabe, B.D. (2009). Drosophila Larval NMJ Dissection. *J Vis Exp*. (24), 1107.

Broadie, K., Baumgartner, S. and Prokop, A. (2011). Extracellular matrix and its receptors in Drosophila neural development. Dev. Neurobiol. 71(11), 1102-30.

Budnik, V., Koh, Y.H., Guan, B., Hartmann, B., Hough, C., Woods, D., Gorczyca, M. (1996). Regulation of synapse structure and function by the Drosophila tumor suppressor gene dlg. Neuron. 17(4), 627-40.

Campbell, R.M., Metzler, M., Granovsky, M., Dennis, J.W. and Marth, J.D. (1995). Complex asparagine-linked oligosaccharides in Mgat1-null embryos. Glycobiology. 5(5), 535-43.

Cantagrel, V., Lefeber, D.J., Ng, B.G., Guan, Z., Silhavy, J.L., Bielas, S.L., Lehle, L., Hombauer, H., Adamowicz, M., Swiezewska, E., De Brouwer, A.P., Blümel, P., Sykut-Cegielska, J., Houliston, S., Swistun, D., Ali, B.R., Dobyns, W.B., Babovic-Vuksanovic, D., van Bokhoven, H., Wevers, R.A., Raetz, C.R., Freeze, H.H., Morava, E., Al-Gazali, L., Gleeson, J.G. (2010). SRD5A3 is required for converting polyprenol to dolichol and is mutated in a congenital glycosylation disorder. *Cell*. 142(2), 203-17.

Chen, Y.C., Lin, Y.Q., Banerjee, S., Venken, K., Li, J., Ismat, A., Chen, K., Duraine, L., Bellen, H.J., Bhat, M.A. (2012). Drosophila neuroligin 2 is required presynaptically and postsynaptically for proper synaptic differentiation and synaptic transmission. *J Neurosci*. 32(45), 16018-30.

Cline, A., Gao, N., Flanagan-Steet, H., Sharma, V., Rosa, S., Sonon, R., Azadi, P., Sadler, K.C., Freeze, H.H., Lehrman, M.A., Steet, R. (2012). A zebrafish model of PMM2-CDG reveals altered neurogenesis and a substrate-accumulation mechanism for N-linked glycosylation deficiency. *Mol Biol Cell*. 23(21), 4175-87.

Dani, N., Broadie, K. (2012). Glycosylated synaptomatrix regulation of trans-synaptic signaling. *Dev Neurobiol*. 72(1), 2-21.

Dani, N., Nahm, M., Lee, S., Broadie, K. (2012). A targeted glycan-related gene screen reveals heparan sulfate proteoglycan sulfation regulates WNT and BMP trans-synaptic signaling. *PLoS Genet*. 8(11), e1003031

Dani N., Zhu H., Broadie, K. (2014). Two protein N-acetylgalactosaminyl transferases regulate synaptic plasticity by activity-dependent regulation of integrin signaling. *J Neurosci*. 34(39), 13047-65.

Dear, M.L., Dani, N., Parkinson, W., Zhou, S., Broadie, K. (2016). Two matrix metalloproteinase classes reciprocally regulate synaptogenesis. *Development* 143(1), 75-87.

Desai, C.J., Popova, E. and Zinn, K. (1994). A Drosophila receptor tyrosine phosphatase expressed in the embryonic CNS and larval optic lobes is a member of the set of proteins bearing the "HRP" carbohydrate epitope. J. Neurosci. 14(12), 7272-83.

Deshpande, M., Rodal, A.A. (2016). The Crossroads of Synaptic Growth Signaling, Membrane Traffic and Neurological Disease: Insights from Drosophila. *Traffic.* 17(2), 87-101.

Engel, A.G., Shen, X.M., Selcen, D., Sine, S.M. (2015). Congenital myasthenic syndromes: pathogenesis, diagnosis, and treatment. *Lancet Neurol*. 14(4), 420-34.

Freeze, H.H., Chong, J.X., Bamshad, M.J., Ng, B.G. (2014). Solving glycosylation disorders: fundamental approaches reveal complicated pathways. *Am J Hum Genet*. 94(2), 161-75.

Freeze, H.H., Eklund, E.A., Ng, B.G., Patterson, M.C. (2015). Neurological Aspects of Human Glycosylation Disorders. *Annu Rev Neurosci*. 38, 105-25.

Geisler, C., Kotu, V., Sharrow, M., Rendić, D., Pöltl, G., Tiemeyer, M., Wilson, I.B., Jarvis, D.L. (2012). The Drosophila neurally altered carbohydrate mutant has a defective Golgi GDP-fucose transporter. *J Biol Chem*. 287(35), 29599-609.

Grasa, P., Kaune, H. and Williams, S.A. (2012). Embryos generated from oocytes lacking complex N- and O-glycans have compromised development and implantation. Reproduction. 144(4), 455-65.

Del Grosso, F., De Mariano, M., Passoni, L., Luksch, R., Tonini, G.P. and Longo, L. (2011). Inhibition of N-linked glycosylation impairs ALK phosphorylation and disrupts pro-survival signaling in neuroblastoma cell lines. BMC Cancer. 11, 525.

Grünewald, S. (2009). The clinical spectrum of phosphomannomutase 2 deficiency (CDG-Ia). *Biochim Biophys Acta*. 1792(9), 827-34.

Haeuptle, M.A., Hennet, T. (2009). Congenital disorders of glycosylation: an update on defects affecting the biosynthesis of dolichol-linked oligosaccharides. *Hum Mutat*. 30(12), 1628-41.

Haghighi, A.P., McCabe, B.D., Fetter, R.D., Palmer, J.E., Hom, S., Goodman, C.S. (2003). Retrograde control of synaptic transmission by postsynaptic CaMKII at the Drosophila neuromuscular junction. *Neuron*. 39(2), 255-67.

Hellbusch, C.C., Sperandio, M., Frommhold, D., Yakubenia, S., Wild, M.K., Popovici, D., Vestweber, D., Gröne, H.J., von Figura, K., Lübke, T., Körner, C. (2007). Golgi GDP-fucose transporter-deficient mice mimic congenital disorder of glycosylation IIc/leukocyte adhesion deficiency II. *J Biol Chem.* 282(14), 10762-72.

Hennet, T. (2012). Diseases of glycosylation beyond classical congenital disorders of glycosylation. Biochimica et Biophysica Acta 1820, 1306-1317.

Henríquez, J.P. and Salinas, P.C. (2012). Dual roles for Wnt signalling during the formation of the vertebrate neuromuscular junction. Acta Physiol. (Oxf). 204(1), 128-36.

Himmelreich, N., Kaufmann, L.T., Steinbeisser, H., Körner, C., Thiel, C.J. (2015). Lack of phosphomannomutase 2 affects Xenopus laevis morphogenesis and the non-canonical Wnt5a/Ror2 signalling. *Inherit Metab Dis*. 38(6), 1137-46.

Jaeken, J., Vanderschueren-Lodeweyckx, M., Casaer, P., Snoeck, L., Corbeel, L., Eggermont, E., Eeckels, R. (1980). Familial psychomotor retardation with markedly fluctuating serum prolactin, FSH and GH levels, partial TBG-deficiency, increased serum arylsulfatase-A and increased CSF protein- new syndrome? *Pediatr Res*. 14:179

Jaeken, J. (2013). Congenital disorders of glycosylation. *Handb Clin Neurol.* 113, 1737-43.

Janssen, M.C., de Kleine, R.H., van den Berg, A.P., Heijdra, Y., van Scherpenzeel, M., Lefeber, D.J., Morava, E. (2014). Successful liver transplantation and long-term follow-up in a patient with MPI-CDG. *Pediatrics*. 134(1), e279-83.

Caramelo, J.J., Parodi, A.J. (2015). A sweet code for glycoprotein folding. *FEBS Lett.* 589(22), 3379-87.

Jumbo-Lucioni P, Parkinson W, Broadie K. (2014). Overelaborated synaptic architecture and reduced synaptomatrix glycosylation in a *Drosophila* classic galactosemia disease model. *Dis Model Mech*. 7(12), 1365-78.

Kamimura, K., Ueno, K., Nakagawa, J., Hamada, R., Saitoe, M. and Maeda, N. (2013). Perlecan regulates bidirectional Wnt signaling at the Drosophila neuromuscular junction. J. Cell Biol. 200(2), 219-33.

Katz, F., Moats, W., Jan, Y.N. (1988). A carbohydrate epitope expressed uniquely on the cell surface of Drosophila neurons is altered in the mutant nac (neurally altered carbohydrate). *EMBO J*. 7(11), 3471-7.

Kim, M.L., Chandrasekharan, K., Glass, M., Shi, S., Stahl, M.C., Kaspar, B., Stanley, P., Martin, P.T. (2008). O-fucosylation of muscle agrin determines its ability to cluster acetylcholine receptors. *Mol Cell Neurosci.* 39(3), 452-64.

Kim, N.C., Marqués, G. (2010). Identification of downstream targets of the bone morphogenetic protein pathway in the Drosophila nervous system. *Dev Dyn*. 239(9), 2413-25.

Kirschner, J. (2013). Congenital muscular dystrophies. *Handb Clin Neurol.* 113, 1377-85.

Kjaergaard, S., Kristiansson, B., Stibler, H., Freeze, H.H., Schwartz, M., Martinsson, T., Skovby, F. (1998). Failure of short-term mannose therapy of patients with carbohydrate-deficient glycoprotein syndrome type 1A. *Acta Paediatr*. 87(8), 884-8.

Koles, K., Lim, J.M., Aoki, K., Porterfield, M., Tiemeyer, M., Wells, L. and Panin, V. (2007). Identification of N-glycosylated proteins from the central nervous system of Drosophila melanogaster. Glycobiology. 17(12), 1388-403.

Korkut, C., Ataman, B., Ramachandran, P., Ashley, J., Barria, R., Gherbesi, N. and Budnik, V. (2009). Trans-synaptic transmission of vesicular Wnt signals through Evi/Wntless. Cell. 139(2), 393-404.

Lahey, T., Gorczyca, M., Jia, X.X. and Budnik, V. (1994). The Drosophila tumor suppressor gene dlg is required for normal synaptic bouton structure. Neuron. 13(4), 823-35.

Lannoo, N., Van Damme, E.J. (2015). Review/N-glycans: The making of a varied toolbox. *Plant Sci.* 239, 67-83.

Long, A.A., Kim, E., Leung, H.T., Woodruff, E. 3rd, An, L., Doerge, R.W., Pak, W.L. and Broadie, K. (2008). Presynaptic calcium channel localization and calcium-dependent synaptic vesicle exocytosis regulated by the Fuseless protein. J. Neurosci. 28(14), 3668-82.

Lu, Q., Hasty, P., Shur, B.D. (1997). Targeted mutation in beta1,4-galactosyltransferase leads to pituitary insufficiency and neonatal lethality. *Dev Biol*. 181(2), 257-67.

Malicdan, M.C., Noguchi, S., Hayashi, Y.K., Nonaka, I., Nishino, I. (2009). Prophylactic treatment with sialic acid metabolites precludes the development of the myopathic phenotype in the DMRV-hIBM mouse model. *Nat Med.* 15(6), 690-5.

Malicdan, M.C., Noguchi, S., Nonaka, I., Hayashi, Y.K., Nishino, I. (2007). A Gne knockout mouse expressing human GNE D176V mutation develops features similar to distal myopathy with rimmed vacuoles or hereditary inclusion body myopathy. *Hum Mol Genet*. 16(22), 2669-82.

Marek, K.W., Vijay, I.K., Marth, J.D. (1999). A recessive deletion in the GlcNAc-1-phosphotransferase gene results in peri-implantation embryonic lethality. *Glycobiology*. 9(11), 1263-71.

Marquardt, T., Denecke, J. (2003). Congenital disorders of glycosylation: review of their molecular bases, clinical presentations and specific therapies. *Eur J Pediatr.* 162(6), 359-79.

Mayatepek, E., Kohlmüller, D. (1998). Mannose supplementation in carbohydrate-deficient glycoprotein syndrome type I and phosphomannomutase deficiency. *Eur J Pediatr*. 157(7), 605-6.

Martin, P.T. (2003). Glycobiology of the neuromuscular junction. *J Neurocyt*. 32(5-8), 915-29.

McCabe, B.D., Marqués, G., Haghighi, A.P., Fetter, R.D., Crotty, M.L., Haerry, T.E., Goodman, C.S. and O'Connor, M.B. (2003). The BMP homolog Gbb provides a retrograde signal that regulates synaptic growth at the Drosophila neuromuscular junction. Neuron. 39(2), 241-54.

Menon, K.P., Carrillo, R.A., Zinn, K. (2013). Development and plasticity of the Drosophila larval neuromuscular junction. *Wiley Interdiscip Rev Dev Biol*. 2(5), 647-70.

Mosca, T.J., Schwarz, T.L. (2010). The nuclear import of Frizzled2-C by Importins-beta11 and alpha2 promotes postsynaptic development. *Nat Neurosci*. 13(8), 935-43.

Muntoni, F., Torelli, S. and Brockington, M. (2008). Muscular dystrophies due to glycosylation defects. Neurotherapeutics. 5(4), 627-32.

Nahm M, Long AA, Paik SK, Kim S, Bae YC, Broadie K, Lee S. (2010). The Cdc42-selective GAP rich regulates postsynaptic development and retrograde BMP transsynaptic signaling. J. Cell Biol. 191(3), 661-75.

Ondruskova, N., Vesela, K., Hansikova, H., Magner, M., Zeman, J., Honzik,T. (2012). RFT1-CDG in adult siblings with novel mutations. *Mol Genet Metab*. 107(4), 760-2.

Pagon, R.A., **Adam, M.P.**, **Ardinger, H.H.**, **Wallace, S.E.**, **Amemiya, A.**, **Bean, L.J.H.**, **Bird, T.D.**, **Fong, C.T.**, **Mefford, H.C.**, **Smith, R.J.H.**, **Stephens, K., Sparks, S.E.**, **Krasnewich, D.M.** (2014). Congenital Disorders of N-linked Glycosylation Pathway Overview. *GeneReviews Internet.*

Parkinson, W., Dear, M.L., Rushton, E., Broadie, K. (2013). N-glycosylation requirements in neuromuscular synaptogenesis. *Development*. 2013 140(24), 4970-81.

Paschinger, K., Rendić, D. and Wilson, I.B. (2009). Revealing the anti-HRP epitope in Drosophila and Caenorhabditis. Glycoconj. J. 26(3), 385-95.

Patel, T.R., Butler, G., McFarlane, A., Xie, I., Overall, C.M., Stetefeld, J. (2012). Site specific cleavage mediated by MMPs regulates function of agrin. *PLoS One.* 7(9), e43669.

Patton, B.L. (2003). Basal lamina and the organization of neuromuscular synapses. J. Neurocytol. 32(5-8), 883-903.

Pownall, S., Kozak, C.A., Schappert, K., Sarkar, M., Hull, E., Schachter, H. and Marth, J.D. (1992). Molecular cloning and characterization of the mouse UDP-N-acetylglucosamine:alpha-3-D-mannoside beta-1,2-N-acetylglucosaminyltransferase I gene. Genomics. 12(4), 699-704.

Puthalakath, H., Burke, J. and Gleeson, P.A. (1996). Glycosylation defect in Lec1 Chinese hamster ovary mutant is due to a point mutation in N-acetylglucosaminyltransferase I gene. J. Biol. Chem. 271(44), 27818-22.

Rohrbough, J., Rushton, E., Woodruff, E., Fergestad, T., Vigneswaran, K. and Broadie, K. (2007). Presynaptic establishment of the synaptic cleft extracellular matrix is required for post-synaptic differentiation. Genes Dev. 21(20), 2607-28.

Rohrbough, J. and Broadie, K. (2010). Anterograde Jelly belly ligand to Alk receptor signaling at developing synapses is regulated by Mind the gap. Development. 137(20), 3523-33.

Rohrbough, J., Kent, K.S., Broadie, K. and Weiss, J.B. (2013). Jelly Belly trans-synaptic signaling to anaplastic lymphoma kinase regulates neurotransmission strength and synapse architecture. Dev. Neurobiol. 73(3), 189-208.

Rushton, E., Rohrbough, J., Deutsch, K. and Broadie, K. (2012). Structure-function analysis of endogenous lectin mind-the-gap in synaptogenesis. Dev. Neurobiol. 72(8), 1161-79.

Sanes, J.R., Lichtman, J.W. (1999). Development of the vertebrate neuromuscular junction.

Annu Rev Neurosci. 22, 389-442.

Sarkar, M., Iliadi, K.G., Leventis, P.A., Schachter, H., and Boulianne, G.L. (2010). Neuronal expression of Mgat1 rescues the shortened life span of Drosophila Mgat11 null mutants and increases life span. Proc. Natl. Acad. Sci. U S A. 107(21), 9677-82.

Sarkar, M., Leventis, P.A., Silvescu, C.I., Reinhold, V.N., Schachter, H., Boulianne, G.L. (2006). Null mutations in Drosophila N-acetylglucosaminyltransferase I produce defects in locomotion and a reduced life span. *J Biol Chem*. 281(18), 12776-85.

Schachter, H. (2010). Mgat1-dependent N-glycans are essential for the normal development of both vertebrate and invertebrate metazoans. Semin. Cell Dev. Biol. 21(6), 609-15.

Schachter, H. and Boulianne, G. (2011). Life is sweet! A novel role for N-glycans in Drosophila lifespan. Fly (Austin). 5(1), 18-24.

Schneider, A., Thiel, C., Rindermann, J., DeRossi, C., Popovici, D., Hoffmann, G.F., Gröne, H.J., Körner, C. (2011). Successful prenatal mannose treatment for congenital disorder of glycosylation-Ia in mice. *Nat Med*. 18(1), 71-3.

Schuster, C.M., Davis, G.W., Fetter, R.D., Goodman, C.S. (1996). Genetic dissection of structural and functional components of synaptic plasticity. II. Fasciclin II controls presynaptic structural plasticity. *Neuron*. 17(4), 655-67.

Schwarzkopf, M., Knobeloch, K.P., Rohde, E., Hinderlich, S., Wiechens, N., Lucka, L., Horak, I., Reutter, W., Horstkorte, R. (2002). Sialylation is essential for early development in mice. *Proc Natl Acad Sci U S A.* 99(8), 5267-70.

Scott, K., Gadomski, T., Kozicz, T., Morava, E. (2014). Congenital disorders of glycosylation: new defects and still counting. *J Inherit Metab Dis*. 37(4), 609-17

Scott, H., Panin, V.M. (2014a). N-glycosylation in regulation of the nervous system. *Adv Neurobiol*. 9, 367-94.

Scott H, Panin VM. (2014b). The role of protein N-glycosylation in neural transmission. *Glycobiology*. 24(5), 407-17.

Sharma, V., Ichikawa, M., He, P., Scott, D.A., Bravo, Y., Dahl, R., Ng, B.G., Cosford, N.D., Freeze, H.H. (2011). Phosphomannose isomerase inhibitors improve N-glycosylation in selected phosphomannomutase-deficient fibroblasts. *J Biol Chem.* 286(45), 39431-8.

Shi, S., Williams, S.A., Seppo, A., Kurniawan, H., Chen, W., Ye, Z., Marth, J.D. and Stanley, P. (2004). Inactivation of the Mgat1 gene in oocytes impairs oogenesis, but embryos lacking complex and hybrid N-glycans develop and implant. Mol. Cell Biol. 24(22), 9920-9.

Slater, C.R. (2015). The functional organization of motor nerve terminals. *Prog Neurobiol*. 134, 55-103.

Spring, A.M., Brusich, D.J., Frank, C.A. (2016). C-terminal Src Kinase Gates Homeostatic Synaptic Plasticity and Regulates Fasciclin II Expression at the Drosophila Neuromuscular Junction. *PLoS Genet*. 12(2), e1005886.

Sun, M. and Xie, W. (2012). Cell adhesion molecules in Drosophila synapse development and function. Sci. China Life Sci. 55(1), 20-6.

Tanaka, K., Kitagawa, Y. and Kadowaki, T. (2002). Drosophila segment polarity gene product porcupine stimulates the posttranslational N-glycosylation of wingless in the endoplasmic reticulum. J. Biol. Chem. 277(15), 12816-23.

Tegtmeyer, L.C., Rust, S., van Scherpenzeel, M., Ng, B.G., Losfeld, M.E., Timal, S., Raymond, K., He, P., Ichikawa, M., Veltman, J., Huijben, K., Shin, Y.S., Sharma, V., Adamowicz, M., Lammens, M., Reunert, J., Witten, A., Schrapers, E., Matthijs, G., Jaeken, J., Rymen, D., Stojkovic, T., Laforêt, P., Petit, F., Aumaître, O., Czarnowska, E., Piraud, M., Podskarbi, T., Stanley, C.A., Matalon, R., Burda, P., Seyyedi, S., Debus, V., Socha, P., Sykut-Cegielska, J., van Spronsen, F., de Meirleir, L., Vajro, P., DeClue,T., Ficicioglu, C., Wada, Y., Wevers, R.A., Vanderschaeghe, D., Callewaert, N., Fingerhut, R., van Schaftingen, E., Freeze, H.H., Morava, E., Lefeber, D.J., Marquardt,T. (2014). Multiple phenotypes in phosphoglucomutase 1 deficiency. *N Engl J Med*. 370(6), 533-42.

Thiel, C., Körner, C. (2013). Therapies and therapeutic approaches in Congenital Disorders of *Glycosylation*. Glycoconj J. 30(1), 77-84.

Thiel, C., Lübke, T., Matthijs, G., von Figura, K., Körner, C. (2006). Targeted disruption of mouse phosphomannomutase 2 causes early embryonic lethality. *Mol Cell Biol*. 26(15), 5615-20.

Wairkar, Y.P., Fradkin, L.G., Noordermeer, J.N. and DiAntonio, A. (2008) Synaptic defects in a Drosophila model of congenital muscular dystrophy. J. Neurosci. 28(14), 3781-9.

Wang, Q., Groenendyk, J., Michalak, M. (2015). Glycoprotein Quality Control and Endoplasmic Reticulum Stress. *Molecules.* 20(8), 13689-704.

Whitlock, K.E. (1993). Development of Drosophila wing sensory neurons in mutants with missing or modified cell surface molecules. *Development*. 117(4), 1251-60.

Wu, H., Xiong, W.C., Mei, L. (2010). To build a synapse: signaling pathways in neuromuscular junction assembly. *Development.* 137(7), 1017-33.

Xing, G., Gan, G., Chen, D., Sun, M., Yi, J., Lv, H., Han, J., Xie, W. (2014). Drosophila neuroligin3 regulates neuromuscular junction development and synaptic differentiation. *J Biol Chem*. 289(46), 31867-77.

Yan, D., Wu, Y., Feng, Y., Lin, S.C., Lin, X. (2009). The core protein of glypican Dally-like determines its biphasic activity in wingless morphogen signaling. Dev Cell. 17(4), 470-81.

Ye, Z. and Marth, J.D. (2004). N-glycan branching requirement in neuronal and postnatal viability. Glycobiology.14(6), 547-58.

Yoshida, C.A., Kawane, T., Moriishi, T., Purushothaman, A., Miyazaki, T., Komori, H., Mori, M., Qin, X., Hashimoto, A., Sugahara, K., Yamana, K., Takada, K., Komori, T. (2014). Overexpression of Galnt3 in chondrocytes resulted in dwarfism due to the increase of mucin-type O-glycans and reduction of glycosaminoglycans. *J Biol Chem*. 289(38), 26584-96.

Yuste-Checa, P., Gámez, A., Brasil, S., Desviat, L.R., Ugarte, M., Pérez-Cerdá, C., Pérez, B. (2015). The Effects of PMM2-CDG-Causing Mutations on the Folding, Activity, and Stability of the PMM2 Protein. *Hum Mutat*. 36(9), 851-60.

CHAPTER II

N-GLYCOSYLATION REQUIREMENTS IN NEUROMUSCULAR SYNAPTOGENESIS

This paper has been published under the same title in *Development*, 2013

William Parkinson, Mary Lynn Dear, Emma Rushton and Kendal Broadie

Department of Biological Sciences,
Kennedy Center for Research on Human Development,
Vanderbilt University, Nashville, TN 37232 USA

Summary

Neural development requires N-glycosylation regulation of intercellular signaling, but the requirements in synaptogenesis have not been well tested**.** All complex and hybrid N-glycosylation requires Mgat1(UDP-GlcNAc:α-3-D-mannoside-β1,2-N-acetylglucosaminyl transferase I) function, and *mgat1* nulls are the most compromised N-glycosylation condition that survive long enough to permit synaptogenesis studies. At the *Drosophila* neuromuscular junction (NMJ), *mgat1* mutants display selective loss of lectin-defined carbohydrates in the extracellular synaptomatrix, and an accompanying accumulation of the secreted endogenous Mind-the-Gap (MTG) lectin, a key synaptogenesis regulator. Null *mgat1* mutants exhibit strongly overelaborated synaptic structural development, consistent with inhibitory roles for complex/hybrid N-glycans in morphological synaptogenesis, and strengthened functional synapse differentiation, consistent with synaptogenic MTG functions. Synapse molecular composition is surprisingly selectively altered, with decreases in presynaptic active zone Bruchpilot (BRP) and postsynaptic glutamate receptor subtype B (GluRIIB), but no detectable change in a wide range of other synaptic components. Synaptogenesis is driven by bidirectional *trans*-synaptic signals that traverse the glycan-rich synaptomatrix, and *mgat1* mutation disrupts both anterograde and retrograde signals, consistent with MTG regulation of *trans*-synaptic signaling. Downstream of intercellular signaling, pre- and postsynaptic scaffolds are recruited to drive synaptogenesis, and *mgat1* mutants exhibit loss of both classic Discs Large (DLG) and newly-defined Lethal Giant Larvae (LGL) scaffolds. We conclude that Mgat1-dependent N-glycosylation shapes the synaptomatrix carbohydrate environment and endogenous lectin localization within this domain, to modulate retention of *trans*-synaptic signaling ligands driving synaptic scaffold recruitment during synaptogenesis.

Introduction

N-glycosylation is the most common posttranslational modification, involving linkage of diverse carbohydrate trees onto asparagine, targeting primarily cell surface and secreted proteins. Mutation of >20 human N-glycosylation genes result in heritable congenital disorders of glycosylation (CDGs), many of which impair nervous system development (Freeze, 2006; Hennet, 2012; Hewitt, 2009). The *mgat1* gene encoded GlcNAcT1 adds GlcNAc to high-mannose sites (Schachter, 2010); an essential early step in producing all complex and hybrid N-glycans (Pownall et al., 1992; Ye and Marth, 2004). Thus, Mgat1 generates the entire repertoire of polymeric branched N-glycans destined for secretion or presentation on the cell surface (Puthalakath et al., 1996); and *mgat1* null mutants, containing high mannose in place of complex/hybrid N-glycans, are the earliest N-glycan pathway block available to study N-glycosylation requirements in neural development (Schachter and Boulianne, 2011). Mouse *mgat1* knockouts are lethal at E9.5, but conditional mutants show movement defects, tremors, paralysis and early death characteristic of neurodevelopmental impairments (Campbell et al., 1995; Grasa et al., 2012; Shi et al., 2004; Ye and Marth, 2004). *Drosophila mgat1* is functionally conserved, and null mutants show the same range of crippling neurological defects, but have the enormous benefit for analysis of being viable.

Drosophila mgat1 null mutants exhibit severely impaired coordinated movement, and the few adults that eclose usually survive only a few days (Sarkar et al., 2006). Importantly, lifespan shortening is due entirely to neuron-specific requirements, and *mgat1* neuronal overexpression increases lifespan (Sarkar et al., 2010; Schachter and Boulianne, 2011). In the central brain Mushroom Body learning/memory center, *mgat1* nulls show fused lobes similar to *fused lobe* (*fdl*) mutants in β-N-acetylglucosaminidase, which removes the Mgat1-added GlcNAc (Leonard et al., 2006; Sakar et al., 2006). Mgat1 is also required for α3 fucose addition, a neuron-specific modification routinely labeled with anti-horse radish peroxidase (HRP) (Desai et al., 1994; Paschinger et al., 2009). Overexpression of the fucose transferase generating HRP glycans increases peripheral sensory neuron clustering, ventral nerve cord growth and glial migration (Rendic et al., 2010). Mgat1-dependent N-glycosylation occurs on many neural

proteins including neurotransmitter receptors, SNAREs, Fasciclins, Neuroglians, Neurexins and Dystroglycans (Koles et al., 2007; Muntoni et al., 2008; Sun and Xie, 2012).

The heavily-glycosylated synaptomatrix is composed of secreted and membrane molecules residing at the interface between presynaptic active zones and postsynaptic receptors. *Drosophila* genetic analyses show synaptomatrix glycan modification/binding has core roles in structural and functional development of the neuromuscular junction (NMJ) synapse (Broadie et al., 2011; Dani and Broadie, 2012). Glycan-dependent synaptogenic events include presynaptic active zone (AZ) differentiation, postsynaptic glutamate receptor (GluR) localization and ECM organization within the synaptic cleft, driven by the secreted endogenous Mind-the-Gap (MTG) lectin, for example (Dani et al., 2012; Long et al., 2008; Rushton et al., 2012). Synaptogenic events are regulated by bidirectional *trans*-synaptic signals that traverse the synaptomatrix, and glycosylation of both ligands and receptors alters localization and binding (Henriquez and Salinas, 2012; Patton, 2003). Three well-characterized *trans*-synaptic signals at the *Drosophila* NMJ are Wnt Wingless (Wg), BMP Glass Bottom Boat (Gbb), and Jelly Belly (Jeb) (Grosso et al., 2011; Kamimura et al., 2013; Rohrbough and Broadie, 2010; Tanaka et al., 2002).

The goal here is to test N-glycosylation requirements during NMJ synaptogenesis using *mgat1* mutants. We found large alterations in synaptomatrix glycan composition, including complete lack of paucimannose glycans, fucosylated HRP epitopes and *Vicia villosa* (VVA) lectin reactivity, coupled to strongly elevated MTG expression. Null *mgat1* mutants display increased NMJ growth (increased synapse area, branching and bouton number) and function (increased transmission and FM1-43 dye cycling), showing that Mgat1-dependent N-glycosylation plays inhibitory roles in synaptogenesis. Consistent with the hypothesis that a modified synaptomatrix would alter *trans*-synaptic signaling, Wg, Gbb and Jeb signaling ligands are all disrupted in the absence of *mgat1* function, together with loss in synaptic recruitment of Discs Large (DLG) and Lethal Giant Larvae (LGL) membrane scaffolds that modulate NMJ synaptogenesis (Humbert et al., 2008; Staples and Broadie, 2013; Wang et al., 2011). Together, these results show requirements for Mgat1-dependent N-glycosylation in *trans*-synaptic signaling and synaptic localization of intracellular scaffolds driving neuromuscular synaptogenesis.

Materials and Methods

Drosophila Genetics

All genotypes were made in the w^{1118} background, with w^{1118} used as genetic control. Df(2R)BSC430 removing *mgat1* was obtained from the Bloomington *Drosophila* Stock Center (Indiana University). Imprecise excision $mgat1^{1}$ and precise excision $mgat1^{+9}$ lines have been characterized (Sarkar et al., 2006). Transgenic studies were done with the pan-neural *elav*-Gal4, muscle 24B-Gal4 and ubiquitous UH1-Gal4 driver lines (Brand and Perrimon, 1993; Lin and Goodman, 1994; Rohrbough et al., 2007) crossed to UAS-*mgat1* (Sarkar et al., 2010) or UAS-RNAi-*mgat1* lines obtained from the Vienna *Drosophila* RNAi Center (VDRC). The Mind-the-Gap (MTG) cDNA fused to GFP coding sequence (UAS-MTG:GFP; Rushton et al., 2009) was placed into *w*; $mgat1^{1}$/Cyo-GFP to express MTG:GFP in the null background.

Immunocytochemistry

Studies were done as described previously (Rushton et al., 2012; Dani et. al., 2012). Briefly; wandering third instars were dissected in physiological saline consisting of 128mM NaCl, 2mM KCl, 4mM $MgCl_2$, 0.2mM $CaCl_2$, 70mM sucrose, 5mM trehalose and 5mM HEPES (pH 7.1). Preparations were fixed in ice-cold methanol for 5 mins (GluRIIA) or 4% paraformaldehyde for 10 mins at room temperature (RT; all other labels). Preparations were then either processed with detergent (PBS + 1% BSA + 0.2% Triton X-100) for cell-permeabilized studies, or detergent-free (PBS with 1% BSA) conditions for non-permeabilized studies. Primary antibodies used included: rabbit anti-horse radish peroxidase (HRP, 1:200, Sigma); mouse anti-Fasciclin 2 (Fas2, 1:10, Developmental Studies Hybridoma Bank (DSHB), University of Iowa); rabbit anti-Dystroglycan (Dg, 1:1000); mouse anti-glutamate receptor IIA (GluRIIA, 1:100 DSHB), rabbit anti-GluRIIB (GluRIIB, 1:1000; Marrus et al., 2004), and rabbit anti-GluRIIC (GluRIIC, 1:500; Marrus et al., 2004); mouse anti-Bruchpilot (BRP, 1:100, DSHB); rabbit anti-vesicular glutamate transporter (vGlut, 1:10,000; Daniels et al., 2004); rabbit anti-Synaptobrevin (Syb, 1:500; Littleton et al., 1993); mouse anti-Cysteine String Protein (CSP, 1:250; Zinsmaier et al., 1990); rabbit anti-Synaptogyrin (GYR, 1:500; Stevens et al., 2012); mouse anti-Wingless (Wg, 1:2;

DSHB); rabbit anti-Glass Bottom Boat (Gbb, 1:100; Dani et al., 2012), guinea pig anti-Jelly Belly (Jeb, 1:2000; Lee et al., 2003); mouse anti-Discs Large (DLG, 1:200; DSHB); rabbit anti-Lethal Giant Larvae (LGL, 1:300; Ohshiro et al., 2000). Lectins used included: *Vicia villosa* agglutinin (VVA-Tritc, 1:200, E.Y. Laboratories); and wheat germ agglutinin (WGA, 1:200), peanut agglutinin (PNA, 1:250), soybean agglutinin (SBA, 1:200), *Erythrina cristagalli* lectin (ECL, 1:250) and *Wisteria floribunda* lectin (WFA, 1:250), all from Vector Labs. Secondary Alexa fluorophore antibodies (Invitrogen) used included: goat anti-mouse 488 and 568 (1:250), goat anti-rabbit 488/568 (1:250), goat anti-guinea pig 488/568 (1:250) and streptavidin 488 (1:250). Primary antibodies and lectins were incubated at 4°C overnight; secondary antibodies were incubated at RT for 2 hrs. Dissections were mounted in Fluoromount-G (Electron Microscopy Sciences). Z-stacks were taken with a Zeiss LSM 510 META laser-scanning confocal using 40x or 63x Plan Apo oil immersion objectives. Optical sections were done starting immediately above and ending immediately below the NMJ. Stacks were projected on the Z-axis, with NMJ signals highlighted and average intensity for each recorded. Intensities were quantified using ImageJ (Abramoff et al., 2004).

Western Blotting

Dissected wandering third instar ventral nerve cords (6) were homogenized in buffer (67mM NaCl, 2M Urea, 1.3% SDS, 1mM EDTA, Tris (pH 8)) and centrifuged for 30 mins at 16,000xg. Soluble fractions with 1X NuPage sample buffer (Invitrogen, Carlsbad, CA) and 5% 2-mercaptoethanol were boiled for 10 mins. Samples were loaded onto 4-12% Bis-Tris SDS gels (Invitrogen), electrophoresed at 200V for 90 mins in 1X MES buffer and transferred to nitrocellulose membranes (Biorad) in 1X NuPage transfer buffer with 300mA for 1 hr at 4^{o}C. Membranes were blocked in 2% BSA (Sigma) in TBS-T (10mM Tris pH 8, 150mM NaCl, 0.05% Tween-20) for 1 hr at RT. Rabbit anti-HRP (Sigma) [1:1000] or biotinylated VVA (EY labs) [1:1000] were diluted in blocking buffer and incubated for one hour at RT and washed for 5 mins in TBS-T (x6). Mouse anti-tubulin (Sigma) [1:5000], rabbit anti-Dg [1:1000] or mouse anti-Fas2 (34B3C2) [1:100] were diluted in blocking buffer and incubated overnight at 4^{o}C. Preparations were washed for 5 mins with TBS-T (x6), and streptavidin-800 (Rockland)

[1:10000], goat anti-mouse 680 (Invitrogen) [1:10000] or goat anti-rabbit 800 (Rockland) [1:10000] were incubated for 1 hr at RT. Blots were washed for 5 mins in TBS-T (x6) and then imaged using an Odyssey Infrared Imaging System.

Electrophysiology

Two-electrode voltage-clamp (TEVC) electrophysiology was performed as previously reported (Rohrbough and Broadie, 2002). Briefly; staged larvae were glued with 3M Vetbond tissue adhesive (World Precision Instruments) to sylgard-coated glass coverslips, cut longitudinally along the dorsal midline, internal organs removed and sides glued down for neuromusculature access. Peripheral nerves were cut near the ventral nerve cord (VNC). Dissections and recordings were performed at 18°C in saline consisting of 128mM NaCl, 2mM KCl, 4mM $MgCl_2$, 1mM $CaCl_2$, 70mM sucrose, 5mM trehalose and 5mM HEPES (pH 7.1). Preparations were imaged using a Zeiss Axioskop microscope with 40X water immersion objective. A fire-polished glass suction electrode was used for evoked nerve stimulation with a 0.5 ms supratheshold stimulus at 0.2 Hz from a Grass S88 stimulator (Rohrbough et al., 2010). Muscle 6 in abdominal segments 2/3 was impaled with two microelectrodes of ~15 MΩ resistance filled with 3M KCl. The muscle was clamped at -60 mV using an Axoclamp-2B amplifier. Excitatory junctional current (EJC) records were filtered at 2 kHz. To quantify EJC amplitudes, 10 consecutive traces were averaged and the peak of the averaged trace recorded. Clampex software was used for all data acquisition, Clampfit software was used for all data analysis, and GraphPad InStat 3 software was used for statistical tests.

FM1-43 Dye Imaging

Synaptic vesicle cycling was imaged using lipophilic dye FM1-43, as previously reported (Long et al., 2010; Nahm et al., 2013). Briefly, for endogenous labeling, dissected preparations were incubated in physiological saline (1.0mM Ca^{2+}) plus 10□M FM1-43 (Invitrogen). To stop loading at staged intervals, the saline was replaced several times in quick succession with Ca^{2+}-free saline lacking FM1-43. For evoked depolarization dye loading, preparations were stimulated with 90mM K^+ plus 10□M FM1-43 for 5 mins. After imaging, preparations were unloaded with

the same depolarizing stimulation without FM1-43 for 2 mins. Z-stacks were taken with a Zeiss LSM 510 META laser-scanning confocal using a 63x water immersion objective. Fifteen slices were acquired and stacks projected in ImageJ. To quantify loaded/unloaded fluorescent intensities, five individual boutons per NMJ were outlined and average intensity measured in ImageJ, with muscle background intensities subtracted.

Statistics

All statistics were performed using GraphPad InStat3 software. ANOVA tests were used for all data sets of $\geq$3 comparisons. Student's t-test was used for pairwise comparisons. Significance is presented as $p \leq 0.05$ (*), $p \leq 0.01$ (**) and $p \leq 0.001$ (***) in figures.

Results

Mgat1 shapes the glycosylated synaptomatrix of the neuromuscular junction

Lectins have been used to define the specialized carbohydrate environment of pre/postsynaptic membranes and perisynaptic extracellular space (Broadie et al., 2011; Dani and Broadie, 2012). For example, the widely employed anti-HRP antibody binds fucosylated N-glycans in the presynaptic membrane, which require *mgat1* for fucose modification (Sarkar et al., 2006). Likewise, *Vicia villosa* (VVA) lectin is a synaptic glycan marker at the *Drosophila* NMJ, which reportedly recognizes primarily postsynaptic Dystroglycan (Haines et al., 2007; Rushton et al., 2012). The endogenous Mind-the-Gap (MTG) lectin patterns the extracellular glycosylated synaptomatrix (Rohrbough et al., 2007), modulates *trans*-synaptic signaling and is essential for functional synaptogenesis (Rushton et al., 2009, Rohrbough and Broadie, 2010). To begin to define synaptogenic roles of Mgat1, we labeled the NMJ with each of these lectins in genetic control, *mgat1* null mutants and *mgat1* rescue conditions (Fig. 4).

Wandering third instar NMJs were first probed with anti-HRP (green) compared to anti-Fasciclin 2 (Fas2, red) in two *mgat1* null conditions ($mgat1^1/mgat1^1$ and $mgat1^1$/Df(2R)BSC430) compared to w^{1118} genetic control (Fig. 4A). The HRP epitope robustly revealed the presynaptic terminal in control, but was undetectable in mutants. Phenotype rescue was assessed with ubiquitous UH1-Gal4 driven UAS-*mgat1* in the *mgat1* null background, showing complete

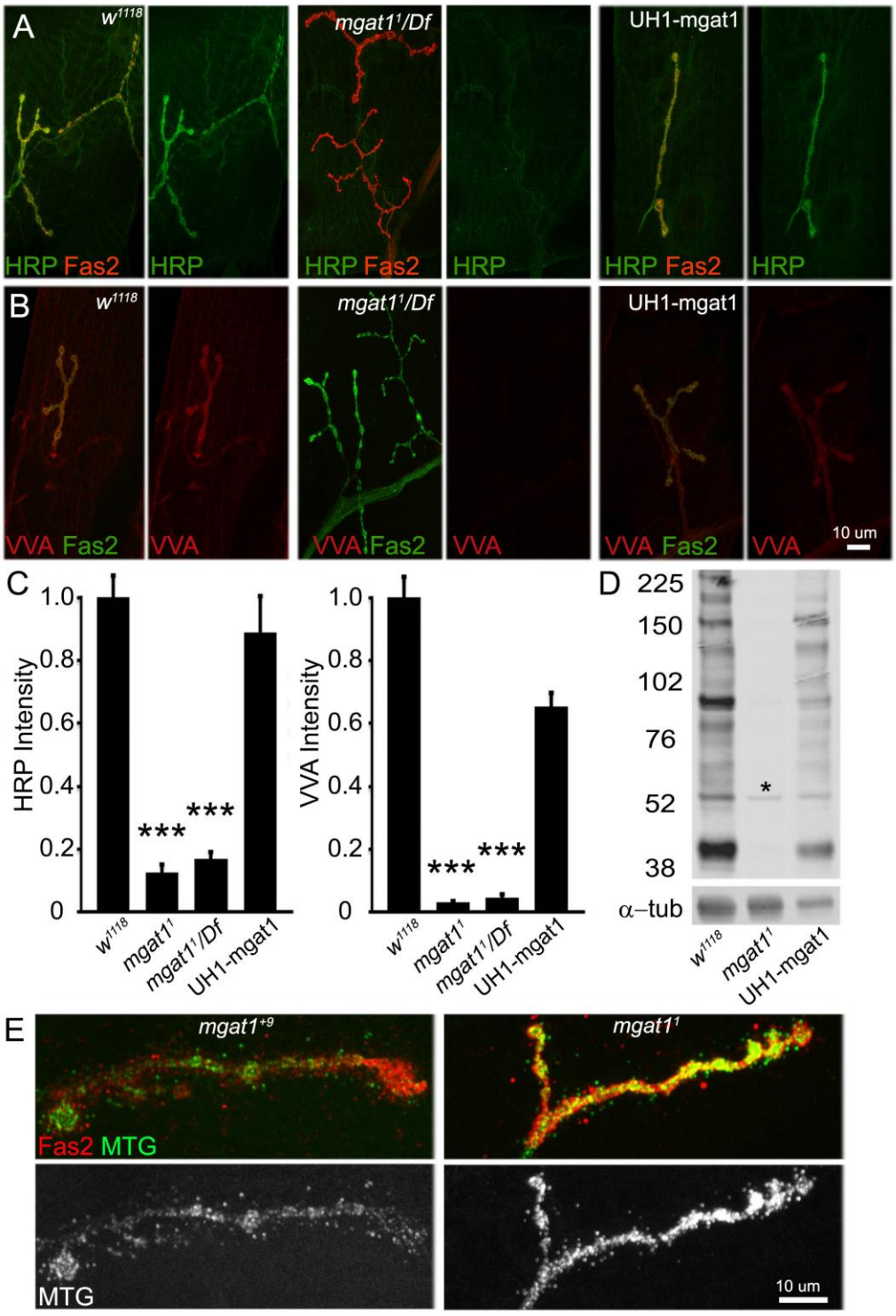
A
w1118
HRP Fas2
HRP
mgat11/Df
HRP Fas2
HRP
UH1-mgat1
HRP Fas2
HRP
B
w1118
VVA Fas2
VVA
mgat11/Df
VVA Fas2
VVA
UH1-mgat1
VVA Fas2
VVA
10 um
C
HRP Intensity
1.0
0.8
0.6
0.4
0.2
0
***
***
w1118
mgat11
mgat11/Df
UH1-mgat1
VVA Intensity
1.0
0.8
0.6
0.4
0.2
0
***
***
w1118
mgat11
mgat11/Df
UH1-mgat1
D
225
150
102
76
52
38
α–tub
*
w1118
mgat11
UH1-mgat1
E
mgat1+9
Fas2 MTG
mgat11
MTG
10 um

Figure 4

Figure 4: Loss of *mgat1* activity dramatically alters the NMJ synaptomatrix.

(A) Representative images of wandering third instar NMJs probed with anti-horse radish peroxidase (HRP, green) and anti-Fasciclin 2 (Fas2, red) in genetic control w^{1118}, $mgat1^{1}$/Df(2R)BSC430 and UH1-GAL4 driven UAS-*mgat1* in $mgat1^{1}$ null background. HRP labeling is undetectable in the *mgat1* null, and fully restored by the genetic rescue. **(B)** Representative NMJ images of *Vicia villosa* (VVA, red) lectin labeling with Fas2 co-labeling (green) in the same genotypes. VVA labeling is undetectable in *mgat1* nulls, and fully restored by genetic rescue. **(C)** Quantification of HRP and VVA intensity normalized to w^{1118}. Statistical analyses with ANOVA shown as $p \leq 0.001$ (***). Sample size is $\geq$10 NMJs from $\geq$5 animals of each genotype. **(D)** Representative anti-HRP Western blot from w^{1118}, *mgat1* null and UH1-*mgat1* rescue conditions. All HRP glycans are undetectable in *mgat1* null, and restored by *mgat1* rescue. The single band (*) represents bleed-through from α-tubulin loading control. **(E)** Representative NMJ images of Mind-the-Gap (MTG-GFP, green) lectin co-labeled with anti-Fas2 (red), and shown alone (MTG, white), in control ($mgat1^{+9}$ precise excision) and *mgat1* null. MTG is greatly increased in mutants ($p \leq 0.0009$; sample size: $\geq$8 NMJs, $\geq$4 animals/genotype).

recovery of the HRP signal (Fig. 4A, right). Quantification of mutants normalized to the control shows significant loss of HRP signal (w^{1118}: 1.0±0.06; $mgat1^{1}$: 0.12±0.02, p<0.001; $mgat1^{1}$/Df: 0.16±0.03. p<0.001; Fig. 4C). Anti-HRP recognizes at least 18 protein bands in Western blots (Fig. 4D; Desai et al., 1994). All these N-glycans are lost in *mgat1* nulls and restored by UH1-Gal4 driven UAS-*mgat1* (Fig. 4D). The VVA lectin signal is similarly lost in *mgat1* mutants and rescued with UH1-Gal4 driven UAS-*mgat1* (w^{1118}: 1.0±0.06; $mgat1^{1}$: 0.02±0.004, p<0.001; $mgat1^{1}$/Df: 0.04±0.01, p<0.001; Fig. 4A,C). In contrast, the endogenous MTG lectin is highly elevated at *mgat1* null NMJs, as revealed by transgenic GFP-tagged MTG (Fig. 4E). Quantification of MTG-GFP within Fas2-labeled synaptic domains shows a ~70% increase in nulls compared to controls ($mgat1^{+9}$ precise excision: 88.53±10.55; $mgat1^{1}$ null: 149.46±9.52; p<0.001). Together, these changes predict strong effects on NMJ synaptogenesis.

Fas2 is the best-characterized HRP-epitope protein, with critical roles in the development of the *Drosophila* NMJ (Desai, et al., 1994; Beumer et al., 2002). Similarly, Dystroglycan (Dg) is reportedly the primary substrate for VVA labeling at the NMJ (Haines et al., 2007; Nakamura et al., 2010). Both HRP and VVA labeling are absent at *mgat1* null NMJs (Fig. 4), allowing analyses of the effects of loss of glycosylation on Fas2 and Dg expression and synaptic localization (Fig. 5). Specific antibodies against Fas2 and Dg show no detectable differences in protein abundance and localization at the NMJ in *mgat1* nulls compared to controls (Fig. 5A). Western blot analyses likewise show no detectable changes in Fas2 or Dg protein stability or expression (Fig. 5B). Quantification of NMJ fluorescent intensities did not show significant changes in *mgat1* nulls compared to controls for Fas2 (normalized w^{1118}: 1.0±0.04; $mgat1^{1}$: 1.03±0.05, $mgat1^{1}$/Df: 0.86±0.08; not significant (n.s.); Fig. 5C) or Dg (w^{1118}: 1.0±0.02; $mgat1^{1}$: 1.06±0.01, $mgat1^{1}$/Df: 1.04±0.04; Fig. 5C). Numerous other lectins used as probes, including WGA, PNA, SBA, ECL and WFA (see Methods), did not show detectable changes in *mgat1* nulls compared to w^{1118} controls. Quantification of fluorescent intensities revealed no significant differences (data not shown). Together, these results show specific lectin changes at *mgat1* null NMJs, with loss of HRP and VVA labeling but not other lectin labels, but no changes in the abundance or synaptic localization of prominent HRP- (Fas2) and VVA-(Dg) labeled proteins.

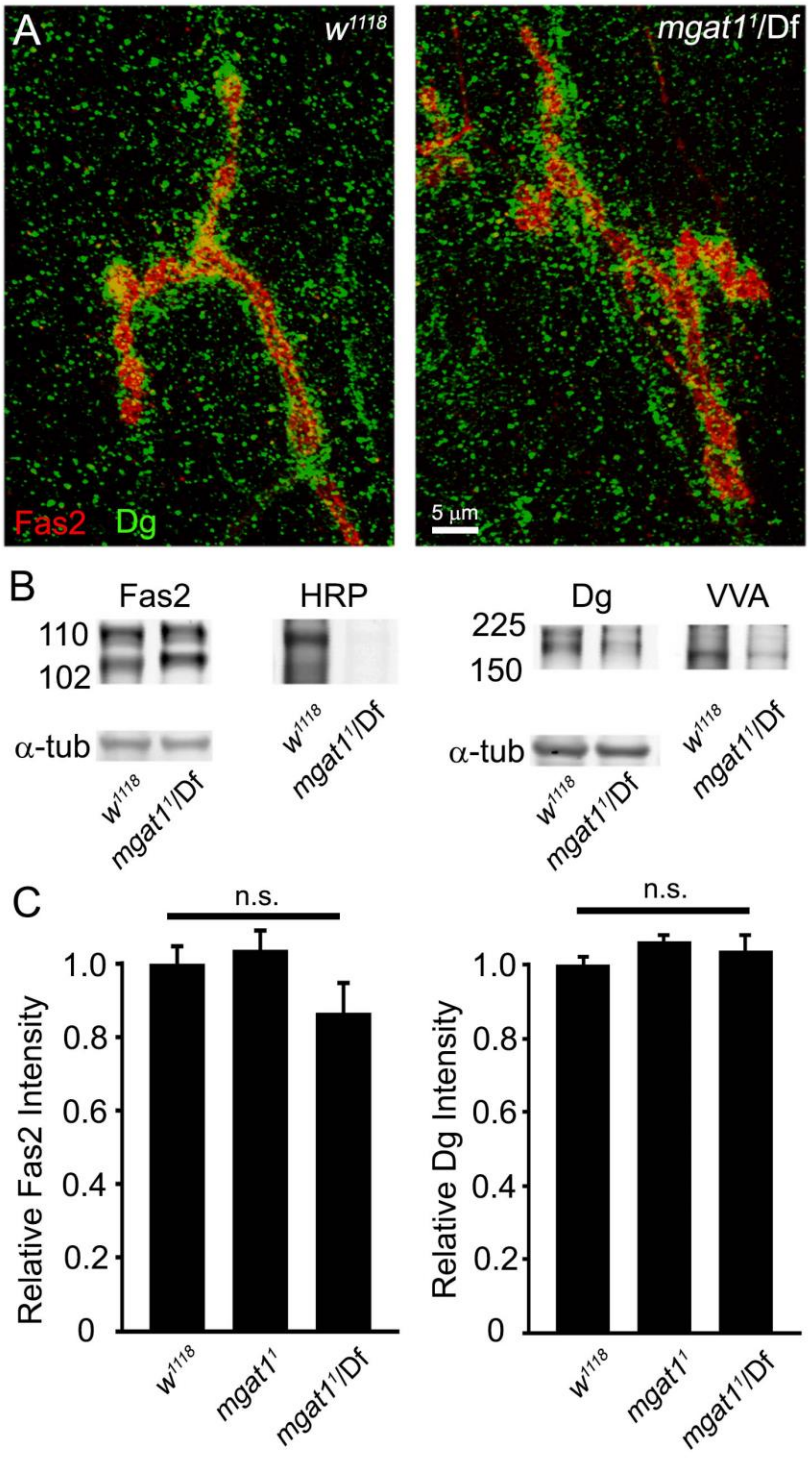
A
w1118
mgat11/Df
Fas2
Dg
5 µm
B
Fas2
HRP
Dg
VVA
110
102
225
150
α-tub
α-tub
w1118
mgat11/Df
C
n.s.
n.s.
Relative Fas2 Intensity
Relative Dg Intensity
1.0
0.8
0.6
0.4
0.2
0
mgat11

Figure 5

Figure 5: Fasciclin 2 and Dystroglycan are normally expressed in *mgat1* nulls.

(A) Representative NMJ images of anti-Fasciclin 2 (Fas2, red) double-labeled with anti-Dystroglycan (Dg, green) in w^{1118} control and $mgat1^{1}$/Df mutant. **(B)** Representative Western blots double-labeled for Fas2 and HRP (left) and Dg and VVA lectin (right) in w^{1118} and $mgat1^{1}$/Df. Alpha tubulin is the loading control. **(C)** Confocal fluorescent intensity quantification shows no significant (n.s.) change in Fas2 or Dg at the NMJ in either homozygous $mgat1^{1}$ or $mgat1^{1}$/Df conditions compared to w^{1118}. ANOVA statistical analyses were done on a sample size of $n \geq 16$ NMJs for each genotype.

Development of NMJ structural overgrowth in the *mgat1* null condition

Our recent genomic survey of glycosylation genes suggested glycan mechanisms largely function to restrict morphological growth during *Drosophila* NMJ synaptogenesis (Dani et al., 2012). Synaptic architecture is determined by axonal growth properties, branch formation and the differentiation of synaptic boutons as sites of synaptic vesicle storage for neurotransmitter release (Broadie et al., 2011; Nahm et al., 2013). To assay these structural parameters in *mgat1* mutants, wandering third instar 6/7 NMJs were labeled with anti-Fas2 and measurements made of NMJ length, branch number (process with $\geq$2 boutons) and bouton number ($\geq$1μm in diameter) in six genotypes; w^{1118} background control, $mgat1^{+9}$ precise excision control, $mgat1^{1}$ homozygous and $mgat1^{1}$/Df null mutants, and muscle 24B-Gal4 and ubiquitous UH1-Gal4 driven UAS-*mgat1* rescue conditions. Neuronally-driven UAS-*mgat1* resulted in early developmental lethality, and is therefore not included. A summary of these data is shown in Figure 6.

Null *mgat1* mutants show a clear increase in NMJ size and structural complexity (Fig. 6A). Quantification of type 1 bouton number shows a highly significant increase in mutants normalized to control, rescued with ubiquitous but not muscle-targeted *mgat1,* suggesting a neuronal requirement (w^{1118}: 1.0±0.03; $mgat1^{+9}$: 1.02±0.08; $mgat1^{1}$: 1.50±0.06, p<0.001; $mgat1^{1}$/Df: 1.58±0.05 p<0.001; 24B-Gal4 driven UAS-*mgat1*: 1.49±0.06; UH1-Gal4 driven UAS-*mgat1*: 0.97±0.08; Fig. 6B, left). Similarly, quantification of synaptic branch number shows a highly significant increase in *mgat1* nulls, rescued only with ubiquitous *mgat1* (w^{1118}: 1.0±0.03; $mgat1^{+9}$: 0.92±0.08; $mgat1^{1}$: 1.36±0.06, p<0.001; m$gat1^{1}$/Df: 1.26±0.03, p<0.001; UH1-Gal4 driven UAS-*mgat1*: 0.89±0.06; Fig. 6B, middle). Finally, synaptic growth, quantified as normalized NMJ length, shows a highly significant increase in *mgat1* mutants, rescue only with ubiquitous *mgat1* (w^{1118}: 1.0±0.03; $mgat1^{+9}$: 1.14±0.09; $mgat1^{1}$: 1.81±0.08, p<0.001; $mgat1^{1}$/Df: 1.53±0.05 p<0.001; 24B-Gal4 driven UAS-*mgat1*: 1.73±0.11 p<0.001; UH1-Gal4 driven UAS-*mgat1*: 0.98±0.05; Fig. 6B, right). Muscle 24B-Gal4 expression of UAS-*mgat1* did not rescue any structural parameters, suggesting that ubiquitous or at least neuronal *mgat1* function is required to restore NMJ developmental growth and normal structural synaptogenesis.

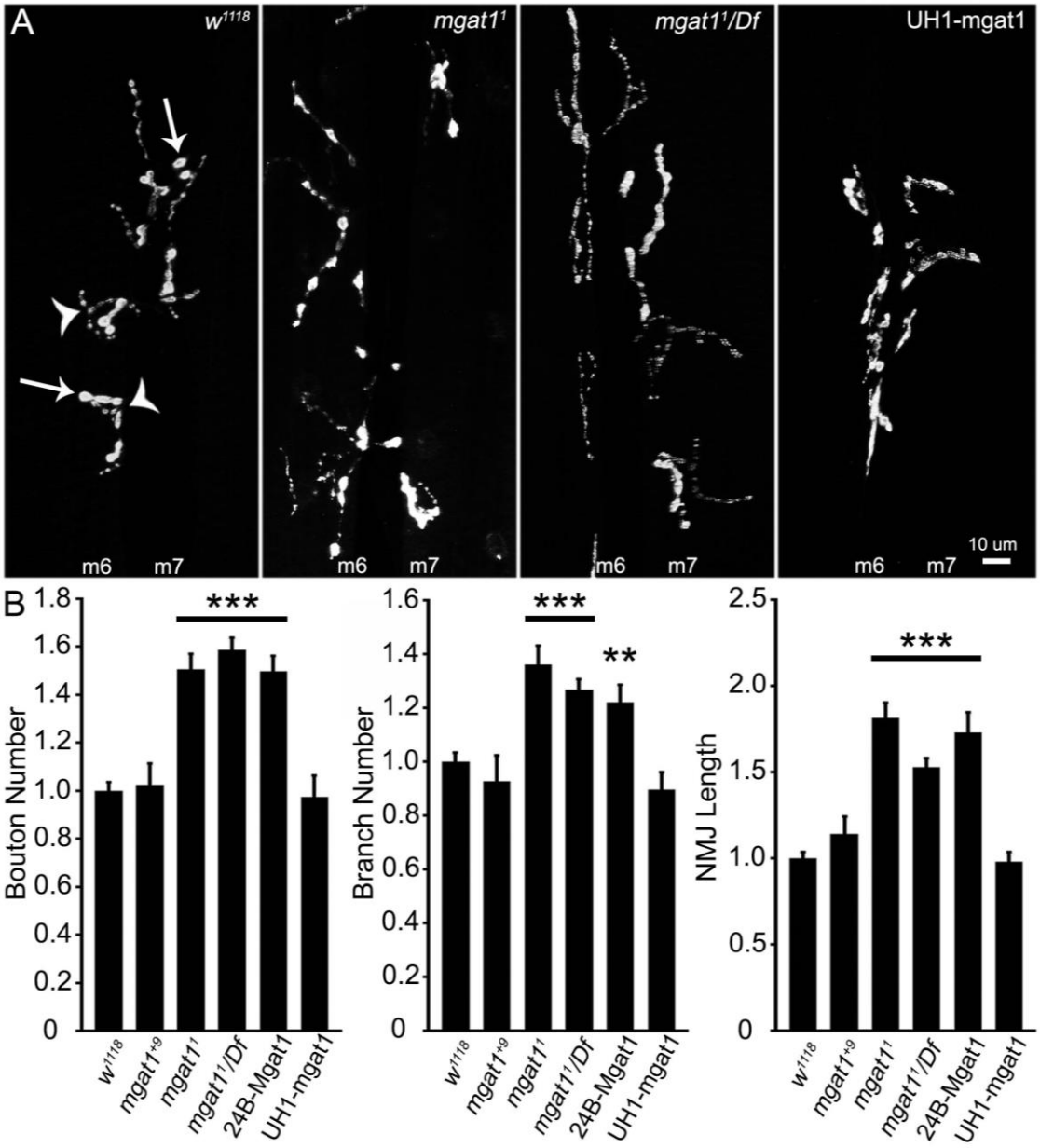
A
w1118
mgat11
mgat11/Df
UH1-mgat1
m6
m7
10 um
B
Bouton Number
Branch Number
NMJ Length
***
**
w1118
mgat1+9
mgat11
mgat11/Df
24B-Mgat1
UH1-mgat1

Figure 6

Figure 6: *Drosophila* NMJ is structurally overgrown in *mgat1* null mutants.

NMJ length, axon branching and synaptic bouton number are increased in *mgat1* nulls. **(A)** Representative images of wandering third instar 6/7 NMJ in genetic control (w^{1118}), $mgat1^{1}$ null, $mgat1^{1}$/Df(2)BSC430 and UH1-Gal4 driven UAS-*mgat1* in null background. Representative axon branch points (arrowheads) and boutons (arrows) are illustrated. **(B)** Quantification of bouton number, branch number and NMJ length normalized to w^{1118} for the $mgat1^{+9}$ precise excision control, $mgat1^{1}$ homozygous null, $mgat1^{1}$/Df and UAS-*mgat1* driven in muscle (24B-Gal4) or ubiquitously (UH1-Gal4) in the $mgat1^{1}$/Df background. All three structural parameters are increased in *mgat1* nulls and fully rescued by ubiquitous UAS-*mgat1* expression, but not muscle-targeted expression. Statistical analysis using ANOVA shown as $p \leq 0.01$ (**) and $p \leq 0.001$ (***) compared to w^{1118}. Sample size is $\geq$8 NMJ's from $\geq$4 animals from each of the 6 genotypes shown.

Pre- and postsynaptic *mgat1* roles restrict synaptic functional differentiation

Regulation of *Drosophila* NMJ structural and functional synaptogenesis is often genetically separable, but N-glycans are causally implicated in both developmental processes (Broadie et al., 2011; Dani et al., 2012). However, there has been no studies to assess overall N-glycan contributions to functional synaptic differentiation. We therefore next tested functional properties of *mgat1* null NMJs by measuring synaptic currents using two-electrode voltage-clamp (TEVC) recording. The motor nerve was stimulated with a glass suction electrode at suprathreshold levels to recruit both motor neuron inputs on muscle 6, and the excitatory junction current (EJC) recorded at 0.5 Hz to measure neurotransmission strength. In total, 12 genotypes were assayed: in addition to those described above, including *mgat1* nulls lacking maternal contribution; ubiquitous, neuron-targeted and muscle-targeted *mgat1* RNAi; and appropriate controls for transgenic conditions. A summary of these data is shown in Figure 7.

NMJ functional strength was clearly and consistently increased in all *mgat1* loss-of-function conditions (Fig. 7A). Null zygotic mutants were comparable to animals lacking both maternal and zygotic expression, showing that a maternal contribution does not mask additional requirements. Mean EJC amplitudes were very significantly elevated in *mgat1* mutants normalized to genetic control (w^{1118}: 1.0±0.02; $mgat1^{1}$: 1.45±0.10, p<0.001; $mgat1^{1}$ without maternal contribution: 1.38±0.06, p<0.001; $mgat1^{1}$/Df: 1.40±0.05, p<0.001; Fig. 7AB). Ubiquitous RNAi *mgat1* knockdown with UH1-Gal4 replicated this phenotype, and the elevated transmission was rescued by ubiquitous expression of UAS-*mgat1* in $mgat1^{1}$/Df (w^{1118}: 1.0±0.02; UH1-Gal4/+ control: 0.99±0.04; UH1-Gal4 UAS-RNAi-*mgat1*: 1.39±0.06, p<0.001; UH1-Gal4 UAS-*mgat1*: 1.07±0.05; Fig. 7C,D). Moreover, postsynaptic *mgat1* RNAi knockdown also increased EJC amplitude, albeit more moderately, and was rescued with postsynaptic 24B-Gal4 UAS-*mgat1* in $mgat1^{1}$/Df (w^{1118}: 1.0±0.02; 24B-Gal4/+ control: 1.04±0.05; 24B-Gal4 UAS-RNAi-*mgat1*: 1.29±0.06, p<0.01; Fig. 7E,D). Finally, presynaptic *mgat1* RNAi also elevated transmission strength (w^{1118}: 1.0±0.02; *elav*-Gal4/+ control: 0.96±0.05; *elav*-Gal4, UAS-RNAi-*mgat1*: 1.51±0.11, p<0.001; Fig. 7G,H). These results reveal separable pre- and postsynaptic *mgat1* roles limiting NMJ functional differentiation.

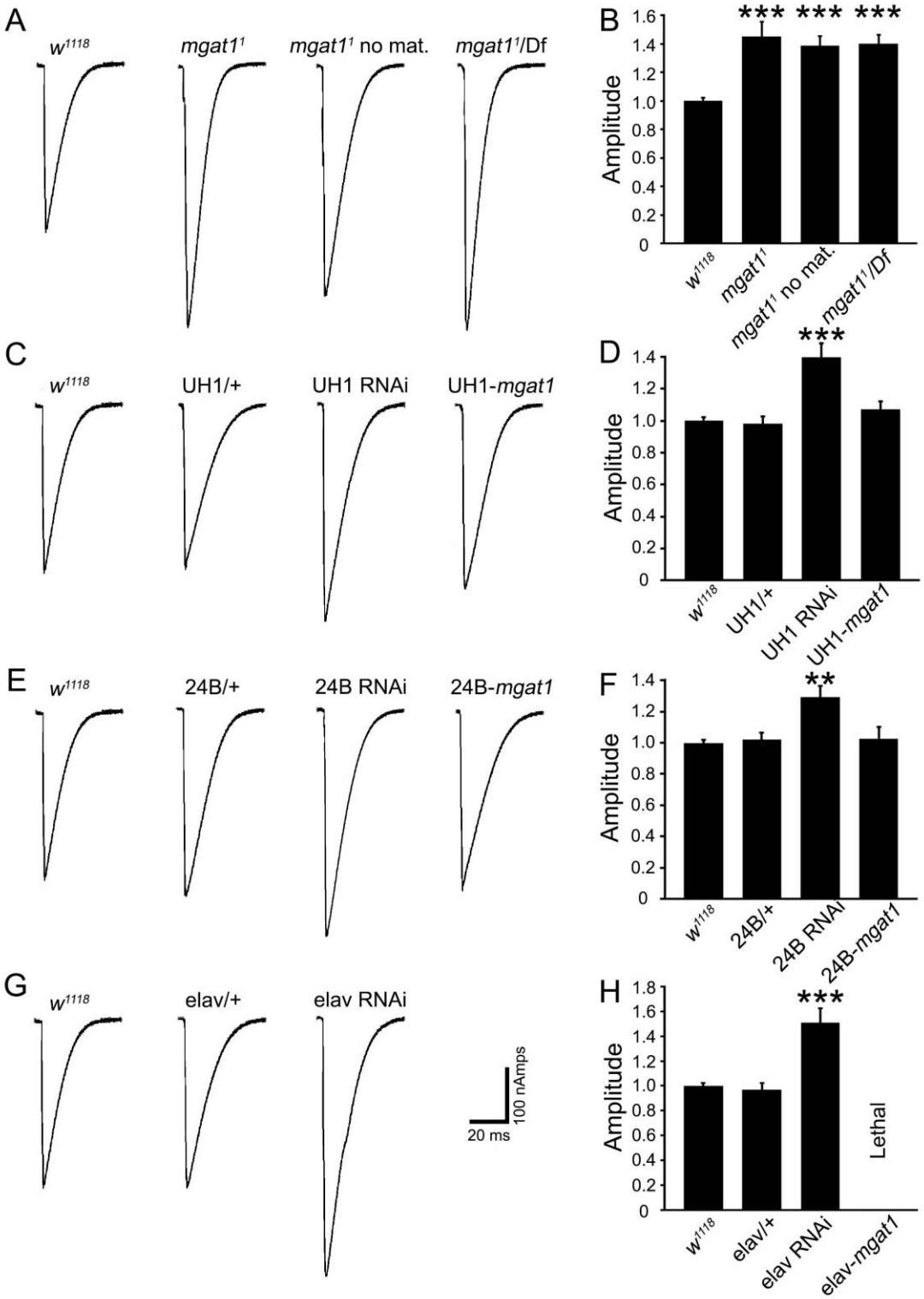
A
w1118
mgat11
mgat11 no mat.
mgat11/Df
B
***
***
***
Amplitude
w1118
mgat11
mgat11 no mat.
mgat11/Df
C
w1118
UH1/+
UH1 RNAi
UH1-mgat1
D
***
Amplitude
w1118
UH1/+
UH1 RNAi
UH1-mgat1
E
w1118
24B/+
24B RNAi
24B-mgat1
F
**
Amplitude
w1118
24B/+
24B RNAi
24B-mgat1
G
w1118
elav/+
elav RNAi
100 nAmps
20 ms
H
***
Amplitude
Lethal
w1118
elav/+
elav RNAi
elav-mgat1

Figure 7

Figure 7: Strengthened synaptic functional differentiation in *mgat1* null mutants.

Neurotransmission measured using two-electrode voltage-clamp (TEVC) of stimulation-evoked excitatory junctional currents (EJC) at the wandering third instar muscle 6 NMJ. **(A)** Representative EJC traces recorded in 1.0mM Ca^{2+} from w^{1118}, $mgat1^{1}$ null, $mgat1^{1}$ without maternal contribution and $mgat1^{1}$/Df. **(B)** EJC quantification for all 4 genotypes normalized to genetic control. Sample size is ≥10 animals per genotype. **(C)** Traces from w^{1118}, UH1/+ control, UH1-GAL4 driven UAS-*mgat1*-RNAi and UH1-GAL4 driven UAS-*mgat1* in $mgat1^{1}$/Df background. Synaptic transmission is elevated by ubiquitous RNAi knockdown and fully restored with reintroduction of ubiqutousUAS-*mgat1*. **(D)** EJC quantification for all 4 genotypes normalized to w^{1118}. Sample size is ≥14 animals per genotype. **(E)** Traces from w^{1118}, 24B-GAL4/+ control, 24B-GAL4 driven UAS-*mgat1*-RNAi and 24B-GAL4 driven UAS-*mgat1* in null background. Transmission elevated by postsynaptic RNAi and rescued with postsynaptic UAS-*mgat1.* **(F)** EJC quantification for 4 genotypes normalized to w^{1118}. Sample size is ≥11 animals per genotype. **(G)** Traces from w^{1118}, *elav*-GAL4/+ control and *elav*-GAL4 driven UAS-*mgat1*-RNAi. Transmission is elevated with neuronal RNAi knockdown. **(H)** EJC quantification normalized to w^{1118}. Sample size is ≥11 animals per genotype. Statistical analyses using ANOVA shown as $p \leq 0.01$ (**) and $p \leq 0.001$ (***).

Mgat1 regulates development of synaptic vesicle cycling properties

Since loss of *mgat1* function increases both synaptic morphogenesis and functional differentiation, the next step was to determine whether the overgrown structure simply mediates more transmission, or if structural and functional defects are due to separable *mgat1* requirements. Synaptic vesicle (SV) cycling with FM1-43 dye measures synaptic function within single boutons, thus allowing a clear separation of structure and function (Long et al., 2010; Nahm et al., 2013). To study SV endocytosis, FM1-43 dye was loaded under endogenous activity conditions over a prolonged period, and in response to acute depolarization with 90mM K+ saline. To study SV exocytosis, NMJ terminals were depolarized a second time in the absence of FM1-43 to drive dye release. The ratio of loading to unloading provides a measure of SV cycling rate within individual synaptic boutons. A summary of these data is shown in Figure 8.

Representative images of endogenous activity loading is shown in control and $mgat1^{1}$/Df NMJs at 1, 10 and 30 minutes in Figure 8A. Faint dye incorporation was present in boutons (arrows) after 1 minute loading in both genotypes, however loading occurred significantly faster in control compared to mutant (Fig. 8A,B). Comparing intensities over time-points revealed a significant decrease in *mgat1* loading (1 min: 23.1±1.9 (w^{1118}) vs. 5.0±0.3 (*mgat1*), $p<0.0001$; 10 min: 79.5±3.5 (w^{1118}) vs. 37.3±2.2 (*mgat1*), $p<0.0001$; 30 min: 124.8±12.6 (w^{1118}) vs. 74.7±6.6 (mgat1), $p<0.006$; Fig. 8B). This difference could represent reduced central activity in locomotor pattern generation, reduced SV cycling in the NMJ or elevated dye release compared to uptake. To distinguish these possibilities, FM1-43 dye was loaded (5 minutes) and then partially unloaded (2 minutes) with acute high [K+] depolarization (Fig. 8C). Representative images control and $mgat1^{1}$/Df NMJs are shown on the left, with higher magnification images of individual boutons shown on the right. Two defects are qualitatively apparent: *mgat1* nulls incorporate less dye, but release dye faster (Fig. 8C). Quantification of mean fluorescent intensities shows decreased loading in *mgat1* nulls normalized to control (w^{1118}: 1.0±0.03; $mgat1^{1}$: 0.83±0.04, $p<0.05$; $mgat1^{1}$/Df: 0.76±0.04, $p<0.001$; Fig. 8D, left). More strikingly, SV cycling rate (unloaded/loaded fluorescent intensity) is increased in *mgat1* nulls compared to control (w^{1118}: 1.0±0.05; $mgat1^{1}$: 0.46±0.05, $p<0.001$; $mgat1^{1}$/Df: 0.37±0.03, $p<0.001$; Fig. 8D, right). Thus, *mgat1* mutants exhibit altered SV cycling within individual boutons, independent

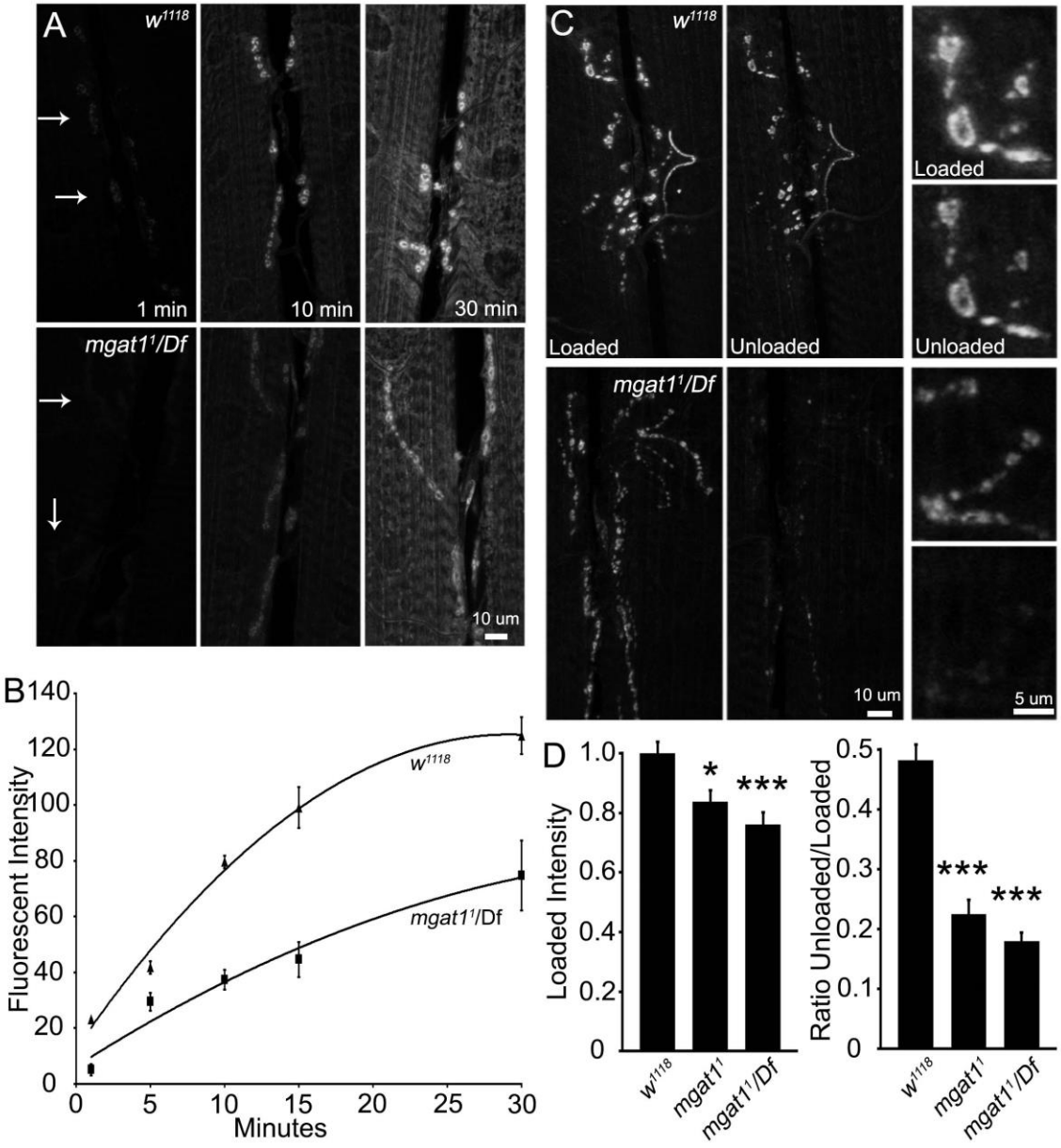
A
w1118
1 min
10 min
30 min
mgat11/Df
10 um
C
w1118
Loaded
Unloaded
Loaded
Unloaded
mgat11/Df
10 um
5 um
B
Fluorescent Intensity
Minutes
w1118
mgat11/Df
D
Loaded Intensity
Ratio Unloaded/Loaded
*
***
***
***
w1118
mgat11
mgat11/Df

Figure 8

Figure 8: Altered NMJ synaptic vesicle cycling in the *mgat1* null mutants.

Assays of synaptic vesicle (SV) loading and cycling rates with FM1-43 dye imaging at the wandering third instar 6/7 NMJ. **(A)** Representative images of FM1-43 loading during endogenous activity at 1, 10 and 30 minutes. Top panels show w^{1118} control and bottom panels show $mgat1^{1}$/Df. Arrows indicate boutons faintly loaded at 1 minute. **(B)** Fluorescence intensity plotted at 1, 5, 10, 15 and 30 minutes of endogenous activity. $\geq$9 animals per genotype used for each time point. **(C)** Representative NMJ images after FM1-43 loading with 90mM K^+ for 5 minutes and unloading for 2 minutes. Top panels show w^{1118} and bottom panels show $mgat1^{1}$/Df, with increased SV turnover indicated by reduced intensity after unloading. Right panels show high magnification images of loaded/unloaded boutons. **(D)** Quantification of loading and ratio of unloaded/loaded fluorescent intensities for w^{1118}, $mgat1^{1}$ homozygous null and $mgat1^{1}$/Df. Statistical analyses compared to genetic control w^{1118} using ANOVA shown as $p \leq 0.05$ (*), $p \leq 0.01$ (**) and $p \leq 0.001$ (***). Sample size is $\geq$18 NMJs for each genotype.

of the increased bouton number, with a strong increase in cycling rate in response to acute depolarization.

Selective loss of pre-and postsynaptic components in *mgat1* null mutants

Functional differentiation of the NMJ requires recruitment and organization of presynaptic SV cycle proteins and active zone (AZ) release sites, and postsynaptic glutamate receptors (GluRs; Featherstone et al., 2005; Long et al., 2008; Richmond and Broadie, 2002). N-glycosylation may be important for localization and maintenance of these key proteins during synaptogenesis, hypothesized to be dependent on Mgat1 function (Dani et al., 2012; Kwon and Chapman, 2012). We therefore next conducted a thorough confocal microscopy expression survey of synaptic proteins in the *mgat1* null condition to test for changes in presynaptic and postsynaptic composition. Most proteins were unchanged in *mgat1* mutants, and only a few molecular changes were identified. A summary of these results is shown in Figure 9.

Postsynaptic GluRs are believed to form tetramers composed of 3 essential subunits (GluRIIC-E) and a single variable subunit (GluRIIA or B) generating two distinct GluR functional classes (Featherstone, et al., 2005; Qin et al., 2005). To assay these receptor classes, we probed control and *mgat1* null NMJs with antibodies specific for GluRIIA, B and C subunits. There was no detectable change in the overall expression of total GluRs (labeled with the essential GluRIIC) or the GluRIIA-class receptors in the *mgat1* null condition (data not shown). In contrast, there was a clear and obvious decrease in GluRIIB-class receptors in *mgat1* nulls, both at low level magnification of the entire NMJ and in higher resolution images of individual synaptic boutons (Fig. 9A). Quantitative measures of fluorescent intensity show a highly significant decrease in GluRIIB labeling in $mgat1^{1}$/Df normalized to the genetic control (w^{1118}: 1.0±0.09; $mgat1^{1}$/Df: 0.73±0.04, $p<0.01$; Fig. 9D, left). This selective loss of GluRIIB shows that this one receptor class alone appears dependent on Mgat1 function.

The presynaptic apparatus includes key AZ protein Bruchpilot (BRP), V/T-SNARES of the core SNARE complex, and a host of SV associated and integral proteins regulating the SV cycle (Chapman, 2002; Hallermann et al., 2010). We assayed a wide range of these presynaptic proteins for changes in *mgat1* null mutants, and found that all did not detectably change, with

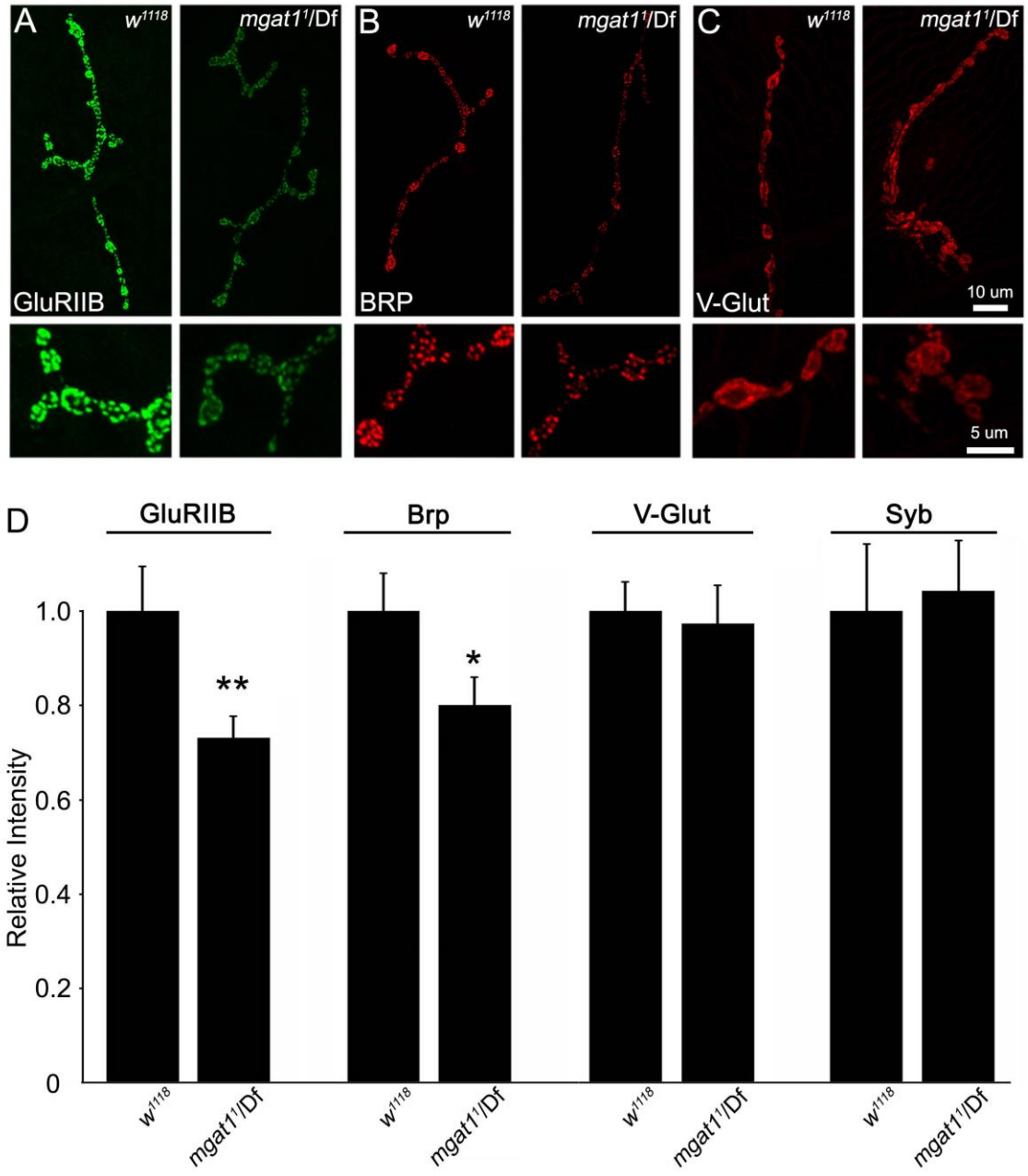
A
w1118
mgat11/Df
GluRIIB
B
w1118
mgat11/Df
BRP
C
w1118
mgat11/Df
V-Glut
10 um
5 um
D
GluRIIB
Brp
V-Glut
Syb
Relative Intensity
1.0
0.8
0.6
0.4
0.2
0
**
*
w1118
mgat11/Df
w1118
mgat11/Df
w1118
mgat11/Df
w1118
mgat11/Df

Figure 9

Figure 9: Pre- and postsynaptic component recruitment reduced at *mgat1* NMJs.

Null *mgat1* mutants show decreased postsynaptic glutamate receptor type IIB (GluRIIB) and presynaptic active zone Bruchpilot (BRP), but are unchanged for multiple other synaptic components. **(A-C)** Representative NMJ images for GluRIIB (A, green), BRP (B, red) and the vesicular glutamate (V-Glut) transporter (C, red) in genetic control w^{1118} and $mgat1^{1}$/Df mutants. High magnification images of synaptic boutons shown below. **(D)** Quantification of fluorescent intensities for GluRIIB ($n \geq 28$), BRP ($n \geq 38$), V-Glut ($n \geq 12$) and Synaptobrevin (Syb; $n \geq 16$) normalized to w^{1118}. V-Glut and Syb exhibit no change, indicating similar synaptic vesicle related density in control and mutant. Statistical analyses using students t-test for each pairwise comparison, with significance shown as $p \leq 0.05$ (*), $p \leq 0.01$ (**) and $p \leq 0.001$ (***).

only a single exception. The BRP punctae marking AZs were clearly decreased in *mgat1* mutants, both in whole NMJs and in high magnification images of synaptic boutons (Fig. 9B). Quantification of BRP labeling intensities showed a significant decrease in $mgat1^{1}$/Df normalized to control (w^{1118}: 1.0±0.07; $mgat1^{1}$/Df: 0.80±0.05, $p<0.05$; Fig. 9D). In contrast, other presynaptic components (e.g. Synaptotagmin, Cysteine String Protein (CSP), Synaptogyrin (GYR), etc.) were not detectably altered in *mgat1* nulls (data not shown). As exemplars of these negative data, we show vesicular glutamate transporter (V-Glut) and V-SNARE Synaptobrevin (Fig. 9D). The selective loss of just BRP shows a focused presynaptic requirement for Mgat1 function.

Multiple *trans*-synaptic signaling pathways altered in *mgat1* null mutants

Active zone (i.e. BRP) and class-specific GluR (i.e. GluRIIB) recruitment are both dependent on tightly regulated *trans*-synaptic signaling between pre- and postsynaptic cells during synaptogenesis (Dani et al., 2012; Margues, 2005; Rohrbough et al., 2013). Moreover, both *trans*-synaptic signaling pathway components and the synaptomatrix they traverse are highly glycosylated, and it is known that glycan mechanisms play key roles in the regulation of this developmental communication (Rohrbough and Broadie, 2010; Rohrbough et al., 2013). We therefore hypothesized that *mgat1* mutants would manifest defects in bidirectional *trans*-synaptic signals. To test this idea, we assayed signaling ligands for three well-characterized *trans*-synaptic pathways; 1) anterograde Wnt Wingless (Wg), 2) retrograde BMP Glass Bottom Boat (Gbb), and 3) newly-defined ligand Jelly Belly (Jeb). Representative NMJ images and the compiled quantification for these studies are shown in Figure 10.

Well-characterized antibodies for all 3 signaling ligands were used to label wandering third instar NMJs, comparing fluorescent intensities within the synaptic domain (dotted white outlines) in $mgat1^{1}$/Df null normalized to the w^{1118} genetic control (Fig. 10). The Wg signal was obviously increased in mutants (Fig. 10A, middle), and quantification of fluorescent intensity confirmed a significant elevation (w^{1118}: 1.0±0.10; $mgat1^{1}$/Df: 1.56±0.16, $p<0.001$; Fig. 10A, right). In contrast, the Gbb signal was clearly reduced and poorly localized to the synaptic domain in mutants (Fig. 10B, middle), and likewise significantly decreased in quantified

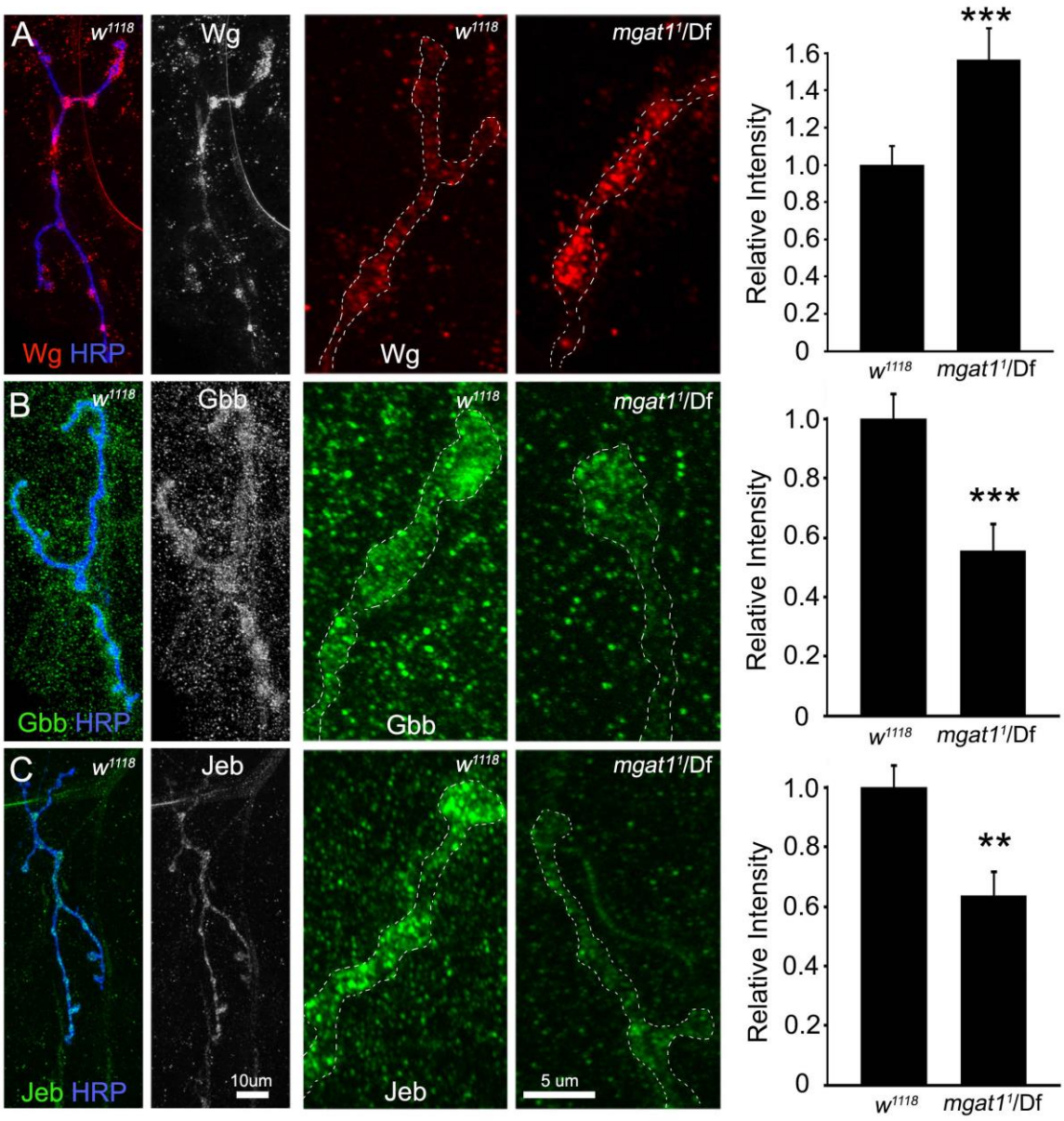
A
w1118
Wg
Wg HRP
w1118
mgat11/Df
Wg
B
w1118
Gbb
Gbb HRP
w1118
mgat11/Df
Gbb
C
w1118
Jeb
Jeb HRP
10um
w1118
mgat11/Df
Jeb
5 um
Relative Intensity
***
1.6
1.4
1.2
1.0
0.8
0.6
0.4
0.2
0
w1118
mgat11/Df
Relative Intensity
1.0
0.8
0.6
0.4
0.2
0
***
w1118
mgat11/Df
Relative Intensity
1.0
0.8
0.6
0.4
0.2
0
**
w1118
mgat11/Df

Figure 10

Figure 10: Multiple *trans*-synaptic signaling pathways altered in *mgat1* null mutant.

Assays of three well-characterized NMJ *trans*-synaptic signals: Wingless (Wg), Glass Bottom Boat (Gbb) and Jelly Belly (Jeb). **(A)** Representative NMJ images of Wg (red) double-labeled with HRP (blue), and shown alone (Wg, white). High magnification bouton comparison of genetic control (w^{1118}) and $mgat1^{1}$/Df. Right: Quantification of relative fluorescent intensity reveals increased Wg in mutant. **(B)** Representative images of Gbb (green) double-labeled with HRP (blue), and shown alone (Gbb, white). High magnification bouton comparison of w^{1118} and $mgat1^{1}$/Df. Right: Quantification shows decreased Gbb in mutant. **(C)** Representative NMJ images of Jeb (green) double-labeled with HRP (blue), and shown alone (Jeb, white). High magnification bouton comparison of w^{1118} and $mgat1^{1}$/Df. Right: Quantification shows decreased Jeb in mutant. Fluorescent intensities measured within the NMJ domain (white dotted line), normalized to genetic control w^{1118}. Statistical analyses were done using student's t-test for pairwise comparisons, with significance shown as $p \leq 0.01$ (**) and $p \leq 0.001$ (***). The sample size is $n \geq 18$ NMJs for each label and each genotype.

intensity (w^{1118}: 1.0±0.08; $mgat1^{1}$/Df: 0.55±0.08, p<0.001; Fig. 10B, right). The third signal Jeb was similarly decreased in $mgat1^{1}$/Df compared to control (w^{1118}: 1.0±0.07; $mgat1^{1}$/Df: 0.63±0.07 p<0.01; Fig. 10C). These results reveal a differential Mgat1 role in modulating *trans*-synaptic signaling, with increased abundance of Wg ligand and decreases in both Gbb and Jeb ligands. A primary role of *trans*-synaptic signaling is to recruit synaptic scaffolds which, in turn, bind synaptic proteins to seed the process of synaptogenesis.

Loss of key synaptic scaffolds driving synaptogenesis in *mgat1* null mutants

Discs Large (DLG) is a particularly well-characterized synaptic scaffold at the *Drosophila* NMJ, which is modulated downstream of Wg, Gbb and Jeb *trans*-synaptic signaling and, in turn, drives the appropriate recruitment of synaptic proteins including cell adhesion molecules, ion channels and GluRIIB-containing receptors (Chen and Featherstone, 2005; Marqués, 2005; Marrus et al., 2004). In addition, we have just recently defined Lethal Giant Larvae (LGL) as another key synaptic scaffold, which presynaptically facilitates the assembly of BRP-containing active zones to regulate SV cycling, and postsynaptically regulates GluR subunit composition (Staples and Broadie, 2013). We hypothesized that, downstream of Mgat1-dependent changes in *trans*-synaptic signaling, defects in recruiting these synaptic scaffolds could explain changes in pre/postsynaptic molecular composition. To test this idea, we imaged DLG and LGL scaffolds at the wandering third instar NMJ, comparing *mgat1* nulls to genetic controls. A summary of these data is shown in Figure 11.

The DLG scaffold is expressed in both pre- and postsynaptic compartments, but is most apparent in the subsynaptic reticulum (SSR) overlapping with postsynaptic glutamate receptors (Fig. 11A). DLG levels are clearly and strongly decreased in *mgat1* null mutants compared to controls. When intensity levels were quantified, there was a very significant decrease in mutants normalized to genetic control (w^{1118}: 1.0±0.08; $mgat1^{1}$: 0.66±0.06, p<0.01; Fig. 11C, top). Similarly, the LGL scaffold is present in the Fas2-labeled NMJ terminals in both presynaptic boutons and the postsynaptic domain, with clearly higher levels of expression in genetic control compared to the *mgat1* null condition (Fig. 11B). Quantification of fluorescent intensity shows a highly significant decrease in LGL (w^{1118}: 1.0±0.07; $mgat1^{1}$: 0.50±0.06, p<0.001; Fig. 11C,

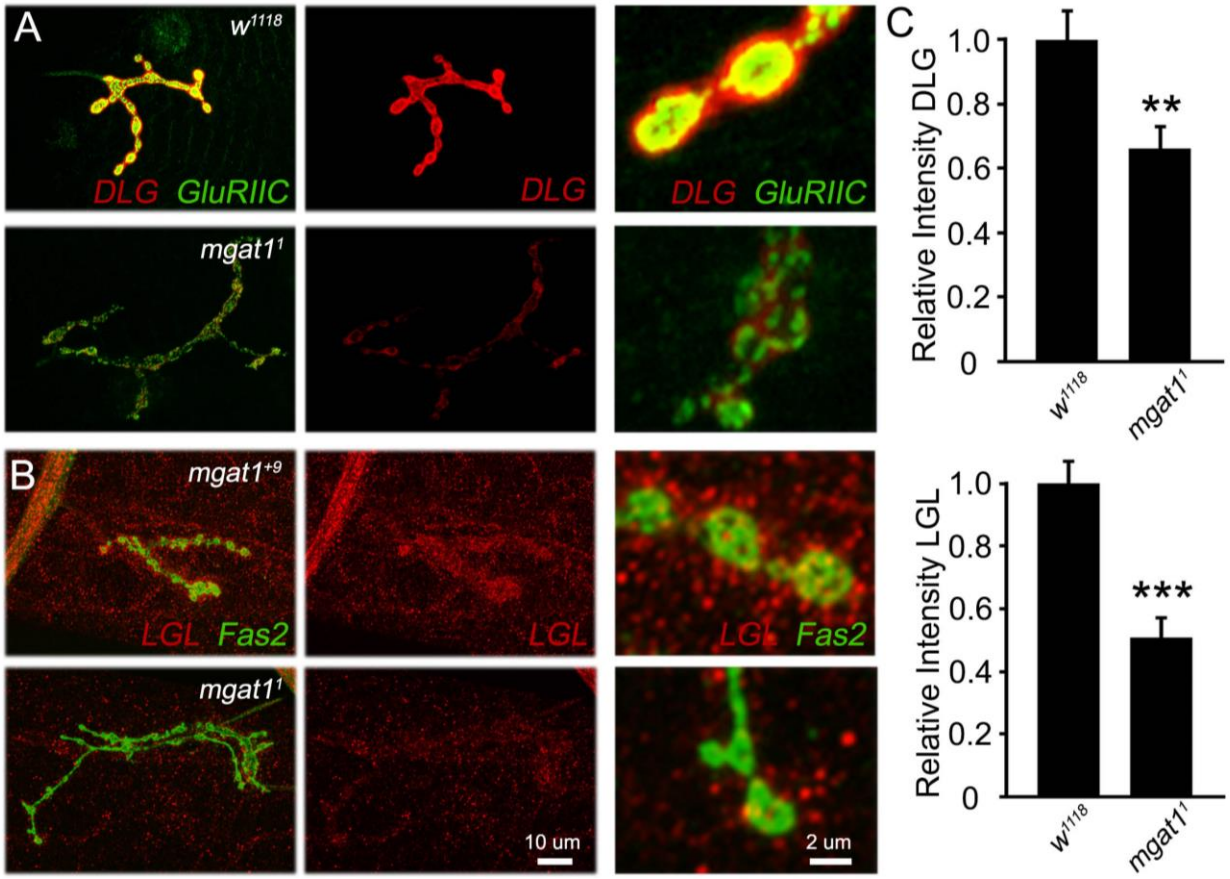
A
w1118
DLG GluRIIC
DLG
DLG GluRIIC
mgat11
B
mgat1+9
LGL Fas2
LGL
LGL Fas2
mgat11
10 um
2 um
C
Relative Intensity DLG
1.0
0.8
0.6
0.4
0.2
0
**
w1118
mgat11
Relative Intensity LGL
1.0
0.8
0.6
0.4
0.2
0
***
w1118
mgat11

Figure 11

Figure 11: Synaptic scaffolds DLG and LGL reduced in the *mgat1* null mutants.

Imaging of Discs Large (DLG) and Lethal Giant Larvae (LGL) synaptic scaffolds at the wandering third instar NMJ. **(A)** Representative images of DLG (red) co-labeled with glutamate receptor type IIC (GluRIIC, green), with higher magnification boutons in side panels. **(B)** Representative images of LGL (red) co-labeled with Fas2 (green), with high magnification boutons in side panels. **(C)** Quantification of DLG fluorescent intensity (top: $mgat1^{1}$ (n=15), w^{1118} (n=22)) and LGL fluorescent intensity (bottom: $mgat1^{1}$ (n=12), w^{1118} (n=12)). Statistical analyses done using student's t-test for pairwise comparisons, with significance shown as $p \leq 0.01$ (**) and $p \leq 0.001$ (***)

bottom). LGL and DLG scaffolds are both known to regulate active zone and glutamate receptor composition, so changes in their abundance and localization are likely to be causal in Mgat1-dependent changes in NMJ synaptogenesis.

Discussion

We began with the hypothesis that disruption of synaptomatrix N-glycosylation would alter *trans*-synaptic signaling underlying NMJ synaptogenesis (Dani and Broadie, 2012). Mgat1 loss transforms the synaptomatrix glycan environment. Complete absence of the HRP epitope, α1-3-fucosylated N-glycans, is expected as it requires Mgat1 activity: key HRP epitope synaptic proteins include Fasciclins, Neurotactin and Neuroglian, among others (Desai et al., 1994; Paschinger et al., 2009). We show that HRP epitope modification of the key synaptogenic regulator Fasciclin 2 is not required for stabilization or localization, suggesting a role in protein function. On the other hand, complete loss of VVA lectin synaptomatrix labeling is surprising because the epitope is a terminal β-GalNAc (Martin, 2003). This result suggests that the N-glycan LacdiNAc is enriched at the NMJ, and that the terminal GalNAc expected on O-glycans/glycosphingolipids may be present on N-glycans in this synaptic context. Importantly, VVA labels Dystroglycan and loss of Dystroglycan glycosylation blocks extracellular ligand binding and complex formation in *Drosophila* (Haines et al., 2007; Nakamura et al., 2010), and causes muscular dystrophies in humans (Ervasti et al., 1997; Muntoni et al., 2008; Tran et al., 2012). This study shows that VVA-recognized Dystroglycan glycosylation is not required for protein stabilization or synaptic localization, but did not test functionality or complex formation, which likely requires Mgat1-dependent modification. Conversely, the secreted endogenous lectin MTG is highly elevated in *mgat1* null synaptomatrix, likely owing to attempted compensation for complex and hybrid N-glycan losses that serve as MTG binding sites. MTG binds GlcNAc in a calcium-dependent manner and pulls down a number of HRP-epitope proteins by immunoprecipitation (Rushton et al., 2012), although the specific proteins have not been identified. It will be of interest to perform immunoprecipitation on *mgat1* samples to identify changes in HRP bands. Importantly, MTG is critical for synaptomatrix glycan patterning and functional synaptic development (Rohrbough et al., 2007). MTG regulates VVA

synaptomatrix labeling (Rushton et al., 2009), suggesting a mechanistic link between the VVA and MTG changes in *mgat1* mutants. The MTG elevation observed in *mgat1* nulls provides a plausible causative mechanism for strengthened functional differentiation (Rohrbough and Broadie, 2010; Rushton et al., 2012).

Consistent with our recent glycosylation gene screen findings (Dani et al., 2012), *mgat1* nulls exhibit increased synaptic growth and structural overelaboration. Therefore, complex and hybrid N-glycans overall provide a brake on synaptic morphogenesis, although individual N-glycans may provide positive regulation. Likely players include Mgat1-dependent HRP-epitope proteins (e.g. Fasciclins, Neurotactin, Neuroglian), and Position Specific (PS) integrin receptors and their ligands, all of which are heavily glycosylated and have well-characterized roles regulating synaptic architecture (Beumer et al., 1999; Rushton et al., 2009; Beck et al., 2012; Enneking et al., 2013). An alternate hypothesis is that *mgat1* phenotypes may result from the presence of high-mannose glycans on sites normally carrying complex/hybrid structures (Schachter, 2010), suggesting possible gain-of-function rather than loss-of-function of specific N-glycan classes. NMJ branch and bouton number play roles in determining functional strength (Thomas and Sigrist, 2012), although active zones and GluRs are also regulated independently (DiAntonio, 2006). Thus, the increased functional strength could be caused by increased structure at *mgat1* null NMJs. However, muscle-targeted UAS-*mgat1* rescues otherwise *mgat1* null function, but has no effect on structural defects, demonstrating that these two roles are separable. On the other hand, presynaptic *mgat1* RNAi also causes strong functional defects, showing there is additionally a presynaptic requirement in functional differentiation. Neuron-targeted *mgat1* causes lethality, indicating that Mgat1 levels must be tightly regulated, but preventing independent assessment of *mgat1* presynaptic rescue of synaptogenesis defects.

Presynaptic glutamate release and postsynaptic glutamate receptor responses drive synapse function. Using lipophilic dye to visualize SV cycling, we found *mgat1* null mutants endogenously cycle less than controls, but have greater cycling capacity upon depolarizing stimulation. The endogenous cycling defect is consistent with the sluggish locomotion of *mgat1* mutants (Sakar et al., 2006), whereas the elevated stimulation-evoked cycling is consistent with electrophysiological measures of neurotransmission. Similarly, mutation of dPOMT1, which

glycosylates VVA-labeled Dystroglycan, decreases SV release probability (Wairkar et al., 2008), although dPOMT1 adds mannose not GalNAc. Null *mgat1* mutants display no change in SV cycle components (e.g. Synaptobrevin, Synaptotagmin, Synaptogyrin, etc.), but exhibit reduced expression of the key active zone component Bruchpilot (Wagh et al., 2006; Kittel et al., 2006). Other examples of presynaptic glycosylation requirements include the *Drosophila* Fuseless (Fusl) glycan transporter, which is critical for Cacophony (Cac) voltage-gated calcium channel recruitment to active zones (Long et al., 2008), and the mammalian GalNAc transferase (Galgt2), whose over-expression causes decreased active zone assembly (Martin, 2003). Postsynaptically, *mgat1* nulls show specific loss of GluRIIB-containing receptors. Similarly, dPOMT1 mutants exhibit specific GluRIIB loss (Wairkar et al., 2008), although *dystroglycan* nulls display GluRIIA loss (Bogdanik et al., 2008). Selective GluRIIB loss in *mgat1* nulls may drive increased neurotransmission owing to channel kinetics differences in GluRIIA vs. GluRIIB receptors (DiAntonio et al., 1999).

Bi-directional *trans*-synaptic signaling regulates NMJ structure, function and pre/postsynaptic composition (Dani et al., 2012; Enneking et al., 2013; Muller and Davis, 2012). This intercellular signaling requires ligand passage through, and containment within, the heavily-glycosylated synaptomatrix (Dani and Broadie, 2012; Martin, 2003), which is strongly compromised in *mgat1* mutants. In testing three well-characterized signaling pathways, we found that Wg accumulates, whereas both Gbb and Jeb are reduced in the *mgat1* null synaptomatrix. Wg has two N-glycosylation sites, but these do not regulate ligand expression (Tang et al., 2012), suggesting Wg buildup occurs due to lost synaptomatrix N-glycosylation. Importantly, Wg overexpression increases NMJ bouton formation similar to the phenotype of *mgat1* nulls (Ataman et al., 2008; Korkut et al., 2009), suggesting a possible causal mechanism. Gbb is predicted to be N-glycosylated at four sites, but putative glycosylation roles have not yet been tested. Importantly, Gbb loss impairs presynaptic active zone development similar to *mgat1* nulls (McCabe et al., 2003; Nahm et al., 2010), suggesting a separable causal mechanism. Jeb is not predicted to be N-glycosylated, indicating Jeb loss is caused by lost synaptomatrix N-glycosylation. Importantly, we have just recently shown that loss of Jeb signaling increases functional synaptic differentiation similar to *mgat1* nulls (Rohrbough et al., 2013). In addition,

jeb mutants exhibit strongly suppressed NMJ endogenous activity, similar to the reduced endogenous SV cycling in *mgat1* nulls (Rohrbough and Broadie, 2010). Moreover, the MTG lectin negatively regulates Jeb accumulation in NMJ synaptomatrix (Rohrbough and Broadie, 2010), consistent with elevated MTG causing Jeb down-regulation in *mgat1* nulls.

Trans-synaptic signaling drives recruitment of scaffolds that, in turn, recruit pre- and postsynaptic molecular components (Ataman et al., 2006; Koles et al., 2012). Specifically, DLG and LGL scaffolds regulate the distribution and density of both active zone components (e.g. BRP) and postsynaptic GluRs (Chen and Featherstone, 2005; Staples and Broadie, 2013), and both of these scaffolds are reduced at *mgat1* null NMJs. Importantly, *dlg* mutants display selective loss of GluRIIB, with GluRIIA unchanged, similar to *mgat1* nulls (Chen and Featherstone, 2005), suggesting a causal mechanism. Moreover, *lgl* mutants display both a selective GluRIIB impairment as well as reduction of BRP aggregation in active zones, similar to *mgat1* nulls (Staples and Broadie, 2013), suggesting a separable involvement for this synaptic scaffold. DLG and LGL are known to interact in other developmental contexts (Humbert et al., 2008), indicating a likely interaction at the developing synapse. Although synaptic ultrastructure has not been examined in *lgl* mutants, *dlg* mutants exhibit impaired NMJ development, including a deformed subsynaptic reticulum (SSR; Lahey et al., 1994). These synaptogenesis requirements predict similar ultrastructural defects in *mgat1* mutants, albeit presumably due to the combined loss of both DLG and LGL scaffolds. Our future work will focus on electron microscopy analyses to probe N-glycosylation mechanisms of synaptic development.

References

Abramoff, M.D., Magalhaes, P.J. and Ram, S.J. (2004). Image Processing with ImageJ. Biophotonics International. 11(7), 36-42.

Ataman, B., Ashley, J., Gorczyca, D., Gorczyca, M., Mathew, D., Wichmann, C., Sigrist, S.J. and Budnik, V. (2006). Nuclear trafficking of Drosophila Frizzled-2 during synapse development requires the PDZ protein dGRIP. Proc. Natl. Acad. Sci. USA. 103(20), 7841-6.

Ataman, B., Ashley, J., Gorczyca, M., Ramachandran, P., Fouquet, W., Sigrist, S.J. and Budnik, V. (2008). Rapid activity-dependent modifications in synaptic structure and function require bidirectional Wnt signaling. Neuron. 57(5), 705-18.

Beck, E.S., Gasque, G., Imlach, W.L., Jiao, W., Jiwon, C.B., Wu, P.S., Kraushar, M.L. and McCabe, B.D. (2012). Regulation of Fasciclin II and synaptic terminal development by the splicing factor beag. J. Neurosci. 32(20), 7058-73.

Beumer, K., Matthies, H.J., Bradshaw, A. and Broadie, K. (2002). Integrins regulate DLG/FAS2 via a CaM kinase II-dependent pathway to mediate synapse elaboration and stabilization during postembryonic development. Development 129(14), 3381-91.

Beumer, K.J., Rohrbough, J., Prokop, A. and Broadie, K. (1999). A role for PS integrins in morphological growth and synaptic function at the postembryonic neuromuscular junction of Drosophila. Development. 126(24), 5833-46.

Bogdanik, L., Framery, B., Frölich, A., Franco, B., Mornet, D., Bockaert, J., Sigrist, S.J., Grau, Y. and Parmentier, M.L. (2008). Muscle dystroglycan organizes the postsynapse and regulates presynaptic neurotransmitter release at the Drosophila neuromuscular junction. PLoS One. 3(4), e2084.

Brand, A.H. and Perrimon, N. (1993). Targeted gene expression as a means of altering cell fates and generating dominant phenotypes. Development. 118(2), 401-15.

Broadie, K., Baumgartner, S. and Prokop, A. (2011). Extracellular matrix and its receptors in Drosophila neural development. Dev. Neurobiol. 71(11), 1102-30.

Campbell, R.M., Metzler, M., Granovsky, M., Dennis, J.W. and Marth, J.D. (1995). Complex asparagine-linked oligosaccharides in Mgat1-null embryos. Glycobiology. 5(5), 535-43.

Chapman, E.R. (2002). Synaptotagmin: a Ca(2+) sensor that triggers exocytosis? Nat Rev. Mol. Cell Biol. 3(7), 498-508.

Chen, K. and Featherstone, D.E. (2005). Discs-large (DLG) is clustered by presynaptic innervation and regulates postsynaptic glutamate receptor subunit composition in Drosophila. BMC Biol. 3:1.

Dani, N. and Broadie, K. (2012). Glycosylated synaptomatrix regulation of trans-synaptic signaling. Dev. Neurobiol. 72(1), 2-21.

Dani, N., Nahm, M., Lee, S., and Broadie, K. (2012). A targeted glycan-related gene screen reveals heparan sulfate proteoglycan sulfation regulates WNT and BMP trans-synaptic signaling. PLoS Genet. 8(11), e1003031.

Daniels, R.W., Collins, C.A., Gelfand, M.V., Dant, J., Brooks, E.S., Krantz, D.E. and DiAntonio, A. (2004). Increased expression of the Drosophila vesicular glutamate transporter leads to excess glutamate release and a compensatory decrease in quantal content. J. Neurosci. 24(46), 10466-74.

Desai, C.J., Popova, E. and Zinn, K. (1994). A Drosophila receptor tyrosine phosphatase expressed in the embryonic CNS and larval optic lobes is a member of the set of proteins bearing the "HRP" carbohydrate epitope. J. Neurosci. 14(12), 7272-83.

DiAntonio, A. (2006). Glutamate receptors at the Drosophila neuromuscular junction. Int. Rev. Neurobiol. 75, 165-79.

DiAntonio, A., Petersen, S.A., Heckmann, M. and Goodman, C.S. (1999). Glutamate receptor expression regulates quantal size and quantal content at the Drosophila neuromuscular junction. J. Neurosci. 19(8), 3023-32.

Enneking, E.M., Kudumala, S.R., Moreno, E., Stephan, R., Boerner, J., Godenschwege, T.A. and Pielage, J. (2013). Transsynaptic Coordination of Synaptic Growth, Function, and Stability by the L1-Type CAM Neuroglian. PLoS Biol. 11(4), e1001537.

Ervasti, J.M., Burwell, A.L. and Geissler, A.L. (1997). Tissue-specific heterogeneity in alpha-dystroglycan sialoglycosylation. Skeletal muscle alpha-dystroglycan is a latent receptor for Vicia villosa agglutinin b4 masked by sialic acid modification. J. Biol. Chem. 272(35), 22315-21.

Featherstone, D.E., Rushton, E., Rohrbough, J., Liebl, F., Karr, J., Sheng, Q., Rodesch, C.K. and Broadie, K. (2005). An essential Drosophila glutamate receptor subunit that functions in both central neuropil and neuromuscular junction. J. Neurosci. 25(12), 3199-208.

Freeze, H.H. (2006). Genetic defects in the human glycome. Nat. Rev. Genet. 7(7), 537-51.

Grasa, P., Kaune, H. and Williams, S.A. (2012). Embryos generated from oocytes lacking complex N- and O-glycans have compromised development and implantation. Reproduction. 144(4), 455-65.

Del Grosso, F., De Mariano, M., Passoni, L., Luksch, R., Tonini, G.P. and Longo, L. (2011). Inhibition of N-linked glycosylation impairs ALK phosphorylation and disrupts pro-survival signaling in neuroblastoma cell lines. BMC Cancer. 11, 525.

Haines, N., Seabrooke, S. and Stewart, B.A. (2007). Dystroglycan and protein O-mannosyltransferases 1 and 2 are required to maintain integrity of Drosophila larval muscles. Mol. Biol. Cell. 18(12), 4721-30.

Hallermann, S., Kittel, R.J., Wichmann, C., Weyhersmüller, A., Fouquet, W., Mertel, S., Owald, D., Eimer, S., Depner, H., Schwärzel, M., Sigrist, S.J. and Heckmann, M. (2010). Naked dense bodies provoke depression. J. Neurosci. 30(43), 14340-5.

Hennet, T. (2012). Diseases of glycosylation beyond classical congenital disorders of glycosylation. Biochimica et Biophysica Acta 1820, 1306-1317.

Henríquez, J.P. and Salinas, P.C. (2012). Dual roles for Wnt signalling during the formation of the vertebrate neuromuscular junction. Acta Physiol. (Oxf). 204(1), 128-36.

Hewitt, J.E. (2009). Abnormal glycosylation of dystorglycan in human genetic disease. Biochimica et Biophysica Acta. 1792, 853-861.

Humbert, P.O., Grzeschik, N.A., Brumby, A.M., Galea, R., Elsum, I. and Richardson, H.E. (2008). Control of tumourigenesis by the Scribble/Dlg/Lgl polarity module. Oncogene. 27(55), 6888-907.

Kamimura, K., Ueno, K., Nakagawa, J., Hamada, R., Saitoe, M. and Maeda, N. (2013). Perlecan regulates bidirectional Wnt signaling at the Drosophila neuromuscular junction. J. Cell Biol. 200(2), 219-33.

Kittel, R.J., Wichmann, C., Rasse, T.M., Fouquet, W., Schmidt, M., Schmid, A., Wagh, D.A., Pawlu, C., Kellner, R.R., Willig, K.I., Hell, S.W., Buchner, E., Heckmann, M. and Sigrist, S.J. (2006). Bruchpilot promotes active zone assembly, Ca2+ channel clustering, and vesicle release. Science. 312(5776), 1051-4.

Koles, K., Lim, J.M., Aoki, K., Porterfield, M., Tiemeyer, M., Wells, L. and Panin, V. (2007). Identification of N-glycosylated proteins from the central nervous system of Drosophila melanogaster. Glycobiology. 17(12), 1388-403.

Koles, K., Nunnari, J., Korkut, C., Barria, R., Brewer, C., Li, Y., Leszyk, J., Zhang, B. and Budnik, V. (2012). Mechanism of evenness interrupted (Evi)-exosome release at synaptic boutons. J. Biol. Chem. 287(20), 16820-34.

Korkut, C., Ataman, B., Ramachandran, P., Ashley, J., Barria, R., Gherbesi, N. and Budnik, V. (2009). Trans-synaptic transmission of vesicular Wnt signals through Evi/Wntless. Cell. 139(2), 393-404.

Kwon, S.E. and Chapman, E.R. (2012). Glycosylation is dispensable for sorting of synaptotagmin 1 but is critical for targeting of SV2 and synaptophysin to recycling synaptic vesicles. J. Biol. Chem. 287(42), 35658-68.

Lahey, T., Gorczyca, M., Jia, X.X. and Budnik, V. (1994). The Drosophila tumor suppressor gene dlg is required for normal synaptic bouton structure. Neuron. 13(4), 823-35.

Lee, H.H., Norris, A., Weiss, J.B., and Frasch, M. (2003). Jelly belly protein activates the receptor tyrosine kinase Alk to specify visceral muscle pioneers. Nature. 425(6957), 507-12.

Léonard, R., Rendic, D., Rabouille, C., Wilson, I.B., Préat, T. and Altmann, F. (2006). The Drosophila fused lobes gene encodes an N-acetylglucosaminidase involved in N-glycan processing. J. Biol. Chem. 281(8), 4867-75.

Lin, D.M. and Goodman, C.S. (1994). Ectopic and increased expression of Fasciclin II alters motoneuron growth cone guidance. Neuron.13(3), 507-23.

Littleton, J.T., Bellen, H.J. and Perin, M.S. (1993). Expression of synaptotagmin in Drosophila reveals transport and localization of synaptic vesicles to the synapse. Development.118(4), 1077-88.

Long, A.A., Kim, E., Leung, H.T., Woodruff, E. 3rd, An, L., Doerge, R.W., Pak, W.L. and Broadie, K. (2008). Presynaptic calcium channel localization and calcium-dependent synaptic vesicle exocytosis regulated by the Fuseless protein. J. Neurosci. 28(14), 3668-82.

Long, A.A., Mahapatra, C.T., Woodruff, E.A., Rohrbough, J., Leung, H.T., Shino, S., An, L., Doerge, R.W., Metzstein, M.M., Pak, W.L. and Broadie, K. (2010). The nonsense-mediated decay pathway maintains synapse architecture and synaptic vesicle cycle efficacy. J. Cell Sci. 123(Pt 19), 3303-15.

Marrus, S.B., Portman, S.L., Allen, M.J., Moffat, K.G., and DiAntonio, A. (2004). Differential localization of glutamate receptor subunits at the Drosophila neuromuscular junction. J. Neurosci. 24(6), 1406-15.

Marqués, G. (2005). Morphogens and synaptogenesis in Drosophila. J. Neurobiol. 64(4), 417-34.

Martin, P.T. (2003). Glycobiology of the neuromuscular junction. J. Neurocytol. 32(5-8), 915-29.

McCabe, B.D., Marqués, G., Haghighi, A.P., Fetter, R.D., Crotty, M.L., Haerry, T.E., Goodman, C.S. and O'Connor, M.B. (2003). The BMP homolog Gbb provides a retrograde signal that regulates synaptic growth at the Drosophila neuromuscular junction. Neuron. 39(2), 241-54.

Müller, M. and Davis, G.W. (2012). Transsynaptic control of presynaptic Ca^{2+} influx achieves homeostatic potentiation of neurotransmitter release. Cur. Biol. 22(12),1102-8.

Muntoni, F., Torelli, S. and Brockington, M. (2008). Muscular dystrophies due to glycosylation defects. Neurotherapeutics. 5(4), 627-32.

Nahm M, Lee MJ, Parkinson W, Lee M, Kim H, Kim YJ, Kim S, Cho YS, Min BM, Bae YC, Broadie K, Lee S. (2013). Spartin regulates synaptic growth and neuronal survival by inhibiting BMP-mediated microtubule stabilization. Neuron. 77(4), 680-95.

Nahm M, Long AA, Paik SK, Kim S, Bae YC, Broadie K, Lee S. (2010). The Cdc42-selective GAP rich regulates postsynaptic development and retrograde BMP transsynaptic signaling. J. Cell Biol. 191(3), 661-75.

Nakamura N, Stalnaker SH, Lyalin D, Lavrova O, Wells L, Panin VM. (2010). Drosophila Dystroglycan is a target of O-mannosyltransferase activity of two protein O-mannosyltransferases, Rotated Abdomen and Twisted. Glycobiology. 20(3), 381-94.

Ohshiro, T., Yagami, T., Zhang, C. and Matsuzaki, F. (2000). Role of cortical tumour-suppressor proteins in asymmetric division of Drosophila neuroblast. Nature. 408(6812), 593-6.

Paschinger, K., Rendić, D. and Wilson, I.B. (2009). Revealing the anti-HRP epitope in Drosophila and Caenorhabditis. Glycoconj. J. 26(3), 385-95.

Patton, B.L. (2003). Basal lamina and the organization of neuromuscular synapses. J. Neurocytol. 32(5-8), 883-903.

Pownall, S., Kozak, C.A., Schappert, K., Sarkar, M., Hull, E., Schachter, H. and Marth, J.D. (1992). Molecular cloning and characterization of the mouse UDP-N-acetylglucosamine:alpha-3-D-mannoside beta-1,2-N-acetylglucosaminyltransferase I gene. Genomics. 12(4), 699-704.

Puthalakath, H., Burke, J. and Gleeson, P.A. (1996). Glycosylation defect in Lec1 Chinese hamster ovary mutant is due to a point mutation in N-acetylglucosaminyltransferase I gene. J. Biol. Chem. 271(44), 27818-22.

Qin, G., Schwarz, T., Kittel, R.J., Schmid, A., Rasse, T.M., Kappei, D., Ponimaskin, E., Heckmann, M. and Sigrist, S.J. (2005). Four different subunits are essential for expressing the synaptic glutamate receptor at neuromuscular junctions of Drosophila. J. Neurosci. 25(12), 3209-18.

Rendić, D., Sharrow, M., Katoh, T., Overcarsh, B., Nguyen, K., Kapurch, J., Aoki, K., Wilson, I.B. and Tiemeyer, M. (2010). Neural-specific α3-fucosylation of N-linked glycans in the Drosophila embryo requires fucosyltransferase A and influences developmental signaling associated with O-glycosylation. Glycobiology. 20(11),1353-65.

Richmond, J.E. and Broadie, KS. (2002). The synaptic vesicle cycle: exocytosis and endocytosis in Drosophila and C. elegans. Curr. Opin. Neurobiol. 12(5), 499-507.

Rohrbough, J. and Broadie, K. (2002). Electrophysiological analysis of synaptic transmission in central neurons of Drosophila larvae. J Neurophysiol. 88(2), 847-60.

Rohrbough, J. and Broadie, K. (2010). Anterograde Jelly belly ligand to Alk receptor signaling at developing synapses is regulated by Mind the gap. Development. 137(20), 3523-33.

Rohrbough, J., Kent, K.S., Broadie, K. and Weiss, J.B. (2013). Jelly Belly trans-synaptic signaling to anaplastic lymphoma kinase regulates neurotransmission strength and synapse architecture. Dev. Neurobiol. 73(3), 189-208.

Rohrbough, J., Rushton, E., Woodruff, E., Fergestad, T., Vigneswaran, K. and Broadie, K. (2007). Presynaptic establishment of the synaptic cleft extracellular matrix is required for post-synaptic differentiation. Genes Dev. 21(20), 2607-28.

Rushton, E., Rohrbough, J. and Broadie, K. (2009). Presynaptic secretion of mind-the-gap organizes the synaptic extracellular matrix-integrin interface and postsynaptic environments. Dev. Dyn. 238(3), 554-71.

Rushton, E., Rohrbough, J., Deutsch, K. and Broadie, K. (2012). Structure-function analysis of endogenous lectin mind-the-gap in synaptogenesis. Dev. Neurobiol. 72(8), 1161-79.

Sarkar, M., Iliadi, K.G., Leventis, P.A., Schachter, H., and Boulianne, G.L. (2010). Neuronal expression of Mgat1 rescues the shortened life span of Drosophila Mgat11 null mutants and increases life span. Proc. Natl. Acad. Sci. U S A. 107(21), 9677-82.

Sarkar, M., Leventis, P.A., Silvescu, C.I., Reinhold, V.N., Schachter, H., and Boulianne, G.L. (2006). Null mutations in Drosophila N-acetylglucosaminyltransferase I produce defects in locomotion and a reduced life span. J. Biol. Chem. 281(18),12776-85

Schachter, H. (2010). Mgat1-dependent N-glycans are essential for the normal development of both vertebrate and invertebrate metazoans. Semin. Cell Dev. Biol. 21(6), 609-15.

Schachter, H. and Boulianne, G. (2011). Life is sweet! A novel role for N-glycans in Drosophila lifespan. Fly (Austin). 5(1), 18-24.

Shi, S., Williams, S.A., Seppo, A., Kurniawan, H., Chen, W., Ye, Z., Marth, J.D. and Stanley, P. (2004). Inactivation of the Mgat1 gene in oocytes impairs oogenesis, but embryos lacking complex and hybrid N-glycans develop and implant. Mol. Cell Biol. 24(22), 9920-9.

Staples, J. and Broadie, K. (2013). The cell polarity scaffold Lethal Giant Larvae regulates synapse morphology and function**.** J. Cell. Sci. (Epub ahead of print)

Stevens, R.J., Akbergenova, Y., Jorquera, R.A., and Littleton, J.T. (2012). Abnormal synaptic vesicle biogenesis in Drosophila synaptogyrin mutants. J. Neurosci. 32(50), 18054-67.

Sun, M. and Xie, W. (2012). Cell adhesion molecules in Drosophila synapse development and function. Sci. China Life Sci. 55(1), 20-6.

Tanaka, K., Kitagawa, Y. and Kadowaki, T. (2002). Drosophila segment polarity gene product porcupine stimulates the posttranslational N-glycosylation of wingless in the endoplasmic reticulum. J. Biol. Chem. 277(15), 12816-23.

Tang, X., Wu, Y., Belenkaya, T.Y., Huang, Q., Ray, L., Qu, J. and Lin, X. (2012). Roles of N-glycosylation and lipidation in Wg secretion and signaling. Dev. Biol. 364(1), 32-41.

Thomas, U. and Sigrist, S.J. (2012). Glutamate receptors in synaptic assembly and plasticity: case studies on fly NMJs. Adv. Exp. Med. Biol. 970, 3-28.

Tran, D.T., Lim, J.M., Liu, M., Stalnaker, S.H., Wells, L., Ten Hagen, K.G. and Live, D. (2012) Glycosylation of α-dystroglycan: O-mannosylation influences the subsequent addition of GalNAc by UDP-GalNAc polypeptide N-acetylgalactosaminyltransferases. J. Biol. Chem. 287(25), 20967-74.

Wagh, D.A., Rasse, T.M., Asan, E., Hofbaue, A., Schwenker,t I., Dürrbeck, H., Buchner, S., Dabauvalle, M.C., Schmidt, M., Qin, G., Wichmann, C., Kittel, R., (2006). Bruchpilot, a protein with homology to ELKS/CAST, is required for structural integrity and function of synaptic active zones in Drosophila. Neuron. 49(6), 833-44.

Wairkar, Y.P., Fradkin, L.G., Noordermeer, J.N. and DiAntonio, A. (2008) Synaptic defects in a Drosophila model of congenital muscular dystrophy. J. Neurosci. 28(14), 3781-9.

Wang, T., Liu, Y., Xu, X.H., Deng, C.Y., Wu, K.Y., Zhu, J., Fu, X.Q., He, M. and Luo, Z.G. (2011). Lgl1 activation of rab10 promotes axonal membrane trafficking underlying neuronal polarization. Dev. Cell. 21(3), 431-44.

Ye, Z. and Marth, J.D. (2004). N-glycan branching requirement in neuronal and postnatal viability. Glycobiology.14(6), 547-58.

Zinsmaier, K.E., Hofbauer, A., Heimbeck, G., Pflugfelder, G.O., Buchner, S. and Buchner, E. (1990). A cysteine-string protein is expressed in retina and brain of Drosophila. J. Neurogenet. 7(1), 15-29.

CHAPTER III

NEUROLOGICAL ROLES FOR PHOSPHOMANNOMUTASE TYPE 2 IN A NEW *DROSOPHILA* CONGENITAL DISORDER OF GLYCOSYLATION DISEASE MODEL

This paper has been accepted for publication under the same title in
Disease Models and Mechanisms, 2016

William M. Parkinson[1], Michelle Dookwah[4], Mary Lynn Dear[1], Cheryl L. Gatto[1,3], Kazuhiro Aoki[5], Michael Tiemeyer[4,5] and Kendal Broadie[1,2,3*]

Department of Biological Sciences[1], Department of Cell and Developmental Biology[2], Kennedy Center for Research on Human Development[3], Vanderbilt University, Nashville, TN 37235 USA

Department of Biochemistry and Molecular Biology[4], Complex Carbohydrate Research Center[5], The University of Georgia, Athens, GA 30602 USA

Translational Impact

1) *Clinical Issue*: The rapidly expanding congenital disorders of glycosylation (CDG) disease family results from mutation of genes encoding glycosylation pathway proteins, which drive the addition of carbohydrate moieties to proteins. The most common CDG, CDG-Ia or PMM2-CDG, is caused by loss of phosphomannomutase type 2 (PMM2), which converts mannose-6-phosphate into mannose-1-phosphate. This obligatory step is required for all N-linked glycosylation, an important and widespread glycan modification of extracellular proteins, which aids in many aspects of protein localization and function. Human CDG-Ia patients present with severe neurological impairments, including loss of coordinated movement and intellectual disability, and are often concomitantly afflicted with multi-organ dysfunction, infection and injury also contributing to reduced lifespan. Here, we generate the first *Drosophila* CDG-Ia disease model, showing phenotypes that strongly parallel patient neurological symptoms and compromised longevity. Previous animal models have revealed important aspects of CDG-Ia disease progression in neurodevelopment and cellular signaling, but are limited by the inability to study tissue-specific reduction of PMM2 function in a temporally and spatially-controlled manner. These capacities are provided in this *Drosophila* disease model, which allows assessment of developmental, cell type-specific PMM2 involvement.
2) *Results*: The new *Drosophila* PMM2-CDG disease model recapitulates the characteristic phenotypes of the human disease state. Using both *pmm2* null mutants and targeted RNAi knockdown, we demonstrate early lethality, severe loss of coordinately movement and reduced/dysregulated glycosylation. We focus on the neuromuscular junction (NMJ) that drives movement to reveal reduced levels of synaptic glycosylation coupled to structural overelaboration and functional strengthening. Based on phenotypes, we hypothesized that compromised NMJ synaptic glycosylation would alter matrix metalloproteinase (MMP) pathways known to modulate Wnt intercellular signaling. In testing this hypothesis, we discovered depressed MMP expression at the NMJ resulting in reduced Wnt Wingless (Wg) *trans*-synaptic signaling that modulates synaptic development and function.

3) *Implications and future directions*: Increasing evidence highlights the importance of glycosylation in neural development and function. The majority of CDG patients present with severe neurological symptoms; however, the causes remain very poorly understood. Here, we present a new *Drosophila* CDG-Ia model identifying a range of phenotypes that closely resemble human patient symptoms. This new model will allow in-depth studies to discover underlying causative mechanisms, decipher them, and ultimately inform drug design. The MMP and Wnt changes identified here represent candidate drug targets for treating CDG-Ia neurological symptoms. Discoveries aided by the relative high speed of *Drosophila* studies combined with the powerful, ever-expanding *Drosophila* genetic toolkit will open up new avenues for CDG-Ia therapeutic intervention.

Abstract

Congenital disorders of glycosylation (CDGs) constitute a rapidly growing family of human diseases resulting from heritable mutations in genes driving production and modification of glycoproteins. The resulting symptomatic hypoglycosylation causes multisystemic defects that include severe neurological impairments, revealing a particularly critical requirement for tightly regulated glycosylation in the nervous system. The most common CDG, CDG-Ia or PMM2-CDG, arises from phosphomannomutase type 2 (PMM2) mutations. Here, we report the generation and characterization of the first *Drosophila* PMM2-CDG model. CRISPR-generated *Drosophila pmm2* null mutants display severely disrupted glycosylation and early lethality, while RNAi-targeted neuronal PMM2 knockdown results in a strong shift in pauci-mannose glycan abundance, progressive incoordination and later lethality, closely paralleling human CDG-Ia symptoms of shortened lifespan, movement impairments and defective neural development. Analyses of the well-characterized *Drosophila* neuromuscular junction (NMJ) reveal synaptic glycosylation loss accompanied by structural architecture and functional neurotransmission defects. NMJ synaptogenesis is driven by intercellular signals traversing an extracellular synaptomatrix co-regulated by glycosylation and matrix metalloproteinases (MMPs). Specifically, Wnt Wingless (Wg) *trans*-synaptic signaling depends on the heparan sulfate proteoglycan (HSPG) co-receptor Dally-like protein (Dlp), which is regulated by synaptic MMP activity. Loss of synaptic MMP2, Wg ligand, Dlp co-receptor and downstream *trans*-synaptic signaling occurs with PMM2 knockdown. Taken together, this *Drosophila* CDG disease model provides a new avenue for the dissection of cellular and molecular mechanisms underlying neurological impairments and a means to discover and test novel therapeutic treatment strategies.

Introduction

Congenital disorders of glycosylation (CDGs) caused by mutation of genes encoding glycosylation pathway proteins are classified into two categories (Freeze et al., 2015): CDG-I disease states include defects in carbohydrate production, lipid-linked oligosaccharide (LLO) formation and attachment of glycan chains to amino acids; CDG-II disease states include defects in modification/maturation of glycan chains after protein attachment. The most common CDG is a CDG-I, called CDG-Ia or PMM2-CDG, resulting from mutations in phosphomannomutase 2 (PMM2) converting mannose-6-phosphate to mannose-1-phosphate, the obligatory precursor for GDP-mannose production and N-linked glycosylation (Andreotti et al., 2014; Freeze et al., 2014; Freeze et al., 2015). Since the first patient in 1980, >100 different mutations in >1000 CDG-Ia patients have been characterized (Freeze et al., 2014; Haeuptle and Hennet, 2009; Jaeken, 2013; Jaeken et al., 1980; Yuste-Checa et al., 2015). CDG-Ia infant mortality is ~20% in the first year, with patients manifesting subsequent increased susceptibility to organ failure, infection and injury (Grunewald, 2009). CDG-Ia patients present with a spectrum of neurological symptoms (Jaeken, 2013), ranging from severe neurological impairments with early death, to mild defects with slight psychomotor delay (Grunewald, 2009; Marquardt and Denecke, 2003). To date, no effective treatments are available, with the only treatment option being symptom management (Grunewald, 2009; Monin et al., 2014; Stefanits et al., 2014).

CDG-Ia modeling is critical for molecular and cellular studies. The initial mouse PMM2 knockout model has been of limited use owing to early embryonic lethality (Thiel et. al., 2006). Heteroallelic combination of two PMM2 mutations allows partial enzymatic activity, protracted embryonic survival and has demonstrated potential maternal dietary intervention in treatment (Schneider et al., 2011). Increased lifespan occurred with mannose feeding prenatally and during gestation, reportedly allowing offspring to develop past critical periods of PMM2-dependent glycan requirement (Schneider et al., 2011; Thiel et al., 2006). Unfortunately, these results have thus far not been successfully replicated in patient trials, where postnatal oral and intravenous mannose administration failed to improve serum protein glycosylation levels (Kjaergaard et al., 1998; Mayatepek and Kohlmuller, 1998). A subsequent zebrafish model established via PMM2 morpholino knockdown revealed increased motor neuron number,

altered cranial development, reduced motility and altered glycan profiles (Cline et al., 2012). Most recently, a similar *Xenopus* morpholino knockdown model demonstrated strong reduction in Wnt signaling, revealing a PMM2 requirement in intercellular communication (Himmelreich et al., 2015). These models have been valuable, but have limitations of morpholino-based approaches with inadequate targeting and concerns about the temporal maintenance of knockdown (Schulte-Merker and Stainier, 2014). We therefore set out to develop a *Drosophila* PMM2-CDG disease model.

The *Drosophila* genome encodes >70% of human disease genes (Reiter et al., 2001), including most linked to glycan-related disorders (Dani et al., 2012; Dani et al., 2014). The human N-linked glycome is more expansive, with higher levels of complex and hybrid branched forms (Katoh and Tiemeyer, 2013), but the N-glycosylation pathway is very highly conserved, with well-mapped glycan profiles and the *Drosophila* genetic toolkit allowing sophisticated manipulation (Altmann et al., 2001; Sarkar et al., 2006). For neurological impairments (Freeze, 2006; Freeze et al., 2015; Jaeken, 2013; Martin, 2003), *Drosophila* provides a host of anatomical, electrophysiological and behavioral assays for neural development and function (Dani el al., 2014; Gatto and Broadie, 2011; Jumbo-Lucioni et al., 2014; Parkinson et al., 2013). In particular, our glycomic RNAi screen uncovered a common role for glycosylation restricting the structure and function of the neuromuscular junction (NMJ) synapse (Dani et al., 2012). Subsequent work on screen hits, including heparan sulfate proteoglycan (HSPG) sulfotranserase (*hs6st*)/sulfatase (*sulf1*), UDP-GlcNAc:α-3-D-mannoside-β1,2-N-acetylglucosaminyl-transferase I (*mgat1*), α-N-acetylgalactosaminyltransferase (*pgant*), galactose-1-phosphate uridyl-transferase (*galt*) and related pathways (Dani et al., 2012; Dani et al., 2014; Jumbo-Lucioni et al., 2014; Parkinson et al., 2013), has shown disruption of *trans*-synaptic signaling to be a common root cause of the compromised NMJ synaptogenesis underlying movement phenotypes.

In this study, we generate a *Drosophila* CDG-Ia disease model. We show that *Drosophila pmm2* is highly conserved and manipulate gene function by making mutants with CRISPR/Cas9 genome editing and tissue-targeted transgenic RNAi. As in human CDG-Ia patients, *Drosophila pmm2* loss-of-function (LOF) mutants exhibit reduced lifespan and psychomotor retardation

proportional to the degree of PMM2 reduction. We show striking impacts on the N-linked glycome: globally in null mutants, neurally in tissue-targeted RNAi knockdown and locally at the NMJ synapse. At the NMJ, targeted pre- and postsynaptic PMM2 knockdown reveals architectural overelaboration, and concurrent reduction on both sides of the synapse strongly increases neurotransmission strength. PMM2 loss strongly impairs the synaptic matrix metalloproteinase (MMP) pathway regulating HSPG co-receptor Dally-like protein (Dlp) to modulate Wnt Wingless (Wg) *trans*-synaptic signaling (Dani et al., 2012; Dear et al., 2016; Freidman et al., 2013). Consistently, PMM2 knockdown reduces Wg, Dlp and the Frizzled Nuclear Import (FNI) pathway. These results suggest a PMM2-dependent extracellular proteinase mechanism modulates Wnt signaling during NMJ synaptogenesis, which underlies coordinated movement and maintained viability. This new *Drosophila* model should lead to novel therapeutic treatments for CDG-Ia.

Results

Degree of *Drosophila PMM2* loss determines lifespan duration

Human *pmm2* contains 8 exons compared to the *Drosophila* CG10688 *pmm2* single reading frame (Fig. 12A), making genetic manipulation and expression studies more amenable. Simplified site-directed CRISPR mutagenesis targeted at one exon reduces the possibility of truncated exons maintaining partial function. Human PMM2 contains 12 active sites that coordinately bind the substrate, mannose-6-phosphate, and convert it to mannose-1-phosphate (Andreotti et al., 2014; Silvaggi et al., 2006). *Drosophila* PMM2 shows 100% conservation of these 12 active sites (Fig. 12A, red) and identifies numerous additional regions of high 90-100% conservation (Fig. 12A, green). Overall, *Drosophila* PMM2 displays 56% amino acid identity compared to human PMM2 (Fig. 12A). To characterize PMM2 requirements, we first made null mutants using CRISPR/Cas9 genome editing directed at both 5' and 3' ends of *Drosophila pmm2* (Fig. 12A; Gratz et al., 2013). A total of 15 mutations were produced, all verified with direct sequencing: 8 frameshifts, 4 insertions, 2 deletions and 1 missense mutation. Two *pmm2* null frameshift mutations were selected for subsequent behavioral, functional and molecular studies, hereafter referred to as $pmm2^{FS1}$ and $pmm2^{FS2}$.

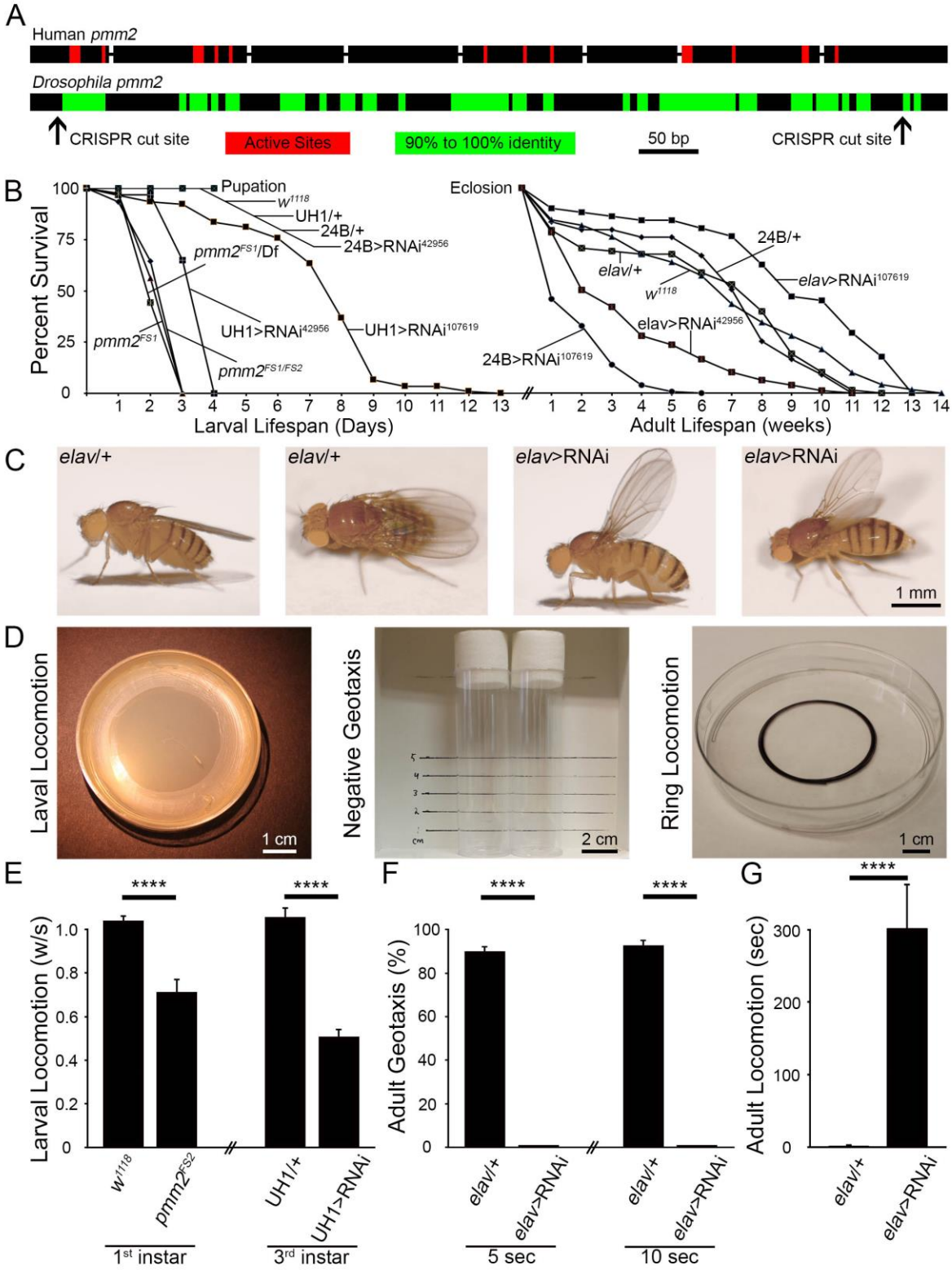
A
Human pmm2
Drosophila pmm2
CRISPR cut site
Active Sites
90% to 100% identity
50 bp
CRISPR cut site
B
Percent Survival
Pupation
w1118
UH1/+
24B/+
24B>RNAi42956
pmm2FS1/Df
UH1>RNAi42956
UH1>RNAi107619
pmm2FS1
pmm2FS1/FS2
Larval Lifespan (Days)
Eclosion
24B/+
elav/+
w1118
elav>RNAi107619
elav>RNAi42956
24B>RNAi107619
Adult Lifespan (weeks)
C
elav/+
elav/+
elav>RNAi
elav>RNAi
1 mm
D
Laval Locomotion
1 cm
Negative Geotaxis
2 cm
Ring Locomotion
1 cm
E
Larval Locomotion (w/s)
****
****
w1118
pmm2FS2
UH1/+
UH1>RNAi
1st instar
3rd instar
F
Adult Geotaxis (%)
****
****
elav/+
elav>RNAi
elav/+
elav>RNAi
5 sec
10 sec
G
Adult Locomotion (sec)
****
elav/+
elav>RNAi

Figure 12

Figure 12: *Drosophila* PMM2 levels determine lifespan and coordinated movement ability.

A) Comparison of human and *Drosophila pmm2* genes. Human *pmm2* contains 8 exons (black boxes) compared to the single reading frame in *Drosophila*. Highly conserved active sites (red) and other regions of high identity (90-100%, green) are depicted. CRISPR-generated null mutants were made at both 5' and 3' ends of *pmm2* (arrows). **B)** Larval lifespan of null mutants (*pmm2*^{FS1}, *pmm2*^{FS1}/Df and heteroallelic *pmm2*$^{FS1/FS2}$), and two driven RNAi lines (RNAi^{42956} and RNAi^{107619}) compared to controls (left). Adult lifespan with targeted neural (*elav*-Gal4) and muscle (24B-Gal4) *pmm2* RNAi compared to controls (right). **C)** Examples of wing posture with neural *pmm2* RNAi. **D)** Behavioral assays: larval locomotion on apple juice plates towards edge yeast attractant (left); adult negative geotaxis climbing to 2 cm height (middle), and adult horizontal locomotion for flies with wings removed exiting a 4 cm ring (right). **E)** Normalized quantification of 1st (left) and 3rd instar (right) larval locomotion (peristaltic waves/second) in genotypes shown. **F)** Quantification of adult negative geotaxis as percent animals climbing to 2cm height at 5 (left) and 10 (right) seconds. **G)** Quantification of adult horizontal locomotion as time to exit 4cm ring). Significance: $p<0.0001$ (****). Sample sizes: $n\geq17$ animals/genotype.

Two independent UAS-RNAi lines (Bloomington *Drosophila* Stock Center #42956 and Vienna *Drosophila* Resource Center v107619) were used to differentially reduce *pmm2* levels. Quantitative PCR (qRT-PCR) with ubiquitous (UH1-Gal4) expression shows both RNAi lines knockdown *pmm2* transcripts by >77%, a significant ($p<0.001$) reduction compared to UH1-Gal4/+ transgenic controls. Of the two lines, 42956 is significantly more effective than 107619 in reducing *pmm2* levels (UH1>RNAi^{107619}, 1.57±0.10; UH1>RNAi^{42956}, 1.27±0.10; n=15, p=0.016) compared to control (UH1-Gal4/+, 7.00±0.79, n=15). Moreover, at 50% lethality of ubiquitous *pmm2* knockdown (42956) (Fig. 12B), *pmm2* levels in UH1-Gal4/+ controls show a sharp increase (1st instar, 1.40±0.15, n=8; 2nd instar 7.00±0.79, n=15), which is paralleled by the surviving ubiquitous *pmm2* knockdown (107619), permitting higher levels of maintained *pmm2* expression. The strong (42956) and weak (107619) PMM2 knockdown phenotypes are likely the result of the significant differences in transcript levels.

Null *pmm2* mutants, heteroallelic combinations and mutants over deficiency all show identical early larval lethality during the late 1st to early 2nd instar transition (Fig. 12B). Half-time survival (HTS) is similar (e.g. *pmm2^{FS1}* HTS 51 hours post-hatching (hph), n=73; *pmm2^{FS1}*/Df HTS 46 hours post-hatching (hph), n=79; *pmm2^{FS2}*/Df HTS 51 hours post-hatching (hph), n=84; *pmm2^{FS1}*/*pmm2^{FS2}* HTS 52 hph, n=75). Ubiquitous *pmm2* knockdown (42956) results in lifespan only marginally longer than *pmm2* nulls (HTS: 68 hph; n=63), whereas the weaker ubiquitous *pmm2* knockdown (107619)allows survival to late larval stages (HTS: 168 hph; n=90) with some pupation (mean 192 hph; Fig. 12B). UH1/+ controls pupate at 96 hph, showing ubiquitous *pmm2* knockdown (107619)exhibits severe developmental delay. Muscle-specific 24B-Gal4 with the stronger RNAi^{42956} produces 100% pupal lethality, whereas weaker 24B>RNAi^{107619} survives with reduced adult lifespan (HTS: 10 days; n=159) compared to control (24B-Gal4/+, HTS: 38 days; n=79; Fig. 12B). Targeted neural *elav*-Gal4 with RNAi^{42956} exhibits similarly reduced adult lifespan (HTS: 17 days; n=92), which is conversely extended with weak *elav*>RNAi^{107619} (HTS: 65 days; n=51) compared to control (*elav*-Gal4/+, HTS: 39 days; n=68; Fig. 12B). This suggests a delicate PMM2 balance, with strong neural loss detrimental but moderate neural loss extending lifespan. Due to these lethality constraints, hereafter weaker RNAi^{107619} is used for ubiquitous knockdown and stronger RNAi^{42956} is used for tissue-targeted neural and muscle knockdown.

Neuronal PMM2 maintains normal posture and coordinated movement

Neurological movement symptoms in CDG-Ia patients range from slight gait ataxia to severe cerebellar ataxia; most children are unable to walk unassisted, and most adults are wheel-chair bound (Barone et al., 2014; Barone et al., 2015; Marquardt and Denecke, 2003; Monin et al., 2014). Loss of *Drosophila* PMM2 results in similarly severe postural and movement phenotypes, largely due to nervous system involvement. Targeted neural *elav*-Gal4 knockdown results in a highly penetrant "held-out wings" posture (Fig. 12C), which is associated with defects in flight muscle control of wing positioning (Muller et al., 2010; Zaffran et al., 1997). Neural *pmm2* knockdown adults have severe ataxia, with profound incoordination, inability to walk in a directed fashion and complete inability to fly. Weak muscle-specific PMM2 knockdown does not yield ataxia. However, strong muscle-specific knockdown allows pupae to develop fully, but not a single pharate adult properly ecloses. A few animals partially eclose before dying, and animals mechanically freed from pupal cases do not move or survive. Based on these severe qualitative movement defects, we conducted a range of quantitative analyses (Fig. 12D).

Larval locomotion requires a CNS pattern generator driving coordinated stimulation of segmental nerves to drive neuromuscular junction (NMJ) transmission evoking coordinated muscle contraction (Gjorgjieva et al., 2013; Kohsaka et al., 2014; Nichols et al., 2012; Sokolowski, 1980). Locomotion was assayed on apple juice agar plates, monitoring movement from the barren center to a yeast reward located along the rim (Fig. 12D, left). At 24 hph, *pmm2* null 1st instar mutants display a significant reduction in coordinated movement, as measured in peristaltic waves/second (*pmm2*^{FS2}, 0.71±0.06 w/s; n=17) compared to genetic control (*w*^{1118}, 1.04±0.02 w/s; n=17; p<0.0001; Fig. 12E). Both lifespan and movement data show ubiquitous *pmm2* knockdown (42956) phenocopies the *pmm2* genetic nulls. Similarly, 3rd instar ubiquitous *pmm2* knockdown (107619)show a comparable reduction in larval locomotion in peristaltic waves/second (0.51±0.04 w/s; n=20) compared to controls (UH1-Gal4/+, 1.06±0.04 w/s; n=20, p<0.0001; Fig. 12E). Thus, global PMM2 loss dramatically impairs coordinated movement needed to maintain viability.

Neural-specific PMM2 involvement was next tested in adults, using a range of established assays (Nichols et al., 2012). Negative geotaxis assays animals the ability to climb vertically (2cm) from the bottom of a vial (Fig. 12D, middle). Neurally-targeted *elav*-Gal4>RNAi^{42956} prevents this simple task, whereas nearly all control animals display the necessary coordinated locomotion at 5 seconds (*elav*-Gal4/+, 90±2.1%, n=50) and 10 seconds (*elav*-Gal4/+, 93±2.4%, n=50; Fig. 12F). Not a single *pmm2* RNAi animal performed the task (n=40, p<0.0001). A less demanding horizontal locomotion assay measures the time required to escape a 4cm diameter circle (Fig. 12D, right). Neurally-targeted *elav*-Gal4>RNAi^{42956} results in a 150-fold delay (302.0±60.02 sec; n=15) compared to controls (*elav*-Gal4/+, 1.93±0.32 sec; n=15; p<0.0001; Fig. 12G). Mutants exit the ring by uncoordinated flailing/kicking, with only a few animals crossing the circle in a directed, purposeful manner. These results show a strong PMM2 role for coordinated movement, similar to CDG-Ia patient symptoms, with a striking PMM2 impact on neurons.

PMM2 loss suppresses N-glycosylation and enhances glycan turnover

To assess N-linked glycoprotein glycosylation levels correlating with movement defects in *pmm2* null mutants and neurally-targeted RNAi knockdown, we next assayed glycome composition. Human CDG-Ia patients display altered glycosylation status, including reduced concanavalin A (ConA) binding but increased fucose-decorated glycoproteins (Dijk et al., 2001). In *Drosophila*, at all stages of development and in all tissues, the major N-linked glycoprotein constituent glycans include high-mannose and pauci-mannose ($\geq$3 mannose residues) classes, whereas human glycosylation is typically more branched and complexly decorated (ten Hagen et al., 2009; Katoh and Tiemeyer, 2013). Complex hybrid and branched N-glycans are present in *Drosophila*, but at much lower relative abundances (Aoki et al., 2007). Here, *Drosophila* N-linked glycans were analyzed by mass spectrometry (MS) throughout the larval body in *pmm2* null mutants and with combined neuronal (*elav*-Gal4) and muscle (24B-Gal4) *pmm2* RNAi, and in adult heads only with neurally targeted *pmm2* RNAi (Fig. 13).

N-linked glycans were released from equal amounts of input *pmm2* null (*pmm2*^{FS1}) compared to genetic background control (*w*^{1118}). Proteins analyzed by MS were dramatically

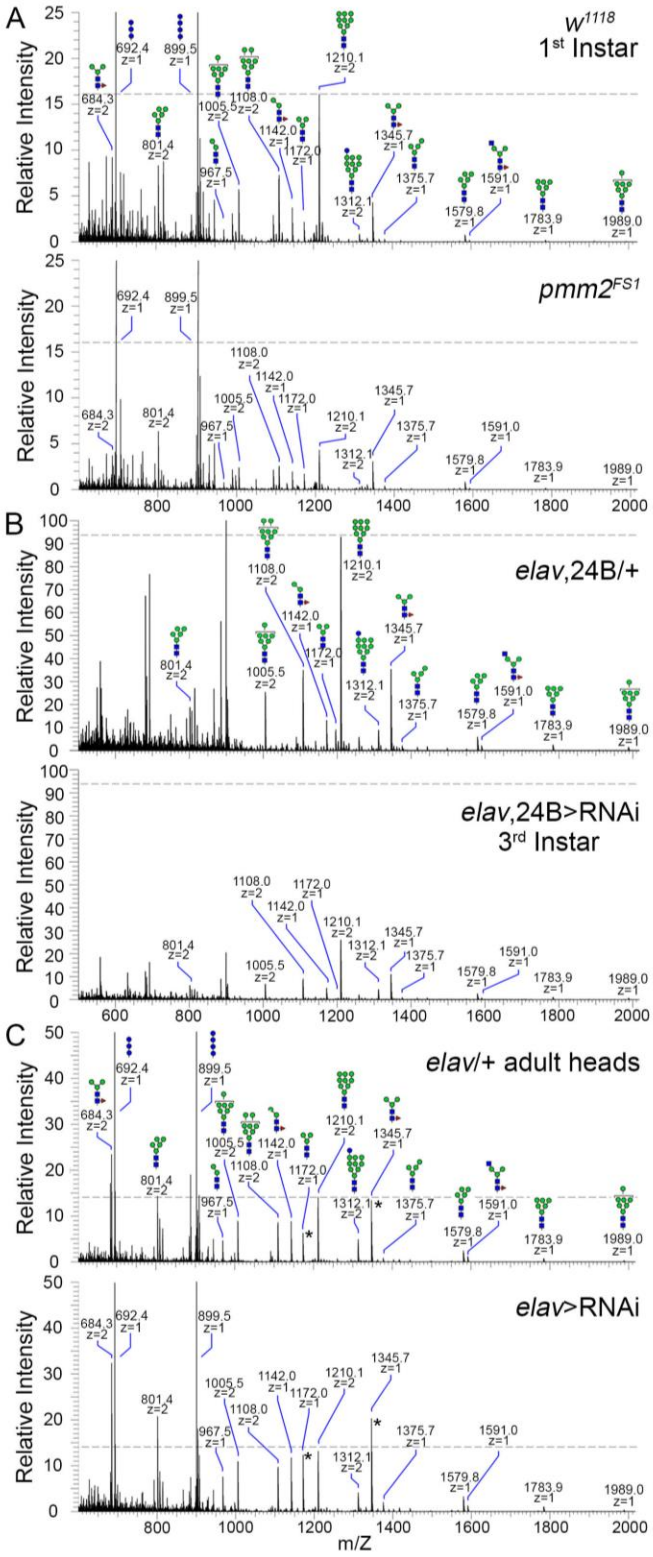
A
w1118
1st Instar
pmm2FS1
B
elav,24B/+
elav,24B>RNAi
3rd Instar
C
elav/+ adult heads
elav>RNAi
Relative Intensity
m/Z

Figure 13

Figure 13: PMM2 loss dramatically alters N-linked glycoprotein glycosylation.

Full mass spectrometry (MS) spectra for permethylated glycans harvested from **(A)** age-matched w^{1118} genetic control (top) and $pmm2^{FS1}$ null (bottom) 1st instars, **(B)** *elav*-Gal4,24B-Gal4/+ transgenic control (top) and *elav*-Gal4,24B-Gal4>RNAi^{42956} (bottom) 3rd instars, and **(C)** *elav*-Gal4/+ transgenic control (top) and *elav*-Gal4>RNAi^{42956} (bottom) adult heads. Dashed lines indicate the relative abundance of $Man_9GlcNAc_2$ (m/z=1210.1, doubly-charged) in each control for comparison with mutants across genotypes. In all panels, mass peaks at m/z=692.4 and 899.5 are Hex_3 and Hex_4 glycans spiked into samples as external calibration standards. The cartoon representations of glycan structures are shown in accordance with glycomics community conventions (Varki and Sharon, 2009).

reduced for all major classes (high-mannose, pauci-mannose and complex; Fig. 13A). For example, the relative abundance of $Man_9GlcNAc_2$ (m/z=1210.1, doubly-charged), a dominant structure in the glycan profile, is down 4-fold in *pmm2* null mutants (Fig. 13A; dashed line). All other detected N-glycans exhibit comparable reductions, consistent with a global suppression of glycoprotein glycosylation. A similar global reduction occurs in 3rd instar larva using paired neural and muscle Gal4s to drive *pmm2* RNAi (*elav*,24B>RNAi^{42956}; Fig. 13B). Interestingly, neurally-targeted *pmm2* RNAi in the adult head does not produce the same phenotype. N-linked glycan quantities are relatively comparable for transgenic control (*elav*-Gal4/+) and this targeted *pmm2* knockdown (*elav*-Gal4>RNAi^{42956}; Figs. 13C). Major complex N-linked glycans (e.g. NM_3N_2F, m/z=1591.0, singly-charged) are not noticeably changed in abundance. However, pauci-mannose glycans display clearly increased abundance. For example, the core-fucosylated trimannosyl glycan M_3N_2F (m/z=1345.7, singly-charged) is increased in relative abundance, as is non-fucosylated M_3N_2 (m/z=1172.0, singly charged), with *pmm2* knockdown (Figs. 13C).

Loss of N-linked glycoprotein glycosylation in *pmm2^{FS1}* mutants implies decreased efficiency in glycosylation initiation by the oligosaccharyltransferase complex (OST) in the endoplasmic reticulum, and/or increased ERAD-mediated protein deglycosylation within the cytoplasm (Gao et al., 2011). Either mechanism should be reflected in increased abundance of free oligosaccharide (FOS), branched oligosaccharides unbound to lipid or protein,, either due to endogenous PNGase release or via lipid-linked precursor hydrolysis by the OST (Cline et al., 2011; Gao et al., 2011). Consistently, FOS abundance is strikingly increased in *pmm2^{FS1}* mutants (Fig. 14A). FOS abundance is detected as products of PNGase and endo-N-acetylglucosaminidase digestion (N1, blue asterisks) or glycans possessing two reducing terminal GlcNAc residues (N2, red asterisks; Fig. 14A), with total ion mapping chromatograms filtered for loss of non-reducing terminal HexNAc residues. Both FOS classes are increased in *pmm2* nulls compared to control (Fig. 14A). Thus, glycomics and FOS assays show striking reduction in mature glycan abundance globally, and altered glycomic repertoire in the nervous system with PMM2 loss. To test for cellular requirements, we next moved to the well-characterized NMJ driving movement.

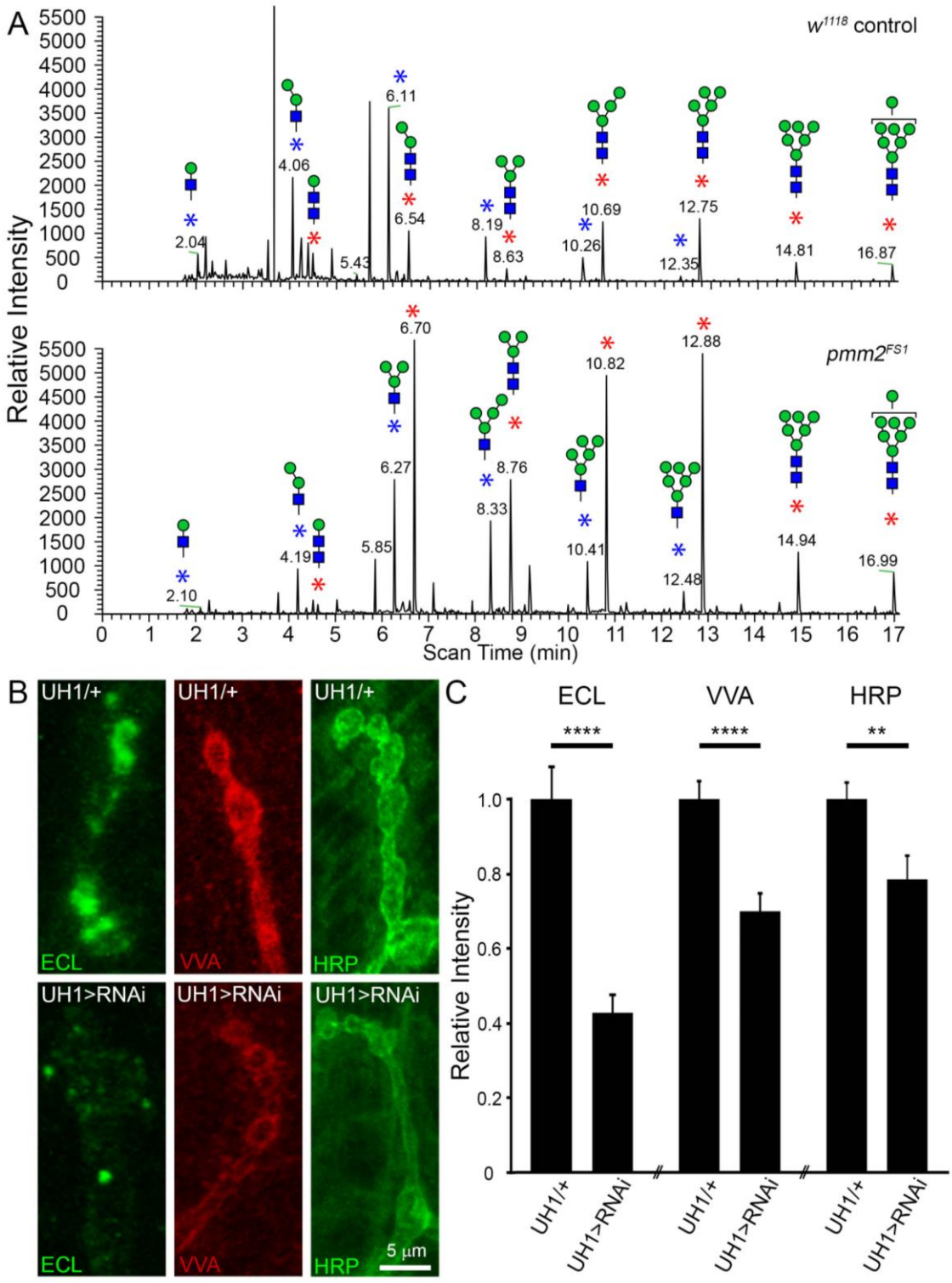
A
w1118 control
pmm2FS1
Relative Intensity
Scan Time (min)
2.04
4.06
5.43
6.11
6.54
8.19
8.63
10.26
10.69
12.35
12.75
14.81
16.87
2.10
4.19
5.85
6.27
6.70
8.33
8.76
10.41
10.82
12.48
12.88
14.94
16.99
B
UH1/+
UH1>RNAi
ECL
VVA
HRP
5 µm
C
ECL
VVA
HRP
****
****
**
Relative Intensity
UH1/+
UH1>RNAi

Figure 14

Figure 14: PMM2 loss increases FOS and reduces NMJ N-linked glycoprotein glycosylation.

A) Free oligosaccharides (FOS) from w^{1118} genetic control and $pmm2^{FS1}$ null 1st instar larvae. FOS detected as products of sequential PNGase and endo-N-acetylglucosaminidase digestion (N1, blue asterisks), or as glycans with 2 reducing terminal GlcNAc residues (N2, red asterisks). Total ion mapping chromatograms filtered for loss of non-reducing terminal HexNAc residues to show the two FOS classes. **B)** Representative images of *Erythrina cristagalli* (ECL, green; left), *Vicia villosa* (VVA, red; middle) and horse radish peroxidase (HRP, green; right) NMJ labeling in *pmm2* knockdowns (bottom) compared to transgenic controls (top). **C)** Quantification of fluorescent labeling intensity in UH1-Gal4/+ transgenic control vs. UH1-Gal4>RNAi^{107619}. Significance: $p \leq 0.01$ (**), $p \leq 0.0001$ (****). Sample sizes: $n \geq 24$ NMJs/12 animals per genotype.

PMM2 maintains the normal glycan environment in the NMJ synaptomatrix

Glycan-binding lectin probes have long been used to chart the cellular carbohydrate landscape at both mammalian and *Drosophila* synapses (Jumbo-Lucioni et al., 2014; Parkinson et al., 2013; Schneider et al., 2011). To assay the composition of the heavily-glycosylated larval NMJ synaptomatrix, we utilized a panel of lectins, including *Erythrina cristagalli* (ECL) to label D-galactose glycans, *Vicia villosa* (VVA) to label N-acetylgalactosamine glycans, and anti-horseradish peroxidase (HRP) to lab alpha1-3-linked fucose moieties (Jumbo-Lucioni et al., 2014; Kurosaka et al., 1991). Both ECL and VVA reveal strong reductions in ubiquitous *pmm2* knockdown (107619) compared to the UH1-Gal4/+ controls (Fig. 14B). Quantification reveals >50% ECL reduction (UH1-Gal4>RNAi^{107619}, 0.43±0.05; UH1-Gal4/+, 1.00±0.08; n=24; $p<0.0001$) and >30% VVA reduction (UH1-Gal4>RNAi^{107619}, 0.69±0.05; UH1-Gal4/+, 1.00±0.05; n=24; $p<0.0001$; Fig. 14C). HRP is reduced by $\geq$20% (UH1-Gal4>RNAi^{107619}, 0.79±0.06; UH1-Gal4/+, 1.00±0.06; n=24; $p\leq0.01$; Fig. 14C). Dual neural and muscle knockdown *elav*-Gal4,24B-Gal4 RNAi also exhibits $\geq$20% HRP loss (*elav*-Gal4,24B>RNAi^{42956}, 0.79±0.06; *elav*-Gal4,24B/+, 1.0±0.04; $n\geq26$, $p<0.008$). These results indicate a robustly altered glycan composition within the NMJ synaptomatrix, which earlier studies have linked to defects in NMJ structural and functional development.

PMM2 restricts NMJ structural growth and synaptic bouton differentiation

Loss of synaptomatrix glycosylation has been shown to result in elevated structural elaboration of the *Drosophila* NMJ, as evidenced by increased branching and excess synaptic boutons (Jumbo-Lucioni et al., 2014; Parkinson et al., 2013). To examine NMJ architecture, we characterized wandering 3rd instar muscle 4 NMJs labeled for HRP and Discs Large (DLG), to illuminate pre- and postsynaptic compartments, respectively (Fig. 15A). Synaptic branches (defined as HRP-positive processes with >2 boutons), boutons (defined as DLG-positive synaptic varicosities >1□m in diameter) and NMJ terminal area (based on DLG-positive labeling) were all quantified (Fig. 15B-D). Cell-specific requirements were tested with neuronal (*elav*) and muscle (24B) targeted Gal4 drivers in comparison to ubiquitous (UH1-Gal4) *pmm2* knockdown. In all cases, loss of PMM2 results in clear NMJ overelaboration, with more branches and

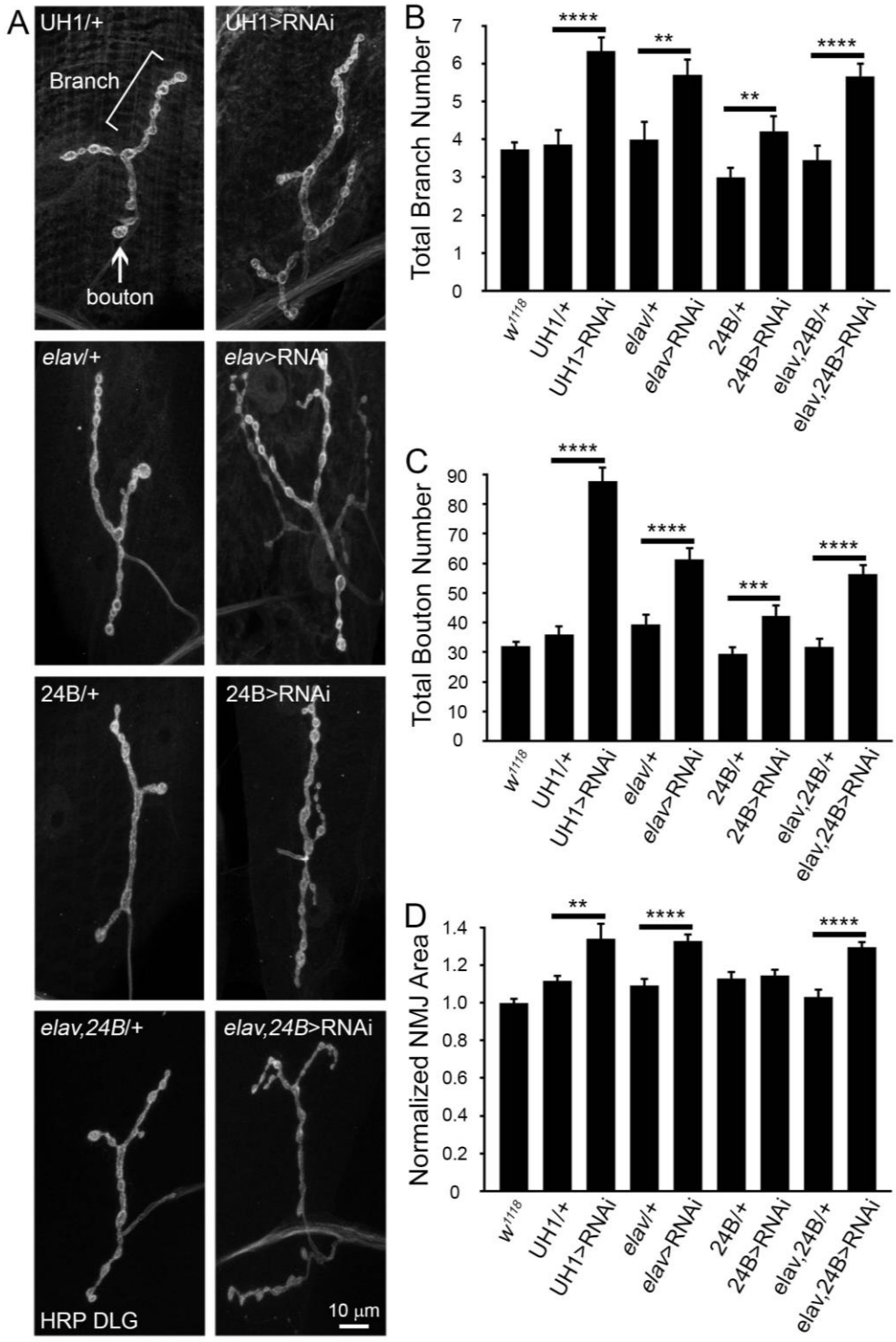
A
UH1/+
UH1>RNAi
Branch
bouton
elav/+
elav>RNAi
24B/+
24B>RNAi
elav,24B/+
elav,24B>RNAi
HRP DLG
10 µm
B
Total Branch Number
C
Total Bouton Number
D
Normalized NMJ Area
w1118
UH1/+
UH1>RNAi
elav/+
elav>RNAi
24B/+
24B>RNAi
elav,24B/+
elav,24B>RNAi

Figure 15

Figure 15: PMM2 loss results in striking NMJ synaptic structural overgrowth.

A) Representative wandering 3rd instar muscle 4 NMJ images of ubiquitous (UH1, top), neural (*elav*, second), muscle (24B, third) and double (*elav*, 24B, bottom) driver controls (left column), compared to RNAi-mediated *pmm2* knockdown (right). NMJs are co-labeled for presynaptic HRP and postsynaptic DLG, merged and shown in black-and-white to best illustrate structure. Quantification of NMJ branch number **(B)**, bouton number **(C)** and terminal area **(D)** in the above 8 genotypes compared to w^{1118} (9 genotypes total). Significance: $p \leq 0.01$ (**), $p \leq 0.001$ (***), $p \leq 0.0001$ (****). Sample sizes: $n \geq 22$ NMJs/12 animals for each genotype.

supernumerary type Is/Ib synaptic boutons, with ubiquitous RNAi resulting in the greatest level of unrestrained NMJ overgrowth (Fig. 15).

PMM2 loss increases NMJ branching, due to both pre- and postsynaptic roles (Fig. 15A). Ubiquitous *pmm2* RNAi increases branch number ~2-fold (UH1-Gal4>RNAi^{107619}, 6.3±0.36 branches, n=24) compared to controls (*w*^{1118}, 3.7±0.19, n=88; UH1-Gal4/+, 3.9±0.38 branches, n=22; p<0.0001; Fig. 15B). Likewise, neural (*elav*) and muscle (24B) knockdown more weakly increase terminal branch number (*elav*, 5.7±0.40; 24B, 4.2±0.39; *elav,*24B, 5.7±0.33 branches) compared to transgenic controls (*elav-Gal4*/+, 4.0±0.47; 24B-Gal4/+, 3.0±0.24; *elav,*24B-Gal4/+, 3.5±0.37 branches; p<0.01, p<0.01 and p<0.0001 respectively; Fig. 15B). Consistently, bouton number is elevated >2-fold with ubiquitous PMM2 removal (UH1-Gal4>RNAi^{107619}, 88±3.9 boutons, n=24) relative to controls (*w*^{1118}, 32±1.4, n=88; UH1-Gal4/+, 36±2.4 boutons, n=22; p<0.0001; Fig. 15C). Bouton number is also elevated with neural and muscle knockdown (*elav*, 61±3.8; 24B, 42±3.0; *elav*,24B, 56.5±2.9 boutons) compared to controls (*elav-Gal4*/+, 39±3.3; 24B-Gal4/+, 30±2.0; *elav*,24B/+, 31.8±2.7 boutons; p<0.0001, p<0.001 and p<0.0001 respectively; Fig. 15C). Finally, analyses of synaptic terminal area show increased size with ubiquitous, neuronal and co-neural/muscle PMM2 loss (p<0.01, p<0.0001 and p<0.0001, respectively), but with no significant change upon muscle-specific PMM2 removal (Fig. 15D).

Synaptic over-elaboration defects occur across the neuromusculature. Compared to the above lateral muscle 4 defects (Fig. 15), ventral muscles 6/7 exhibit comparable NMJ phenotypes. For example, the synaptic area in *elav*-Gal4,24B-Gal4/+ transgenic controls (380.82□m^2) is dramatically expanded in neural and muscle combined knockdown *elav*-Gal4,24B-Gal4<RNAi^{42956} (526.82□m^2), a highly significant (p>0.0001) increase. Early lethal *pmm2* genetic null mutants also exhibit similarly increased NMJ growth and structural elaboration in the 1st instar prior to developmental arrest (Fig. 16). Using the structural parameters as above, *pmm2* nulls manifest increased synaptic branch number (*w*^{1118}, 1.6±0.11; *pmm2*^{FS2}, 2.2±0.14 branches; p=0.007; Fig. 16B), more bouton formation (*w*^{1118}, 5.6±0.21; *pmm2*^{FS2}, 7.0±0.32 boutons; p=0.0006; Fig. 16C) and dramatically increased synaptic area (*w*^{1118}, 1.0±0.07; *pmm2*^{FS2}, 1.5±0.05 ; p=0.0001; Fig. 16D). Consistently, *pmm2* null mutants exhibit a loss of synaptic N-linked glycosylation, including ≥20% decrease in HRP glycan labeling

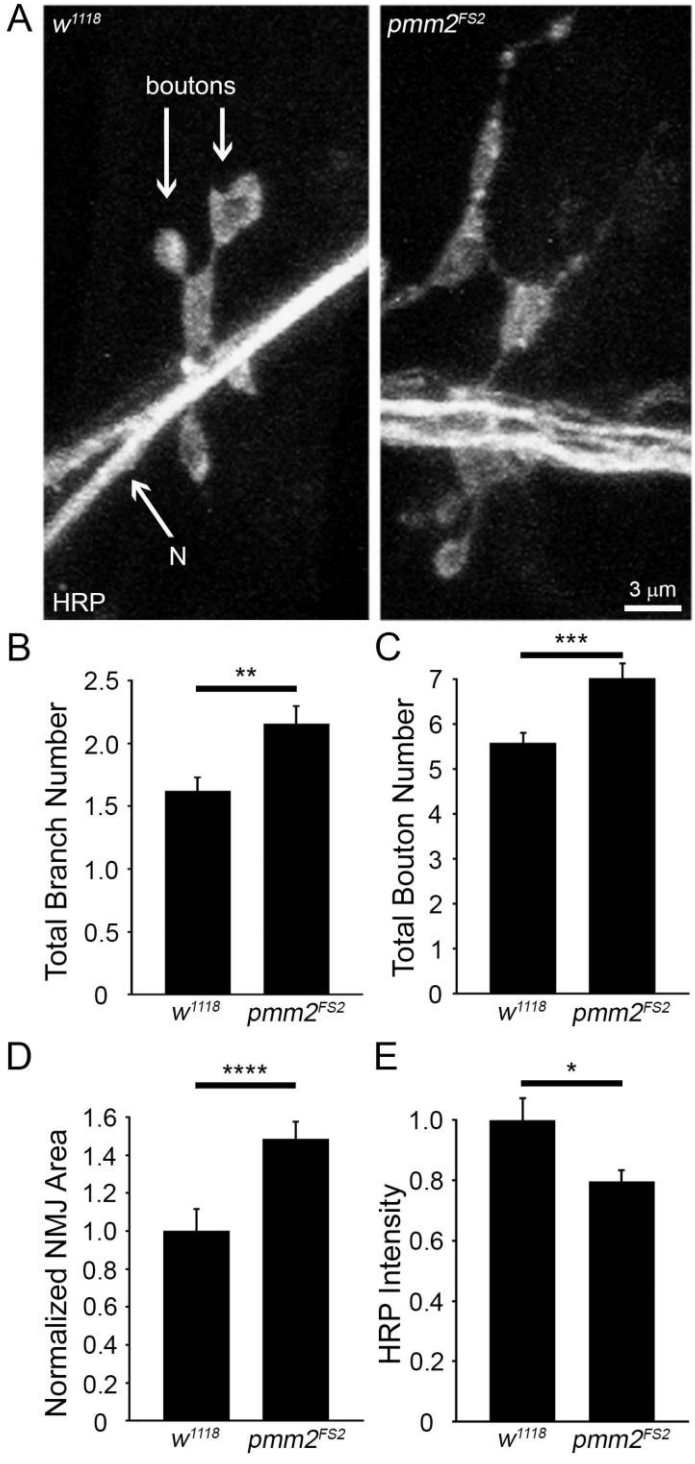
A
w1118
pmm2FS2
boutons
N
HRP
3 μm
B
Total Branch Number
**
C
Total Bouton Number
***
D
Normalized NMJ Area
****
E
HRP Intensity
*

Figure 16

Figure 16: Early lethal *pmm2* null mutants exhibit NMJ overgrowth and loss of N-glycans.

A) Representative 1st instar muscle 4 NMJ images from genetic background control (w^{1118}, left) and *pmm2* null mutant ($pmm2^{FS2}$, right). NMJs are labeled for the presynaptic anti-HRP. Quantification of synaptic branch number **(B)**, bouton number **(C)**, synaptic terminal area **(D)** and HRP fluorescence labeling intensity **(E)**. Significance: $p \leq 0.05$ (*), $p \leq 0.01$ (**), $p \leq 0.001$ (***) and $p < 0.0001$ (****). Sample sizes: $n \geq 30$ NMJs/13 animals per genotype.

(w^{1118}, 1.0±0.08; $pmm2^{FS2}$, 0.80±0.04; n≥30, p≤0.05; Fig. 16E). To determine how NMJ overgrowth compares to synaptic function, we next turned to electrophysiological studies.

Coupled pre- and postsynaptic PMM2 function limits NMJ transmission strength

Glycosylation has been shown to play key roles in NMJ functional differentiation and the determination of neurotransmission strength (Dani et al., 2012; Dani et al., 2014; Parkinson et al., 2013). The severely impaired coordinated locomotion and alterations in NMJ structure similarly suggest PMM2 roles in synaptic function. We tested neurotransmission in the two-electrode voltage-clamp (TEVC) recording configuration, by stimulating the motor nerve with a glass suction electrode and measuring the evoked excitatory junctional current (EJC) from the voltage-clamped muscle (Parkinson et al., 2013). To compare EJC transmission properties, 10 consecutive stimulation recordings were made at 0.2Hz, and then averaged to calculate the mean peak transmission amplitude. Cell-specific roles in functional differentiation were tested with targeted neuronal (*elav*) and muscle (24B) Gal4 drivers, alone and in combination, in comparison to ubiquitous (UH1-Gal4) *pmm2* RNAi knockdown (Fig. 17).

PMM2 loss dramatically increases neurotransmission strength due to an unusual coupled role in both pre- and postsynaptic cells (Fig. 17A). Sample recordings show that all transgenic controls and the genetic background control (w^{1118}) have comparable EJC properties, and only ubiquitous and combined pre- and postsynaptic PMM2 knockdown strongly and equally increase transmission amplitude (Fig. 17A). Ubiquitous RNAi increases peak EJC values by ~75% (UH1-Gal4>RNAi^{107619}, 1.73±0.09 (450.2±23.72nA), n=21; w^{1118}, 1.00±0.03 (253.68±8.26nA), n=44; UH1-Gal4/+, 1.11±0.06 (288.57±14.39nA), n=21; p<0.0001; Fig. 17B). Strong PMM2 knockdown in either neuron (*elav*-Gal4>RNAi^{42956}, 1.03±0.04 (301.8±12.66nA), n=16) or muscle (24B-Gal4>RNAi^{42956}, 1.20±0.05 (320.7±13.41nA), n=18) has no significant impact on amplitude compared to controls (*elav*-Gal4/+, 0.99±0.04 (289.9±12.09nA), n=17; 24B-Gal4/+, 1.20±0.04 (302.4±10.90nA), n=16; Fig. 17B). However, coincident *pmm2* RNAi driven in both the presynaptic neuron and postsynaptic muscle again shows significantly (p<0.0001) increased EJCs (*elav*-Gal4,24B-Gal4>RNAi^{42956}, 1.91±0.05 (397.61±11.58nA), n=23)

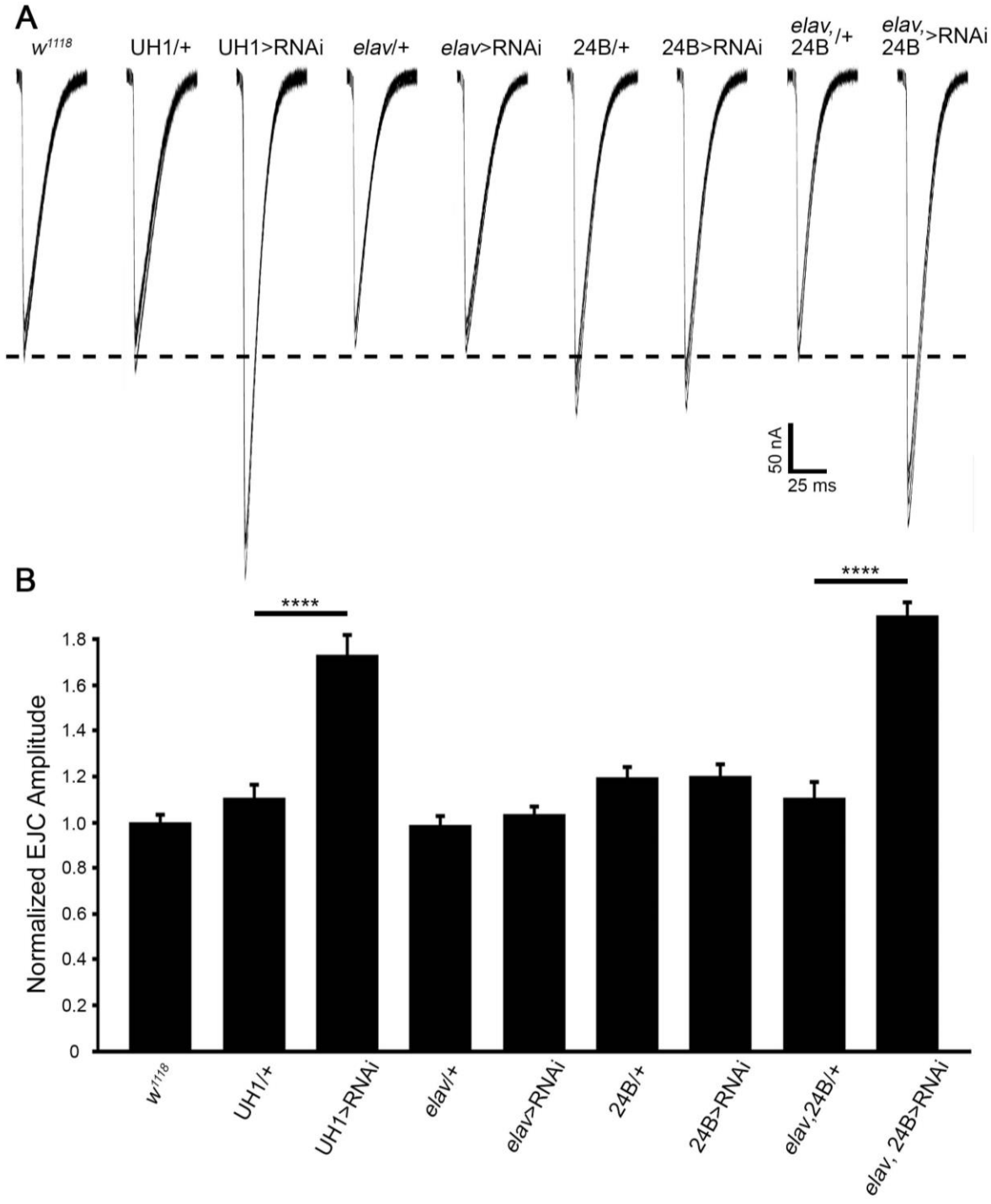
A
w1118
UH1/+
UH1>RNAi
elav/+
elav>RNAi
24B/+
24B>RNAi
elav, 24B/+
elav, 24B>RNAi
50 nA
25 ms
B
****
****
Normalized EJC Amplitude
0
0.2
0.4
0.6
0.8
1.0
1.2
1.4
1.6
1.8
w1118
UH1/+
UH1>RNAi
elav/+
elav>RNAi
24B/+
24B>RNAi
elav;24B/+
elav; 24B>RNAi

Figure 17

Figure 17: Coupled pre- and postsynaptic PMM2 removal increases neurotransmission.

A) Representative two-electrode voltage-clamp (TEVC) recordings of nerve-stimulation evoked excitatory junctional currents (EJCs) from wandering 3rd instar muscle 6. Superimposed traces are shown in response to nerve stimulation at 1.0mM Ca^{2+} comparing UH1-Gal4>RNAi^{107619}, *elav*-Gal4>RNAi^{42956}, 24B-Gal4>RNAi^{42956} and *elav*-Gal4, 24B-Gal4>RNAi^{42956} to w^{1118} and Gal4 diver alone controls. Quantification of peak EJC amplitude normalized to w^{1118} **(B)** and neurotransmission quantal content **(C)** Significance: $p \leq 0.0001$ (****). Sample sizes: $n \geq 16$ NMJs/8 animals per genotype.

compared to the dual driver control alone (*elav*-Gal4,24B-Gal4/+, 1.11±0.07 (231.0±14.56nA), n=23; Fig. 17B). We next recorded miniature evoked junction currents (mEJC) in neural and muscle combined knockdown *elav*-Gal4,24B-Gal4>RNAi^{42956} but did not detect any significant change in either frequency (*elav*-Gal4,24B-Gal4/+, 1.80±0.11 Hz; *elav*-Gal4,24B-Gal4/42956, 1.93±0.14 Hz; n.s. n=20) or amplitude (*elav*-Gal4,24B-Gal4/+, 0.66±0.02 nA; *elav*-Gal4,24B-Gal4/42956, 0.61±0.03 nA; n.s. n=20) compared with control but quantal content (QC) was elevated >80% (*elav*-Gal4,24B-Gal4/+, 362.0±13.9 QC; *elav*-Gal4,24B-Gal4/42956, 677.6±29.9 QC; Fig. 17C)). Thus, PMM2 specifically regulates evoked quantal content (Fig. 17C). These results indicate the NMJ functional defect is not cell autonomous, as either pre- or postsynaptic PMM2 is sufficient to properly regulate neurotransmission strength. We therefore began to test non-cell autonomous molecular mechanisms that could underlie the PMM2 function.

PMM2 positively regulates the synaptic extracellular matrix proteinase pathway

Extracellular mechanisms in the highly-glycosylated NMJ synaptomatrix provide an obvious answer to PMM2 non-cell autonomous phenotype. We were first guided to consider extracellular matrix metalloproteinase (MMP) pathways owing to common tracheal break and melanization mutant phenotypes (Glasheen et al., 2010; Page-McCaw et al., 2007; Zhang and Ward, 2009) shared with PMM2 loss-of-function (data not shown). Subsequently, recent work has shown that *mmp* mutants exhibit both NMJ structural and functional phenotypes strikingly similar to PMM2 loss-of-function (Dear et al., 2016). Therefore, we examined the matrix metalloproteome at the NMJ, which includes secreted MMP1, GPI-anchored MMP2 and their shared secreted tissue inhibitor of MMP (TIMP) (Dear et al., 2016; Kessenbrock et al., 2010; Page-McCaw et al., 2007). We hypothesized that PMM2-dependent glycan modification of these extracellular proteins, and/or their synaptic substrates, could provide a mechanism regulating NMJ structure and function. Consistent with this hypothesis, utilizing PNGaseF and EndoH to remove N-linked glycosylation (Song et al., 2011) reveals a clear reduction in MMP size (Fig. 18A), showing a high level of glycosylation (Glasheen et al., 2009; Jia et al., 2014). This change is much greater for membrane-anchored MMP2, in which all major isoforms show

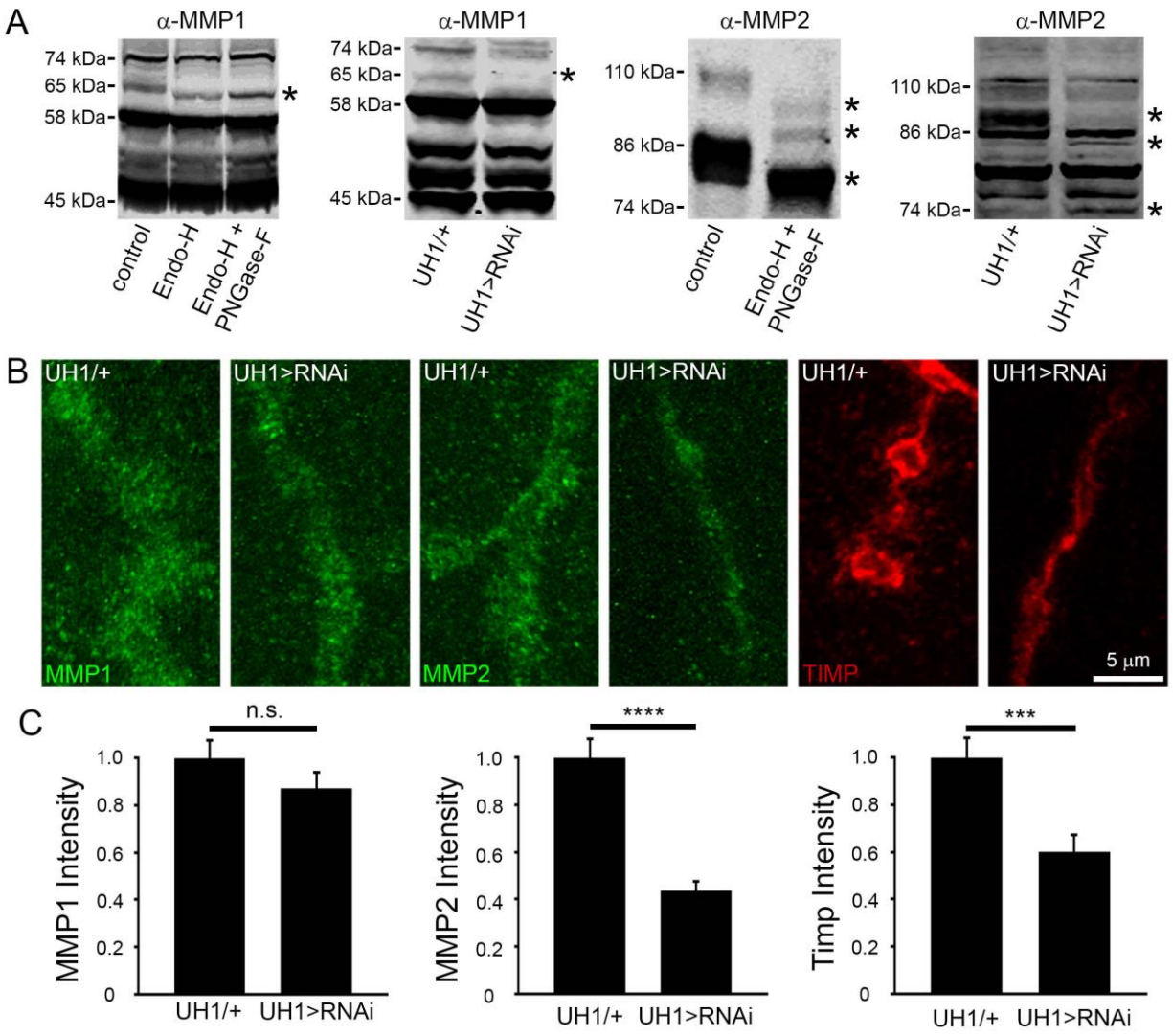
A
α-MMP1
74 kDa
65 kDa
58 kDa
45 kDa
control
Endo-H
Endo-H + PNGase-F
α-MMP1
74 kDa
65 kDa
58 kDa
45 kDa
UH1/+
UH1>RNAi
α-MMP2
110 kDa
86 kDa
74 kDa
control
Endo-H + PNGase-F
α-MMP2
110 kDa
86 kDa
74 kDa
UH1/+
UH1>RNAi
B
UH1/+
UH1>RNAi
MMP1
MMP2
TIMP
5 μm
C
n.s.
MMP1 Intensity
****
MMP2 Intensity
***
Timp Intensity
1.0
0.8
0.6
0.4
0.2
0
UH1/+ UH1>RNAi

Figure 18

Figure 18: Loss of PMM2 down-regulates the synaptic matrix proteinase pathway.

A) Representative Western blots for MMP1 (left) and MMP2 (right); 1) with/without PNGaseF and EndoH enzymatic treatment to remove glycosylation, and 2) in UH1-Gal4/+ transgenic control and UH>RNAi^{107619} PMM2 knockdown conditions. The asterisks denote shifted bands. **B)** Representative NMJ images for anti-MMP1 (green, left), anti-MMP2 (green, center) and anti-TIMP (red, right) in UH1-Gal4/+ controls and UH1-Gal4>RNAi^{107619}. **C)** Normalized quantification of fluorescent intensities for all three proteins. Significance: $p \leq 0.001$ (***), $p \leq 0.0001$ (****) and not significant (n.s.). Sample sizes: $n \geq 20$ NMJs/12 animals per genotype.

glycosylation-dependent shifts in size (Fig. 18A, asterisks), compared to secreted MMP1, in which only one minor isoform displays glycosylation. We next tested for non-glycosylated MMP forms in mutants using UH1-Gal4 driven *pmm2* knockdown (Fig. 18A). Loss of PMM2 results in multiple shifted (non-glycosylated) MMP bands compared to controls. Again, the effect is much greater for MMP2, with multiple bands showing a PMM2-dependent loss of glycosylation (Fig. 18A, asterisks). Consistently, NMJ labeling in *pmm2* RNAi compared to controls shows the synaptic matrix metalloproteome is compromised, again particularly for MMP2 (Fig. 18B). PMM2 ubiquitous knockdown results in >50% reduction in MMP2 levels (UH1-Gal4>RNAi^{107619}, 0.44±0.04, n=32) normalized to control (UH1-Gal4/+, 1.00±0.08, n=32; $p<0.0001$; Fig. 18C). In contrast, there is no significant change in MMP1 expression, although there is a slight decreasing trend (UH1-Gal4>RNAi^{107619}, 0.87± 0.07, n=20; UH1-Gal4/+, 1.00±0.07, n=24; Fig. 18B.C). TIMP is also reduced with PMM2 loss (UH1-Gal4>RNAi^{107619}, 0.60±0.07, n=24) compared to control (UH1-Gal4/+, 1.00±0.08, n=24; $p<0.001$; Fig. 18B,C). These results show synaptic MMP2 is strongly reduced by PMM2 removal, with a reduction also in synaptic TIMP levels. Given the importance of the synaptic metalloproteome in shaping Wnt *trans*-synaptic signaling (Dear et al., 2016), we next tested predicted PMM2 involvement.

PMM2 positively regulates the Wnt Wingless *trans*-synaptic signaling pathway

MMPs play an important role in Wnt Wingless (Wg) intercellular signaling by directly regulating the HSPG Dally-like protein (Dlp) Wg co-receptor (Wang and Page-McCaw, 2014). Importantly, the same Wg/Dlp signaling pathway is a critical driver of structural and functional development at the *Drosophila* NMJ (Ataman et al., 2006, 2008; Kerr et al., 2014; Mathew et al., 2005) and is known to be modulated by glycan mechanisms (Dani et al., 2012; Jumbo-Lucioni et al., 2014; Parkinson et al., 2013). Wg binds the Frizzled-2 (Fz2) receptor, which is internalized and the C-terminus proteolytically cleaved (Fz2C) for transport via the Fz2C nuclear import (FNI) pathway (Ataman et al., 2006; Mathew et al., 2005) to modulate NMJ structure/function (Speese et al. 2012). Based on this extensive work, we hypothesized that PMM2 regulates MMP2-dependent Wg signaling to regulate NMJ structure and function underlying coordinated movement and maintained viability.

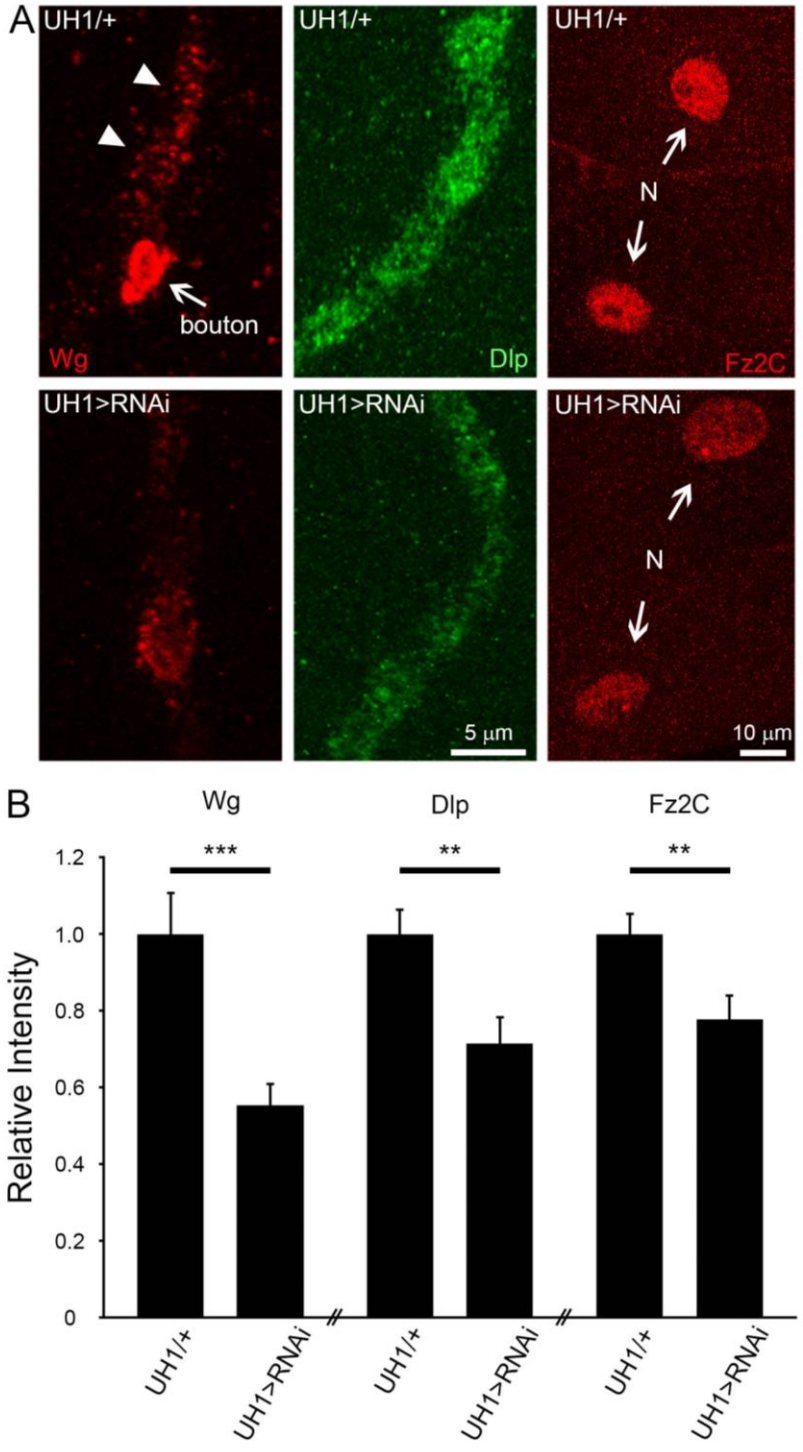
A
UH1/+
UH1/+
UH1/+
bouton
Wg
Dlp
Fz2C
N
N
UH1>RNAi
UH1>RNAi
UH1>RNAi
5 μm
10 μm
B
Wg
Dlp
Fz2C
***
**
**
Relative Intensity
1.2
1.0
0.8
0.6
0.4
0.2
0
UH1/+
UH1>RNAi
UH1/+
UH1>RNAi
UH1/+
UH1>RNAi

Figure 19

Figure 19: Loss of PMM2 down-regulates the *trans*-synaptic Wnt signaling pathway.

A) Representative NMJ images for anti-Wg (red, left), anti-Dlp (green, middle) and anti-Fz2C (red, right) in UH1-Gal4/+ controls (top) and UH1-Gal4>RNAi^{107619} (bottom). Left: Arrow indicates high Wg-expressing bouton, and arrowheads show low Wg-expressing boutons in control NMJ. Right: The arrows indicate two postsynaptic nuclei in control and mutant muscle. **B)** Normalized quantification of Wg, Dlp and Fz2C fluorescent labeling intensities. Significance: $p \leq 0.01$ (**) and $p \leq 0.001$ (***). Sample sizes: $n \geq 24$ NMJs or nuclei/12 animals per genotype.

All 3 components of the signaling pathway show clear down-regulation with PMM2 loss (Fig. 19). Qualitative comparison of Wg ligand and Dlp co-receptor at the NMJ, and Fz2C cleavage/import into the postsynaptic muscle nuclei, all show reduction of pathway components and impairment of downstream signaling (Fig. 19A). Quantification of the extracellular Wg levels shows a ~50% reduction with PMM2 ubiquitous knockdown (UH1-Gal4>RNAi^{107619}, 0.55±0.05, n=32) normalized to control (UH1-Gal4/+ 1.00±0.11, n=30; $p<0.001$; Fig. 19B, left). Wg co-receptor Dlp is also reduced (UH1-Gal4>RNAi^{107619}, 0.72±0.07, n=24) compared to control (UH1-Gal4/+, 1.00± 0.06, n=24, $p<0.01$; Fig. 19B, middle). Finally, consequent Fz2C import into the muscle nucleus via the FNI pathway to mediate downstream signaling is significantly impaired with PMM2 ubiquitous knockdown (UH1-Gal4>RNAi^{107619}, 0.78±0.05, n=24) compared to control (UH1-Gal4/+, 1.00±0.04, n=24), showing a significant decrease in *trans*-synaptic signaling ($p<0.01$; Fig 19B). These results agree well with the recent report of strongly reduced Wnt signaling in the *Xenopus* PMM2-CDG model (Himmelreich et al., 2015). We conclude that neurological impairments in the *Drosophila* PMM2-CDG model similarly map to impaired Wnt signaling, to misregulate NMJ synaptogenesis underlying coordinated movement.

Discussion

We set forth to establish a *Drosophila* CDG-Ia (aka PMM2-CDG) genetic model through manipulation of the causative phosphomannomutase type 2 (PMM2) gene (Freeze et al., 2014). Using CRISPR-generated *pmm2* null mutants and transgenic RNAi, we found PMM2 levels correlated to coordinated movement abilities and lifespan (Fig. 12), as in CDG-Ia patients (Cylwik et al., 2013; Jaeken, 2013; Lonlay et al., 2001). Human patients with identical *pmm2* mutations present with a wide spectrum of movement defects (Marquardt and Denecke, 2003; Schneider et al., 2011), attributed to genetic and/or environmental factors readily controlled in *Drosophila*. With tissue-specific drivers, we found a neural PMM2 impairment for coordinated movement (Fig. 12). Interestingly, weak neural knockdown of *pmm2* resulted in increased lifespan. Similarly, moderate impairments of oxidative stress and dietary restriction pathways have also been reported to extend lifespan (Mair et al., 2005; Min and Tartar, 2006; Ristow and

Schmeiser, 2011). Like PMM2, severe impairments of these pathways result in reduced lifespan and early death, but more modest impairments extend lifespan via changes in metabolic rate, developmental conditioning and/or defense mechanisms. Null *pmm2* mutants display severe attenuation of glycoprotein glycosylation (Fig. 13), with reduced N-linked glycosylation diversity (Aoki et al., 2007). Similar global N-glycan losses occur with strong *pmm2* RNAi throughout the larval neuromusculature, but not with weaker neural-targeted *pmm2* RNAi in the adult head (Fig. 13). Lipid-linked oligosaccharides (LLO) used for protein attachment by oligosaccharyltransferase (OST) activity are regulated at many levels (Gao et al., 2011). PMM2 loss should reduce LLO levels by inhibiting mannose-1-phosphate production and elevating the mannose-6-phosphate pool acting as a signal mediating LLO destruction, thereby increasing free oligosaccharides (FOS; Fig. 14A; Gao et al., 2011). However, the increase in pauci-mannose structures with adult neuronal *pmm2* knockdown differentially alters glycan maturation. The mannose-6-phosphate increase may change the mannose phosphoisomerase (MPI) equilibrium, leading to interconversion of mannose-6-phosphate to fructose-6-phosphate to siphon LLO-toxic mannose-6-phosphate and mitigate LLO elimination.

Null *pmm2* mutants display elevated FOS levels (Fig. 14A). Increased phosphorylated FOS levels, predicted to be cleaved from LLO intermediates, likewise occur in CDG-Ia patient cells (Vleugels et al., 2011). Similarly, the zebrafish morpholino model shows increased FOS levels, with phenotype rescue via MPI co-reduction, suggesting causative mannose-6-phosphate elevation (Cline et al., 2012). Viable human CDG-Ia patients are typically heterozygous for *pmm2* mutations, resulting in partial loss of PMM2 (Matthijs et al., 1998; Monin et al., 2014). In *Drosophila*, partial loss-of-function from neuron-targeted RNAi results in surprising resistance to glycosylation changes (Fig. 13C). Pauci-mannose glycans are increased, but high mannose and complex glycans unchanged. PMM2 regulates GDP-mannose availability for glycan production, but following glycosylation by OST further processing should be GDP-mannose independent (Cylwik et al., 2013). The increased pauci-mannose glycans resulting from PMM2 partial loss suggests GDP-mannose levels influence glycan processing beyond the role as synthetic donors for mannosylation. Pauci-mannose glycan production is driven by the balance between Golgi exomannosidases, GlcNAc-Transferase 1 and a hexosaminidase

removing GlcNAc from nascent complex glycans (Stanley et al., 2009). Precursor abundances, including donor and acceptor, influence expression and activity of glycan-processing enzymes. Reduced GDP-mannose likely skews the balance of enzyme activities that trim high-mannose to pauci-mannose, before they increase in complexity. Impacts on glycosylation independent of GDP-mannose is also evident in reduced NMJ lectin labeling with PMM2 loss (Fig. 14B). Importantly, both ECL and VVA bind mannose-free structures, most likely on O-linked glycoprotein backbones.

The nervous system is tightly regulated by glycans at multiple levels of development and function (Koles et al., 2007; Scott and Panin, 2014a,b; Seppo and Tiemeyer, 2000). NMJ architectural overelaboration and functional strengthening has been identified in many glycan mutants in our systematic genetic screens, including *sulf1*, *mgat1*, *galt* and *pgant* (Dani et al., 2012; Dani et al., 2014; Jumbo-Lucioni, 2014; Parkinson et al, 2013). Consistently, PMM2 loss shows striking NMJ overelaboration (Fig. 15), supporting the conclusion that glycans primarily inhibit synaptic morphogenesis. Null *pmm2* mutants already exhibit strong synaptic architecture defects within a day after hatching (Fig. 16), showing that PMM2-dependent glycan mechanisms brake the earliest stages of synaptic growth and differentiation. Glycosylation mechanisms also have key roles modulating neurotransmission (Koles et al., 2007; Scott and Panin, 2014a,b), and PMM2 loss strongly increases NMJ function (Fig. 17). There is no effect on spontaneous synaptic vesicle release or postsynaptic amplitude, indicating a specific PMM2 role in limiting stimulus evoked quantal content. Interestingly, neural- and muscle-targeted PMM2 knockdown have no effect on transmission, however combined neural and muscle knockdown fully replicates the ubiquitous PMM2 loss phenotype (Fig. 17), indicating that the elevated transmission needs concomitant PMM2 removal both pre- and postsynaptically. One explanation is that semi-synaptic glycosylation may be sufficient to normalize transmission: loss of glycosylation from one side may be compensated for by the other side, as synapse transmission is highly regulated by both pre- and postsynaptic cells (Dani and Broadie, 2012). Another idea is that glycosylation could be provided by extracellular components from either synaptic partner cell.

The non-cell-autonomous defect occurring with PMM2 loss prompted us to investigate extracellular signaling mechanisms, which are tightly regulated by glycosylation at the NMJ (Dani et al. 2012; Dani et al., 2014; Parkinson et al., 2013; Jumbo-Lucioni et al., 2014; Rushton et al., 2012). In particular, matrix metalloproteinases (MMPs) play critical roles shaping synapse structure and function (Dear et al., 2016; Kessenbrock et al., 2010; Page-McCaw et al., 2007; Sternlicht and Werb, 2001). PMM2 loss could impair MMP glycosylation or ability to cleave improperly glycosylated substrates (Godenschwege et al., 2000; Llano et al., 2000; Llano et al., 2002; Pohar et al., 1999). PNGaseF and EndoH treatment to remove N-linked glycans shows MMP2 isoforms are highly glycosylated, whereas only a tiny subset of MMP1 isoforms are glycosylated (Fig. 18A). GPI-anchored MMP2 also requires GDP-mannose, although GPI anchors require fewer donor mannose than N-linked glycans (Morena-Bario et al., 2013). Importantly, *pmm2* RNAi similarly removes glycosylation from multiple MMP2 isoforms, with only a minor change to MMP1 (Fig. 18A). As predicted by PMM2-dependent glycosylation changes, MMP2 is strongly reduced at the NMJ synapse with *pmm2* RNAi, whereas MMP1 is not significantly altered (Fig. 18B,C). The TIMP regulator is also reduced in abundance with removal of PMM2, which would be predicted to help alleviate consequences of MMP2 loss, perhaps as a compensation mechanism (Dear et al., 2016). Importantly, recent work from our lab has shown that MMPs play critical roles regulating NMJ structural and functional synaptogenesis via control of heparan sulfate proteoglycan (HSPG) receptors that modulate Wnt *trans*-synaptic signaling (Dear et al., 2016).

Recent work utilizing PMM2 morpholino knockdown in *Xenopus* revealed altered glycosylation of Wingless-type MMTV integration site family growth factor (Wnt) and reduction of Wnt signaling (Himmelreich et al., 2015). Similarly, we find that *pmm2* RNAi knockdown in *Drosophila* suppressing Wnt Wingless (Wg) signaling at the developing NMJ synapse (Fig. 19). With PMM2 loss, synaptic levels of Wg ligand and its HSPG co-receptor Dally-like Protein (Dlp) are both strongly reduced, and downstream signaling through the Frizzled Nuclear Import (FNI; Speese et al., 2012) pathway is consistently down-regulated (Fig. 19). These defects have been previously associated with the loss of synaptic MMP2, which acts via Dlp to regulate Wg *trans*-synaptic signaling to modulate both structural and functional NMJ development in the same

direction (Dear et al., 2016). However, we have shown that PMM2 loss has myriad consequences on N-linked glycoprotein glycosylation, and therefore quite likely impacts NMJ synaptogenesis at multiple levels. Indeed, specifically targeted reduction in Wg signaling alone has previously been associated with decreased NMJ structural development and reduced function (Ataman et al., 2008; Kerr et al., 2014; Packard et al., 2002), which differs from the Wg attenuation associated with PMM2 loss. Therefore, PMM2 roles at the NMJ synapse likely reflect roles in multiple intersecting pathways that jointly control growth, structural differentiation and neurotransmission strength. Our future work will aim at deciphering other PMM2-dependent glycoprotein contributions, which combinatorially result in the structural and functional NMJ defects characterizing this CDG-Ia disease state model.

We hope this new *Drosophila* model will prove instrumental for tackling the disease, and related CDGs, especially in regard to neurological symptoms (Grunewald, 2009; Jaeken, 2010). One avenue will be to dissect roles played by glycan precursors and mannose-6-phosphate buildup, by examining genetic interactions shifting the relative abundance of alternatively processed glycans and to alleviate increased FOS levels. For example, using genetic MPI reduction or pharmaceutical MPI inhibitors in the benzoisothiazolone series (Sharma et al., 2011). One such agent, MLS0315771, has been shown to favor mannose-1-phosphate production in CDG-Ia patient fibroblasts and zebrafish embryos. Pharmacological tests in *Drosophila* could include assays to prolong lifespan, improve coordinated movement and prevent NMJ structural and functional defects. The current standard of care for CDG-Ia patients is simply symptomatic treatment and disease management (Grunewald, 2009; Jaeken, 2013). The mouse model suggests beneficial dietary intervention, common for other metabolic disorders like Classic Galactosemia (Jumbo-Lucioni et al., 2014). However, mannose treatment has not been effective in restoring N-linked glycoprotein glycosylation levels in CDG-Ia patients (Thiel and Korner, 2013). Drug avenues to increase PMM2-dependent glycosylation are hypothesized, but there are no studies (Thiel and Korner, 2013). We expect the relatively high speed of *Drosophila* disease model studies utilizing the powerful *Drosophila* genetic toolkit will open up new avenues for disease intervention. We propose here that targeting the matrix

metalloproteome and Wnt signaling pathways offers potential new candidates to consider in developing future CDG-Ia treatments.

Materials and Methods

Drosophila Genetics

Drosophila stocks were grown on standard cornmeal/agar/molasses food in a 12 hour light:dark cycle at 25°C. Mutants were generated with CRISPR/Cas9 (Gratz et al., 2013). Briefly, chiRNA targeting 5'CATTGAAGCGTGATGAAATC and 3'AGGATACGCAACGATTCTC sequences of *pmm2* were incorporated into a pU6-BbsI-chiRNA plasmid (Addgene #45946). F1 progeny from w^{1118} vas-Cas9 males (BDSC# 51324) crossed to w^{1118} Lig4 females (BDSC# 28877) were injected with both targeting plasmids (BestGene Inc., Chino Hills, CA). Injected animals were then crossed to a double balanced (TM3Sb/TM6Tb) mate. F1 males were then crossed to deficiency/balancer females (w^{1118}; Df(3L)BSC380/TM6C, Sb^1cu^1 (BSCD #24404)) to identify lethal *pmm2* mutations. F1 males were recollected and mated with double balanced females to produce the *pmm2* mutant stocks. Mutant backcrossing and sequencing were performed with standard *Drosophila* genetic and PCR techniques. The w^{1118} background stock was used as the control. RNAi studies were performed with neuronal-specific *elav*-Gal4, muscle-specific 24B-Gal4 and ubiquitous UH1-Gal4 transgenic drivers (Brand and Perrimon, 1993; Lin and Goodman, 1994; Rohrbough et al., 2007). Two *pmm2* UAS-RNAi lines, v107691 (Vienna *Drosophila* RNAi Center) and BDSC42956 (Bloomington *Drosophila* Stock Center) were used, with Gal4 drivers alone as transgenic controls.

PCR Methods

For reverse transcription quantitative PCR (RT-qPCR), total RNA was extracted using a Zymo Research Direct-zol RNA Miniprep Plus Kit with TRI reagent (R2070) with on column DNase treatment. The Superscript VILO cDNA synthesis kit (11754-050) was used for cDNA synthesis. RT-qPCR was run on a Biorad CFX96 with equal amounts of cDNA (2ng for each trial). For expression quantification, the Pfaffl Method was used with standards of known transcript number to quantify absolute cDNA number for target and reference genes. For the reference,

ribosomal protein L32 (CG7939) levels were used for normalization of absolute cDNA quantity ((target/reference)*100). The following primers were used for target and reference: *pmm2* forward AGGCTCGGATCTGGAGAAGA, *pmm2* reverse AATGTCGTACTCGGCGAACA; *L32* forward CGGTTACGGATCGAACAAGC, *L32* reverse CTTGCGCTTCTTGGAGGAGA. Samples and standards were run with gene specific primers in duplicate trials.

Behavioral Assays

Egg lays were collected overnight on apple juice agar plates. Plates were then cleared of larvae, and newly-hatched larvae collected after 1 hour (t=0). Larval lifespan analyses involved daily counts. Adult lifespan analyses required two separate methods. For strong neural *elav*-Gal4>RNAi *pmm2* knockdown and *elav*-Gal4/+ controls, adults were collected at eclosion and maintained in laying pots with filter paper covering apple juice plates with yeast. For all other lifespan assays, adults were maintained in normal fly tubes on cornmeal/agar/molasses food. Adult survival was measured 3 times/week, with animals transferred to fresh plates or tubes. The comparative quantification of survival is reported as the time to which 50% of the animals remain viable (half-time survival, HTS). Adult and larval locomotion were assayed as previously described (Nichols et al., 2012; Sokolowski, 1980). Briefly, larvae were tested on apple juice agar plates with yeast paste spread around edges as an attractant. Individual larvae were placed in the middle of a plate and time-lapse recorded under a dissection microscope with a Cannon Rebel DSLR camera (Melville, NY). Locomotion was assayed as peristaltic waves per second (Gjorgjieva et al., 2013). Adult motility was assayed by negative geotaxis and a ring locomotion assay. For geotaxis, adults were place in empty fly vials for 15 mins to acclimate, and then tubes were sharply tapped to put animals at the bottom (Nichols et al., 2012). Movement was recorded with a Canon Rebel DSLR camera and the percentage of animals to climb above 2cm measured at timed intervals. To assay horizontal locomotion, a 4cm circle was drawn in a large dish, and flies with amputated wings were placed in the middle of the circle. Movement was recorded with a Canon Rebel DSLR camera and the time required to traverse the circle measured.

Glycomic Analyses

Glycoproteins and free oligosaccharides (FOS) were prepared from staged collections of *pmm2* null 1st instars or *elav*-Gal4>RNAi^{42956} adult heads by homogenization in aqueous/organic solvents and subsequent protein precipitation as described previously (Aoki et al., 2007). Briefly, the aqueous/organic homogenate was centrifuged with glycoproteins recovered in the pellet and FOS from the supernatant (Katoh et al., 2013). Precipitated proteins were washed with cold acetone and dried under a stream of nitrogen to produce samples stored desiccated at -20^{o}C. Protein content was determined by BCA assay of resolubilized material (Pierce). N-linked glycoprotein glycans were prepared from 1 mg aliquots by digestion with trypsin/chymotrypsin, followed by enzymatic release of glycans with PNGaseF (Aoki et al., 2007). FOS were separated by passage over a Sep-pak C_{18} cartridge column (Katoh et al., 2013). N-linked glycans and FOS were permethylated and analyzed by mass spectrometry (MS) using nanospray ionization coupled to linear iontrap and orbital Fourier transform mass analyzers (Discover NSI-LTQ/OrbitrapFT, Thermo-Fisher Scientific). MS spectra were collected over the range m/z=200-2000 and MS/MS fragmentation by collision-induced dissociation (CID; 30-40% normalized collision energy) was acquired over the same m/z range using the total ion mapping function of the XCalibur instrument software (version 2.0). Annotated glycans were validated by exact mass in full MS and by manual inspection of MS/MS spectra at each of the detected m/z values.

Immunocytochemistry Imaging

Immunocytochemistry studies were performed as described previously (Parkinson et al., 2013). Briefly, all animals were dissected, fixed and labeled identically in the same dish. Wandering 3rd or 1st instars were dissected in physiological saline containing 128mM NaCl, 2mM KCl, 4mM $MgCl_2$, 0.25mM $CaCl_2$, 70mM sucrose, 5mM trehalose and 5mM HEPES (pH 7.1). Preparations were fixed in 4% paraformaldehyde for 10 mins at room temperature (RT) in phosphate buffered saline (PBS). Preparations were then either processed with detergent (PBS + 1% bovine serum albumin (BSA) + 0.2% Triton X-100) for intracellular labeling, or detergent-free (PBS with 1% BSA) for extracellular studies. Primary antibodies included: rabbit anti-horseradish

peroxidase (HRP, 1:200; Sigma, St. Louis, MO); conjugated CY2, CY3 or CY5-HRP (1:250, Jackson Labs, West Grove, PA); mouse anti-Wingless (Wg, 1:2; Developmental Studies Hybridoma Bank (DSHB), University of Iowa, Iowa City, Iowa); mouse anti-Discs Large (DLG, 1:200; DSHB). Lectins included: *Vicia villosa* agglutinin (VVA-Tritc, 1:200, E.Y. Laboratories, San Mateo, CA) and *Erythrina cristagalli* lectin (ECL-biotin, 1:250, Vector Labs). Secondary Alexa fluorophore antibodies (Invitrogen, Grand Island, NY) included: goat anti-mouse 488 and 568 (1:250), goat anti-rabbit 488 and 568 (1:250), and streptavidin 488 and 594 (1:250). Primary antibodies and lectins were incubated at 4°C overnight; secondary antibodies were incubated at RT for 2 hours. Samples were mounted in Fluoromount-G (Electron Microscopy Sciences, Hatfield, PA). All preparations were imaged using identical parameters. Z-stacks were taken with a Zeiss LSM510 META laser-scanning confocal using a 63X Plan Apo oil immersion objective. Optical sections were imaged starting above and ending below the NMJ or muscle nuclei to encompass their entirety. Stacks were projected on the Z-axis for maximum intensity, with NMJ or nuclei signals highlighted and average intensity quantified using ImageJ (Abramoff et al., 2001).

Western Blot analyses

Tissues were homogenized in buffer (1% SDS, 50mM Tris-HCl, 150mM NaCl) with protease inhibitors, heated (70°C, 10 mins) and centrifuged (16,100xg, 10 mins). Supernatant was split into two tubes (+/- enzyme) and glycosidase treatment done following manufacturer instructions (New England Biolabs (NEB), Ipswich, MA). Briefly, samples in denaturing buffer (NEB) were heated (10 mins, at 95°C) then cooled to RT. Denatured samples were treated with or without (buffer alone) Endoglycosidase-H (NEB) and PNGase-F (NEB) at 1 microliter enzyme/ 20 microgram protein in 1X G5 buffer (NEB) overnight at 37°C. Samples were assayed with Western blot SDS-PAGE using 10% Bis-Tris gels and Western blot analysis. Membranes were blocked in 2% milk in tris-buffered saline (TBS) for 1 hour at RT. Mmp antibodies (1:1500) were incubated overnight 4°C, then washed for 5 mins (x6) in TBS + 0.1% Tween-20 (TBST). Goat secondaries (1:10,000; Rockland, Limerick, PA) were incubated for 1 hour RT. Blots washed for 5 mins (x6) in TBS-T were imaged using an Odyssey Infrared Imaging System.

Electrophysiology

Excitatory junctional current (EJC) recordings made using two-electrode voltage-clamp (TEVC) were done as previously reported (Parkinson et al., 2013). Briefly, wandering 3rd instars were glued with 3M Vetbond adhesive (World Precision Instruments, Sarasota, FL) to sylgard-coated glass coverslips, cut longitudinally along the dorsal midline, internal organs removed and sides affixed down for neuromusculature access. Peripheral nerves were cut at the ventral nerve cord. Recordings were done at 18°C in saline consisting of 128mM NaCl, 2mM KCl, 4mM $MgCl_2$, 1mM $CaCl_2$, 70mM sucrose, 5mM trehalose and 5mM HEPES (pH 7.1), imaged using a Zeiss Axioskop microscope with 40X immersion objective. A fire-polished glass suction electrode was used for evoked nerve stimulation with 0.5 millisecond supratheshold stimuli at 0.2Hz from a Grass S88 stimulator (Rohrbough et al., 2007). Muscle 6 in abdominal segments 2/3 was impaled with two microelectrodes of 10-15 MΩ resistance filled with 3M KCl, and clamped (-60 mV) using an Axoclamp-2B amplifier (Molecular Devices, Sunnyvale, CA). EJC records were filtered at 2kHz. To quantify EJC amplitudes, 10 consecutive traces were averaged. Spontaneous miniature EJC (mEJC) records were made in 2-minute sessions and filtered at 200Hz with a low-pass Gaussian filter prior to quantification. Clampex software was used for all data acquisition, and Clampfit software for all data analyses (Molecular Devices, Sunnyvale, CA).

Statistics

All statistical analyses were performed using GraphPad InStat3 software (La Jolla, CA). Student's T-tests were used for pairwise comparisons, and ANOVA with appropriate post-hoc testing was used for all data sets of 3 or more comparisons. Nonparametric methods were used for data sets lacking normal distribution. Fisher's exact tests were used to analyze contingency tables for adult behavioral data. Data are shown as mean±SEM in all figures, with significance presented as $p \leq 0.05$ (*), $p \leq 0.01$ (**), $p \leq 0.001$ (***) and $p \leq 0.0001$ (****).

References

Abramoff, M.D., Magalhaes, P.J., Ram, S.J. (2001). Image Processing with ImageJ. *Biophotonics International*. 11(7), 36-42.

Altmann, F., Fabini, G., Ahorn, H., Wilson, I.B. (2001). Genetic model organisms in the study of N-glycans. *Biochimie*. 83(8), 703-12.

Andreotti, G., Cabeza de Vaca, I., Poziello, A., Monti, M.C., Guallar, V., Cubellis, M.V. (2014). Conformational response to ligand binding in phosphomannomutase2: insights into inborn glycosylation disorder. *J. Biol. Chem*. 289(50), 34900-10.

Aoki, K., Perlman, M., Lim, J.M., Cantu, R., Wells, L., Tiemeyer, M. (2007). Dynamic developmental elaboration of N-linked glycan complexity in the *Drosophila melanogaster* embryo. *J. Biol. Chem*. 282(12), 9127-42.

Ataman, B., Ashley, J., Gorczyca, D., Gorczyca, M., Mathew, D., Wichmann, C., Sigrist, S.J., Budnik, V. (2006). Nuclear trafficking of *Drosophila* Frizzled-2 during synapse development requires the PDZ protein dGRIP. *Proc Natl Acad Sci U S A*. 103(20), 7841-6.

Ataman, B., Ashley, J., Gorczyca, M., Ramachandran, P., Fouquet, W., Sigrist, S.J., Budnik, V. (2008). Rapid activity-dependent modifications in synaptic structure and function require bidirectional Wnt signaling. *Neuron*. 57(5), 705-18.

Barone, R., Fiumara, A., Jaeken, J. (2014). Congenital disorders of glycosylation with emphasis on cerebellar involvement. *Semin Neurol*. 34(3), 357-66.

Barone, R., Carrozzi, M., Parini, R., Battini, R., Martinelli, D., Elia, M., Spada, M., Lilliu, F., Ciana, G., Burlina, A., Leuzzi, V., Leoni, M., Sturiale, L., Matthijs, G., Jaeken, J., Di Rocco, M., Garozzo, D., Fiumara, A. (2015). A nationwide survey of PMM2-CDG in Italy: high frequency of a mild neurological variant associated with the L32R mutation. *J Neurol*. 262(1), 154-64.

Brand, A.H., Perrimon, N. (1993). Targeted gene expression as a means of altering cell fates and generating dominant phenotypes. *Development*. 118(2), 401-15.

Cline, A., Gao, N., Flanagan-Steet, H., Sharma, V., Rosa, S., Sonon, R., Azadi, P., Sadler, K.C., Freeze, H.H., Lehrman, M.A., Steet, R. (2012). A zebrafish model of PMM2-CDG reveals altered neurogenesis and a substrate-accumulation mechanism for N-linked glycosylation deficiency. *Mol Biol Cell*. 23(21), 4175-87.

Cylwik, B., Naklicki, M., Chrostek, L., Gruszewska, E. (2013). Congenital disorders of glycosylation. Part I. Defects of protein N-glycosylation. *Acta Biochim Pol*. 60(2), 151-61.

Dani, N., Broadie, K. (2012). Glycosylated synaptomatrix regulation of trans-synaptic signaling. *Dev Neurobiol*. 72(1), 2-21.

Dani, N., Nahm, M., Lee, S., Broadie, K. (2012). A targeted glycan-related gene screen reveals heparan sulfate proteoglycan sulfation regulates WNT and BMP trans-synaptic signaling. *PLoS Genet*. 8(11), e1003031

Dani N., Zhu H., Broadie, K. (2014). Two protein N-acetylgalactosaminyl transferases regulate synaptic plasticity by activity-dependent regulation of integrin signaling. *J Neurosci*. 34(39), 13047-65.

Dear, M.L., Dani, N., Parkinson, W., Zhou, S., Broadie, K. (2016). Two matrix metalloproteinase classes reciprocally regulate synaptogenesis. *Development* 143(1), 75-87.

Van Dijk, W., Koeleman, C., Van het Hof, B., Poland, D., Jakobs, C., Jaeken, J. (2001). Increased alpha3-fucosylation of alpha(1)-acid glycoprotein in patients with congenital disorder of glycosylation type IA (CDG-Ia). *FEBS Lett.* 494(3), 232-5.

Freeze, H.H., Chong, J.X., Bamshad, M.J., Ng, B.G. (2014). Solving glycosylation disorders: fundamental approaches reveal complicated pathways. *Am J Hum Genet*. 94(2), 161-75.

Freeze, H.H., Eklund, E.A., Ng, B.G., Patterson, M.C. (2015). Neurological Aspects of Human Glycosylation Disorders. *Annu Rev Neurosci*. 38, 105-25.

Gao, N., Shang, J., Huynh, D., Manthati, V.L., Aria,s C., Harding, H.P., Kaufman, R.J., Mohr, I., Ron, D., Falck, J.R., Lehrman, M.A. (2011). Mannose-6-phosphate regulates destruction of lipid-linked oligosaccharides. *Mol Biol Cell*. 22(17), 2994-3009.

Gatto, C.L., and Broadie, K. (2011). *Drosophila* modeling of heritable neurodevelopmental disorders. *Curr Opin Neurobiol.* 21(6), 834-41.

Gjorgjieva, J., Berni, J., Evers, J.F., Eglen, S.J. (2013). Neural circuits for peristaltic wave propagation in crawling *Drosophila* larvae: analysis and modeling. *Front Comput Neuro*. 7, 24.

Glasheen, B.M., Kabra, A.T., Page-McCaw, A. (2009). Distinct functions for the catalytic and hemopexin domains of *Drosophila* matrix metalloproteinase. *Pro Nat Acad Sci* 106(8), 2659-64.

Glasheen, B.M., Robbins, R.M., Piette, C., Beitel, G.J., Page-McCaw, A. (2010). A matrix metalloproteinase mediates airway remodeling in *Drosophila*. *Dev Biol*. 344(2), 772-83.

Godenschwege, T.A., Pohar, N., Buchner, S., Buchner, E. (2000). Inflated wings, tissue autolysis and early death in tissue inhibitor of metalloproteinases mutants of *Drosophila*. *Eur J Cell Biol*. 79(7), 495-501.

Gratz, S.J., Cummings, A.M., Nguyen, J.N., Hamm,, D.C., Donohue, L.K., Harrison, M.M., Wildonger, J., O'Connor-Giles, K.M. (2013). Genome engineering of *Drosophila* with the CRISPR RNA-guided Cas9 nuclease. *Genetics*. 194(4), 1029-35.

Grünewald, S. (2009). The clinical spectrum of phosphomannomutase 2 deficiency (CDG-Ia). *Biochim Biophys Acta*. 1792(9), 827-34.

Haeuptle, M.A., Hennet, T. (2009). Congenital disorders of glycosylation: an update on defects affecting the biosynthesis of dolichol-linked oligosaccharides. *Hum Mutat*. 30(12), 1628-41.

ten Hagen, K.G., Zhang, L., Tian, E., Zhang, Y. (2009). Glycobiology on the fly: developmental and mechanistic insights from *Drosophila*. *Glycobiology*. (2), 102-11.

Himmelreich, N., Kaufmann, L.T., Steinbeisser, H., Körner, C., Thiel, C.J. (2015). Lack of phosphomannomutase 2 affects Xenopus laevis morphogenesis and the non-canonical Wnt5a/Ror2 signalling. *Inherit Metab Dis*. 38(6), 1137-46.

Jaeken, J., Vanderschueren-Lodeweyckx, M., Casaer, P., Snoeck, L., Corbeel, L., Eggermont, E., Eeckels, R. (1980). Familial psychomotor retardation with markedly fluctuating serum prolactin, FSH and GH levels, partial TBG-deficiency, increased serum arylsulfatase-A and increased CSF protein- new syndrome? *Pediatr Res*. 14:179

Jaeken J. (2010). Congenital disorders of glycosylation. *Ann N Y Acad Sci*. 1214, 190-8.

Jaeken, J. (2013). Congenital disorders of glycosylation. *Handb Clin Neurol.* 113, 1737-43.

Jia, Q., Liu, Y., Liu, H., Li, S. (2014). Mmp1 and Mmp2 cooperatively induce Drosophila fat body cell dissociation with distinct roles. *Sci Rep*. 4:7535.

Jumbo-Lucioni P, Parkinson W, Broadie K. (2014). Overelaborated synaptic architecture and reduced synaptomatrix glycosylation in a *Drosophila* classic galactosemia disease model. *Dis Model Mech*. 7(12), 1365-78.

Katoh, T., Takase, J., Tani, Y., Amamoto, R., Aoshima, N., Tiemeyer, M., Yamamoto, K., Ashida, H. (2013). Deficiency of α-glucosidase I alters glycoprotein glycosylation and lifespan in *Caenorhabditis elegans*. *Glycobiology*. 23(10), 1142-51.

Katoh, T., Tiemeyer, M. (2013). The N's and O's of *Drosophila* glycoprotein glycobiology. *Glycoconj J.* 30(1), 57-66.

Kerr, K.S., Fuentes-Medel, Y., Brewer, C., Barria, R., Ashley, J., Abruzzi, K.C., Sheehan, A., Tasdemir-Yilmaz, O.E., Freeman, M.R., Budnik, V. (2014). Glial wingless/Wnt regulates glutamate receptor clustering and synaptic physiology at the *Drosophila* neuromuscular junction. *J Neurosci*. 34(8), 2910-20.

Kessenbrock, K., Plaks, V., Werb, Z. (2010). Matrix metalloproteinases: regulators of the tumor microenvironment. *Cell*. 141(1), 52-67.

Kjaergaard, S., Kristiansson, B., Stibler, H., Freeze, H.H., Schwartz, M., Martinsson, T., Skovby, F. (1998). Failure of short-term **mannose therapy** of patients with carbohydrate-deficient glycoprotein syndrome type 1A. *Acta Paediatr.* 87(8), 884-8.

Kohsaka, H., Takasu, E., Morimoto, T., Nose, A. (2014). A group of segmental premotor neurons regulates speed of axial locomotion in *Drosophila* larvae. *Curr Biol.* 24(22), 2632-42.

Koles, K., Lim, J.M., Aoki, K., Porterfield, M., Tiemeyer, M., Wells, L., Panin, V. (2007). Identification of N-glycosylated proteins from the central nervous system of *Drosophila melanogaster*. *Glycobiology*. 17(12), 1388-403.

Kurosaka, A., Yano, A., Itoh, N., Kuroda, Y., Nakagawa, T., Kawasaki, T. (1991). The structure of a neural specific carbohydrate epitope of horseradish peroxidase recognized by anti-horseradish peroxidase antiserum. *J Biol Chem.* 266(7), 4168-72.

Llano, E., Adam, G., Pendás, A.M., Quesada, V., Sánchez, L.M., Santamariá, I., Noselli, S., López-Otín, C. (2002). Structural and enzymatic characterization of *Drosophila* Dm2-MMP, a membrane-bound matrix metalloproteinase with tissue-specific expression. *J Biol Chem*. 277(26), 23321-9.

Llano, E., Pendás, A.M., Aza-Blanc, P., Kornberg, T.B., López-Otín, C. (2000). Dm1-MMP, a matrix metalloproteinase from *Drosophila* with a potential role in extracellular matrix remodeling during neural development. *J Biol Chem*. 275(46), 35978-85.

Lin, D.M., Goodman, C.S. (1994). Ectopic and increased expression of Fasciclin II alters motoneuron growth cone guidance. *Neuron*. 13(3), 507-23.

de Lonlay, P., Seta, N., Barrot, S., Chabrol, B., Drouin, V., Gabriel, B.M., Journel, H., Kretz, M., Laurent, J., Le Merrer, M., Leroy, A., Pedespan, D., Sarda, P., Villeneuve, N., Schmitz, J., van Schaftingen, E., Matthijs, G., Jaeken, J., Korner, C., Munnich, A., Saudubray, J.M., Cormier-Daire, V. (2001). A broad spectrum of clinical presentations in congenital disorders of glycosylation I: a series of 26 cases. *J Med Genet*. 38(1), 14-9.

Mair, W., Piper, M.D., Partridge, L. (2005). Calories do not explain extension of life span by dietary restriction in Drosophila. *PLoS Biol*. 3(7):e223.

Marquardt, T., Denecke, J. (2003). Congenital disorders of glycosylation: review of their molecular bases, clinical presentations and specific therapies. *Eur J Pediatr.* 162(6), 359-79.

Martin, P.T. (2003). Glycobiology of the neuromuscular junction. *J Neurocyt*. 32(5-8), 915-29.

Mathew, D., Ataman, B., Chen, J., Zhang, Y., Cumberledge, S., Budnik, V. (2005). Wingless signaling at synapses is through cleavage and nuclear import of receptor DFrizzled2. *Science*. 310(5752), 1344-7.

Matthijs, G., Schollen, E., Van Schaftingen, E., Cassiman, J.J., Jaeken, J. (1998). Lack of homozygotes for the most frequent disease allele in carbohydrate-deficient glycoprotein syndrome type 1A. *Am J Hum Genet*. 62(3), 542-50.

Min, K.J., Tatar, M. (2006) Restriction of amino acids extends lifespan in *Drosophila melanogaster*. *Mech Ageing Dev*. 127(7), 643-6.

Mayatepek, E., Kohlmüller, D. (1998). **Mannose** supplementation in carbohydrate-deficient glycoprotein syndrome type I and phosphomannomutase deficiency. *Eur J Ped.* 157(7), 605-6.

Monin, M.L., Mignot, C., De Lonlay, P., Héron, B., Masurel, A., Mathieu-Dramard, M., Lenaerts, C., Thauvin, C., Gérard, M., Roze, E., Jacquette, A., Charles, P., de Baracé, C., Drouin-Garraud, V., Khau Van Kien, P., Cormier-Daire, V., Mayer, M., Ogier, H., Brice, A., Seta, N., Héron, D. (2014). 29 French adult patients with PMM2-congenital disorder of glycosylation: outcome of the classical pediatric phenotype and depiction of a late-onset phenotype. *Orphanet J Rare Dis*. 11, 9:207.

de la Morena-Barrio, M.E., Hernández-Caselles, T., Corral, J., García-López, R., Martínez-Martínez, I., Pérez-Dueñas, B., Altisent, C., Sevivas, T., Kristensen, S.R., Guillén-Navarro, E., Miñano, A., Vicente, V., Jaeken, J., Lozano, M.L. (2013). GPI-anchor and GPI-anchored protein expression in PMM2-CDG patients. *Orphanet J Rare Dis*. 8, 170.

Müller, D., Jagla, T., Bodart, L.M., Jährling, N., Dodt, H.U., Jagla, K., Frasch, M. (2010). Regulation and functions of the lms homeobox gene during development of embryonic lateral transverse muscles and direct flight muscles in *Drosophila*. *PLoS One*. 5(12), e14323.

Nichols, C. D., Becnel, J., Pandey, U. B. (2012). Methods to Assay *Drosophila* Behavior. *J. Vis. Exp.* (61), e3795.

Packard, M., Koo, E.S., Gorczyca, M., Sharpe, J., Cumberledge, S., Budnik, V. (2002). The *Drosophila* Wnt, wingless, provides an essential signal for pre- and postsynaptic differentiation. *Cell*. 111(3), 319-30.

Page-McCaw, A., Ewald, A.J., Werb, Z. (2007). Matrix metalloproteinases and the regulation of tissue remodelling. *Nat Rev Mol Cell Biol*. 8(3), 221-33.

Parkinson, W., Dear, M.L., Rushton, E., Broadie, K. (2013). N-glycosylation requirements in neuromuscular synaptogenesis. *Development*. 2013 140(24), 4970-81.

Pohar, N., Godenschwege, T.A., Buchner, E. (1999). Invertebrate tissue inhibitor of metalloproteinase: structure and nested gene organization within the synapsin locus is conserved from Drosophila to human. *Genomics*. 57(2), 293-6.

Reiter, L.T., Potocki, L., Chien, S., Gribskov, M., Bier, E. (2001). A systematic analysis of human disease-associated gene sequences in *Drosophila*. *Genome Res*. 11(6), 1114-25.

Ristow, M., Schmeisser, S. (2011) Extending life span by increasing oxidative stress. *Free Radic Biol Med.* 51(2), 327-36.

Rohrbough, J., Rushton, E., Woodruff, E. 3rd., Fergestad, T., Vigneswaran, K., Broadie, K. (2007). Presynaptic establishment of the synaptic cleft extracellular matrix is required for post-synaptic differentiation. *Genes Dev*. 21(20), 2607-28.

Rushton, E., Rohrbough, J., Deutsch, K., Broadie, K. (2012). Structure-function analysis of endogenous lectin mind-the-gap in synaptogenesis. *Dev Neurobiol*. 72(8), 1161-79.

Sarkar, M., Leventis, P.A., Silvescu, C.I., Reinhold, V.N., Schachter, H., Boulianne, G.L. (2006). Null mutations in Drosophila N-acetylglucosaminyltransferase I produce defects in locomotion and a reduced life span. *J Biol Chem*. 281(18), 12776-85.

Schneider, A., Thiel, C., Rindermann, J., DeRossi, C., Popovici, D., Hoffmann, G.F., Gröne, H.J., Körner, C. (2011). Successful prenatal mannose treatment for congenital disorder of glycosylation-Ia in mice. *Nat Med*. 18(1), 71-3.

Schulte-Merker, S., and Stainier, D.Y. (2014). Out with the old, in with the new: reassessing morpholino knockdowns in light of genome editing technology. *Development*. 141(16), 3103-4.

Scott, H., Panin, V.M. (2014a). N-glycosylation in regulation of the nervous system. *Adv Neurobiol*. 9, 367-94.

Scott H, Panin VM. (2014b). The role of protein N-glycosylation in neural transmission. *Glycobiology*. 24(5), 407-17.

Seppo, A., Tiemeyer, M. (2000). Function and structure of Drosophila glycans. *Glycobiology*. 10(8), 751-60.

Sharma, V., Ichikawa, M., He, P., Scott, D.A., Bravo, Y., Dahl, R., Ng, B.G., Cosford, N.D., Freeze, H.H. (2011). Phosphomannose isomerase inhibitors improve N-glycosylation in selected phosphomannomutase-deficient fibroblasts. *J Biol Chem.* 286(45), 39431-8.

Silvaggi, N.R., Zhang, C., Lu, Z., Dai, J., Dunaway-Mariano, D., Allen, K.N. (2006). The X-ray crystal structures of human alpha-phosphomannomutase 1 reveal the structural basis of congenital disorder of glycosylation type 1a. *J Biol Chem*. 281(21), 14918-26.

Speese, S.D., Ashley, J., Jokhi, V., Nunnari, J., Barria, R., Li, Y., Ataman, B., Koon, A., Chang, Y.T., Li, Q., Moore, M.J., Budnik, V. (2012). Nuclear envelope budding enables large ribonucleoprotein particle export during synaptic Wnt signaling. *Cell.* 149(4), 832-46.

Sokolowski, M.B. (1980). Foraging strategies of *Drosophila melanogaster*: a chromosomal analysis. *Behav Genet*. 10(3), 291-302.

Song, W., Henquet, M.G., Mentink, R.A., van Dijk, A.J., Cordewener, J.H., Bosch, D., America, A.H., van der Krol, A.R. (2011). N-glycoproteomics in plants: perspectives and challenges. *J Proteomics*. 74(8), 1463-74.

Stanley, P., Schachter, H., Taniguchi, N. (2009). N-Glycans. In: *Essentials of Glycobiology*. (ed. A. Varki, R.D. Cummings, J.D. Esko, H.H. Freeze, P. Stanley, C.R. Bertozzi, G.W. Hart, M.E. Etzler), pp. 101-114. Cold Spring Harbor (NY): Cold Spring Harbor Laboratory Press.

Stefanits, H., Konstantopoulou, V., Kuess, M., Milenkovic, I., Matula, C. (2014). Initial diagnosis of the congenital disorder of glycosylation PMM2-CDG (CDG1a) in a 4-year-old girl after neurosurgical intervention for cerebral hemorrhage. *J Neurosurg Pediatr*. 14(5), 546-9.

Sternlicht, M.D. and Werb, Z. (2001). How Matrix metalloproteinases regulate cell behavior. *Annu Rev Cell Biol*. 17, 463–516.

Thiel, C., Lübke, T., Matthijs, G., von Figura, K., Körner, C. (2006). Targeted disruption of mouse phosphomannomutase 2 causes early embryonic lethality. *Mol Cell Biol*. 26(15), 5615-20.

Thiel, C., Körner, C. (2013). Therapies and therapeutic approaches in Congenital Disorders of Glycosylation. *Glycoconj J*. 30(1), 77-84.

Thiel, C., Meßner-Schmitt, D., Hoffmann, G.F., Körner, C. (2013). Screening for congenital disorders of glycosylation in the first weeks of life. *J Inherit Metab Dis*. 36(5), 887-92.

Wang, X., Page-McCaw, A. (2014). A matrix metalloproteinase mediates long-distance attenuation of stem cell proliferation. *J Cell Biol*. 206(7), 923-36.

Varki, A., Sharon, N. (2009). Historical background and overview. In: *Essentials of Glycobiology*. (ed. A. Varki, R.D. Cummings, J.D. Esko, H.H. Freeze, P. Stanley, C.R. Bertozzi, G.W. Hart, M.E. Etzler), pp. 1-22. Cold Spring Harbor (NY): Cold Spring Harbor Lab Press.

Vleugels, W., Duvet, S., Peanne, R., Mir, A.M., Cacan, R., Michalski, J.C., Matthijs, G., Foulquier, F. (2011). Identification of phosphorylated oligosaccharides in cells of patients with a congenital disorders of glycosylation (CDG-I). *Biochimie.* 93(5), 823-33.

Yuste-Checa, P., Gámez, A., Brasil, S., Desviat, L.R., Ugarte, M., Pérez-Cerdá, C., Pérez, B. (2015). The Effects of PMM2-CDG-Causing Mutations on the Folding, Activity, and Stability of the PMM2 Protein. *Hum Mutat*. 36(9), 851-60.

Zaffran, S., Astier, M., Gratecos, D., Sémériva, M. (1997). The held out wings (how) Drosophila gene encodes a putative RNA-binding protein involved in the control of muscular and cardiac activity. *Development*. 124(10), 2087-98.

Zhang, L., Ward, R.E. (2009). *uninflatable* encodes a novel ectodermal apical surface protein required for tracheal inflation in Drosophila. *Dev Biol*. 336(2), 201-12.

CHAPTER IV

CONCLUSIONS AND FUTURE DIRECTIONS

This work was initiated to comprehensively test the role of N-linked glycosylation in synaptic mechanisms, using the *Drosophila* glutamatergic NMJ as a genetic model. The anticipation was that the loss of glycosylation would result in catastrophic failure of synaptogenesis and/or neurotransmission, so it was surprising to find much more subtle requirements. Before this work, relatively little study had been done on glycosylation enzymes in the *Drosophila* model (Geisler et al., 2012; Katz et al., 1988; Whitlock, 1993), other than the identification of predicted glycosylation sites on proteins and a few examples of lost glycan modifications causing proteins to not fold properly, fail to form a complex or lack function (Koles et al., 2007). Parallel glycosylation studies at the *Drosophila* NMJ conducted in the Broadie Lab in the same time-frame as this thesis (Dani et al., 2012, 2014; Jumbo-Lucioni et al., 2014) revealed increased synaptic structural and functional development in the absence of proper modification, validating similar outcomes with Mgat1 and PMM2 genetic manipulations. Together, these studies have revealed key glycosylation roles in the extracellular synaptomatrix that modulate intercellular signaling to inhibit synaptic development and neurotransmission function (Dani et al., 2012, 2014; Jumbo-Lucioni et al., 2014; Parkinson et al., 2013). With this new hypothesis, the focus has become understanding the intersection between extracellular glycosylation and *trans*-synaptic signaling pathways driving synaptogenesis.

Mgat1 Conclusions

The goal here has been to understand how loss of higher order N-glycosylation would affect synaptic development and function by utilizing *mgat1* null mutants unable to produce all hybrid and complex N-glycans (Sarkar et al., 2006; Schachter and Boulianne, 2011). The critical role of these species at multiple levels of nervous system development and function predicted a profound impact on synaptic mechanisms (Koles et al., 2007; Scott and Panin, 2014; Seppo and

Tiemeyer, 2000). Surprisingly, therefore, *mgat1* null mutants showed not a failure of synaptogenesis but rather accelerated synaptic growth, overelaborated architecture and increased neurotransmission strength at the *Drosophila* NMJ (Chapter 2). This result was validated by a transgenic RNAi screen that identified a general trend for structural overelaboration and increased neurotransmission with the knockdown of most glycosylation pathways (Dani et al., 2012). This result was further substantiated by mutant studies on multiple glycosylation enzyme genes, including *sulf1*, *galt* and *pgant* (Dani et al., 2012; Dani et al., 2014; Jumbo-Lucioni, 2014), which all showed the same accelerated synapse development and elevated synaptic function. To probe specific glycan changes in *mgat1* null NMJs, synaptomatrix composition was probed for bi-fucosylated N-glycans with anti-HRP (Desai et al., 1994; Katz et al., 1988; Kurosaka et al., 1991) and terminal GalNAc glycans with *Vicia villosa* (VVA) lectin (Haines et al., 2007). Both glycan classes were grossly reduced at the mutant NMJ (Chapter 2). This was a counter-intuitive result since key synaptic proteins with HRP (Fasciclins, Neurotactin and Neuroglian) and VVA (Dystroglycan) glycan modification are generally required to stabilize the synapse (Desai et al., 1994; Haines et al., 2007; Nakamura et al., 2010; Paschinger et al., 2009). It therefore appears that N-glycosylation of these proteins must serve to inhibit their function, which is elevated in the *mgat1* mutant condition.

Trans-synaptic signaling requires passage through, and containment within, the heavily-glycosylated synaptomatrix (Dani and Broadie, 2012; Martin, 2003), which is strongly compromised in *mgat1* mutants. A range of known bi-directional signals regulate both NMJ structural development and synaptic strength (Enneking et al., 2013; Muller and Davis, 2012). The Broadie Lab has focused on three specific *trans*-synaptic cascades, mediated by the Wg, Gbb and Jeb signaling ligands (Grosso et al., 2011; Kamimura et al., 2013; Rohrbough and Broadie, 2010; Tanaka et al., 2002), and all three pathways were disrupted by the absence of *mgat1* function (Chapter 2). The difficulty with current imaging of these *trans*-synaptic signals is that static pictures are taken, and thus signaling kinetics are completely unknown. An increase in the signal could occur from increased release, inappropriate sequestration, or lack of ligand uptake, among other possibilities. Parallel studies showed that *trans*-synaptic signaling regulates NMJ structure and function via recruitment of synaptic scaffolds which, in turn,

recruit pre- and postsynaptic molecular components (Ataman et al., 2006; Dani et al., 2012; Enneking et al., 2013; Koles et al., 2012; Muller and Davis, 2012). Consistently, two synaptic scaffolds, DLG and LGL, were reduced in *mgat1* null mutants (Chapter 2), which normally regulate the distribution and density of both pre- and postsynaptic elements (Chen and Featherstone, 2005; Staples and Broadie, 2013). Importantly, *dlg* mutants exhibit impaired NMJ development, including deformed subsynaptic reticulum (SSR; Lahey et al., 1994), and preliminary ultrastructural analyses of *mgat1* mutants reveals similar defects (Fig. 20). SSR phenotypes may be attributed to disrupted DLG and LGL scaffolds, but also may include other glycan contributions. The elevated synaptic vesicle number likely contributes to the increased neurotransmission and activity-dependent FM1-43 dye unloading in *mgat1* mutants (Chapter 2). Together, these results show Mgat1-dependent N-glycosylation regulates *trans*-synaptic signaling and thereby downstream synaptic localization of intracellular scaffolds driving neuromuscular synaptogenesis.

Mgat1 Future Directions

Immediate future studies on the role of hybrid and complex N-glycans in neuromuscular synaptogenesis will likely progress along two avenues. The first goal will be to comprehensively catalog the glycan changes occurring at the *mgat1* null NMJ. The work done here only scratches the surface of available probes (Varki et al., 2009), and the extent of the synaptomatrix glycan changes remains largely unknown. A key hypothesis arising from this work is that Mgat1-dependent glycosylation of known synaptic proteins puts the brakes on structural and functional NMJ development. Specifically, the hypothesis is that loss of HRP-epitope additions on known target proteins (Fasciclins, Neurotactin and Neuroglian; Paschinger et al., 2009) as well as VVA glycan additions on other targets (e.g. Dystoglycan; Haines et al., 2007) contribute to the *mgat1* null phenotypes of over-elaborated synaptic architecture and increased neurotransmission strength, respectively (Chapter 2). To test this hypothesis, the glycosylation state of candidate proteins can be queried in *mgat1* nulls compared to transgenic rescue conditions. Rescue of *mgat1* synaptic phenotypes could also be assayed with over-expression of these candidate targets, although it is unknown whether this would overcome the glycosylation

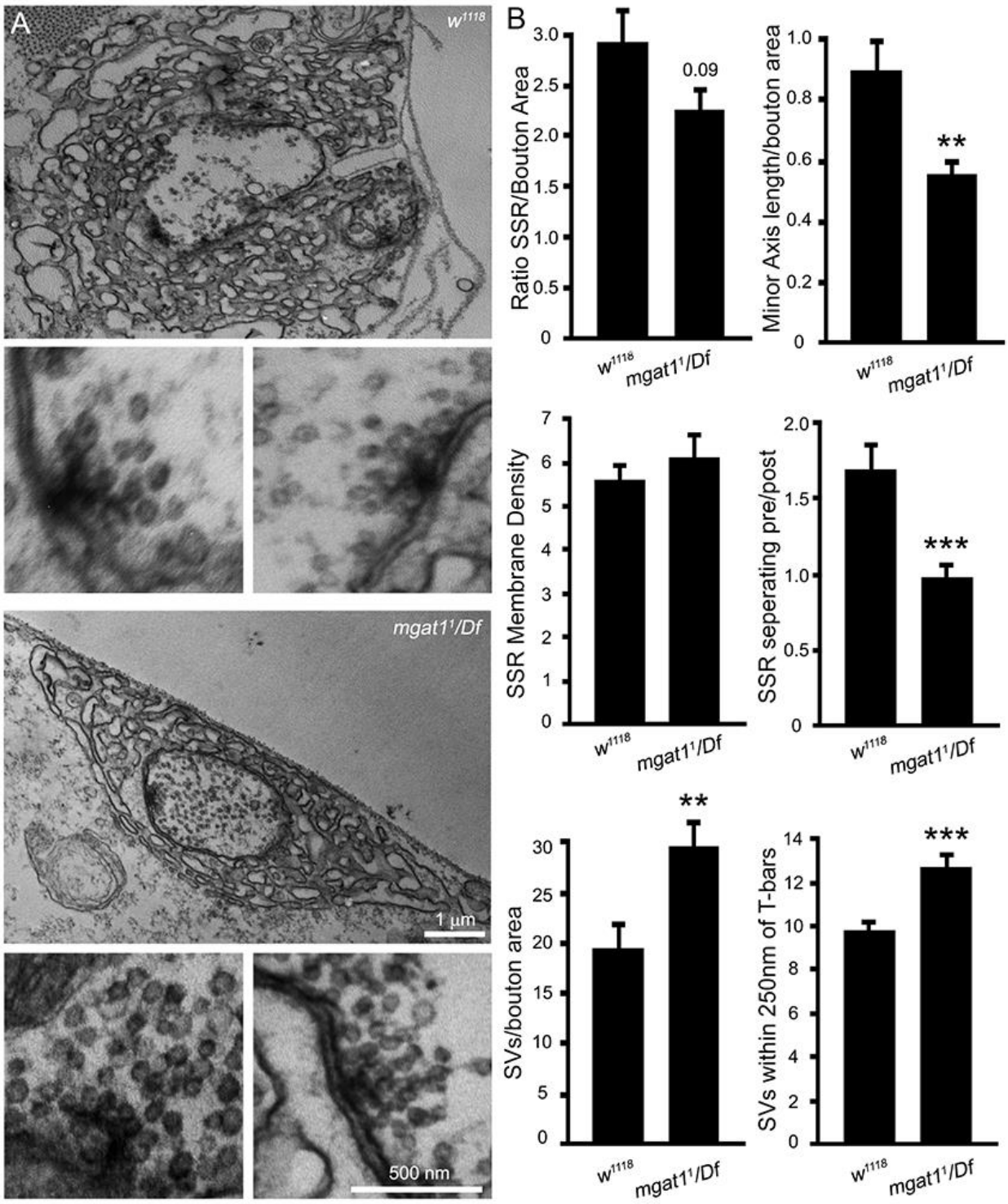
A
w1118
mgat1¹/Df
1 µm
500 nm
B
Ratio SSR/Bouton Area
0.09
Minor Axis length/bouton area
**
SSR Membrane Density
SSR seperating pre/post
***
SVs/bouton area
**
SVs within 250nm of T-bars
***
w1118
mgat1¹/Df

Figure 20

Figure 20: Ultrastructural analysis reveals SSR development and SV concentration phenotypes

SSR distribution and SV concentrations are altered in the *mgat1*^{1} null mutant. (A) Representative images of wandering third instar 6/7 boutons and T-bars in genetic control (*w*^{1118}) and *mgat1*^{1}/Df(2)BSC430. (B) Quantification of SSR/bouton area, Minor Axis length/bouton area, SSR membrane density as number of membranes/um, the distance of SSR separating the bouton and muscle along the minor axis, total SV number/bouton area and number of SV within 250 nm of clearly defined T-bars. Results show a trend for decreased ratio of SSR/Bouton area in the mutant, significant decrease in the minor axis length/bouton area and specifically the SSR separating the bouton from muscle but no change in the SSR membrane density measured by the number of plasma membranes per um. There is a strong increase in total number of SVs/bouton and SVs within 250nm of t-bars in the mutant. Statistical analysis using T-test shown as p≤0.01 (**) and p≤0.001 (***) compared to *w*^{1118}.

requirements. Second, the role of *trans*-synaptic signaling defects in *mgat1* null synaptogenic phenotypes needs to be more rigorously tested, and the mechanism directly addressed. Specifically, it is well-known that changes in signaling ligand abundance in the extracellular space can result in numerous possible outcomes for the actual relay of *trans*-synaptic signals (Dear et al., 2016). Changes in ligand abundance can be caused by changes in release, sequestration, degradation or presentation to cognate receptors, as put forth in the 'exchange factor' model of signaling (Yan et al., 2009). Thus, for each of the target pathways (Wg, Gbb, Jeb) downstream signaling needs to be tested via the Fz2-C nuclear import pathway, p-MAD and pERK signaling, respectively (Dani et al., 2012). Once the direction and degree of each signaling defect is defined, pathways can be individually or combinatorially corrected to test their impact on *mgat1* null synaptic outcomes, as the Broadie Lab has done previously in other mutant contexts (Dani et al., 2012). Together, this future work will define the molecular mechanisms underlying Mgat1-dependent neuromuscular synaptogenesis.

A severe short-coming of this Mgat1 work was the inability to identify and test specific glycan modifications on synaptic proteins. At the time of these studies this type of analysis was daunting; however, the technology is quickly becoming available to perform systematic assays (Koles et al., 2007; Kurz et al., 2015; Nilsson, 2016). Using older and newer techniques together, proteins can be 1) immuno-precipitated with lectins for specific glycan patterns, 2) cleave all glycan branches leaving a modified asparagine to then 3) identify all sites of previous glycans. A major direction will be the identification of specific branching patterns on candidate proteins to allow a directed approach for dissecting glycosylation roles. Although a monumental endeavor, producing mutants lacking glycosylation sites would be ideal for dissecting *mgat1* mutant phenotypes. This work should reveal the role for specific glycan modifications in synaptic mechanisms. However, it may still be difficult to discern the temporal roles that glycosylation plays. For instance, an "early" glycan that is initially attached to a protein may be required for protein folding, and a "mature" glycan may be required for complex formation with other proteins at the final destination (Varki et al., 2009). Loss of either "early" or "mature" forms of the same glycan could result in the same outcome (i.e. loss of the protein at its intended target). One path forward could be to replicate studies on additional glycosylation enzymes that

are required for the addition or removal of hybrid and complex glycans (Baas et al., 2011; Leonard et al., 2006). In this manner, a smaller subset of glycosylation events could be studied, possibly reducing the number of total modifications. For instance, instead of using an *mgat1* mutant to block all hybrid and complex glycan formation, a future focus could be on the fucose transferase responsible for HRP epitope production (Rendic et al., 2006). In this manner, a dozen proteins might be affected instead of hundreds. The overall goal for this future work will be to identify the mechanisms by which specific glycan attachments mediate synaptic growth, structural integrity and functional communication properties.

PMM2 Conclusions

This study set forth to establish a new *Drosophila* PMM2-CDG disease model through mutation of the causative phosphomannomutase type 2 (*pmm2*) gene (Freeze et al., 2014). This was the first work to investigate *Drosophila pmm2,* so the study began by producing genetic nulls using CRISPR and characterizing transgenic RNAi lines. N-glycosylation is required for viability in all metazoa, plants and yeast cells (Varki et al., 2009), predicting very early lethality in *Drosophila pmm2* null animals, with cellular viability only temporarily sustained by maternal contribution. As expected, loss of *pmm2* reduced lifespan corresponding to PMM2 level; null mutants survive only briefly and are developmentally delayed as first instars almost immediately after hatching (Chapter 3). The presence of maternally contributed *pmm2* mRNA was verified with quantitative reverse transcription PCR. Abundant transcripts were present in unfertilized eggs, explaining the embryonic survival of the null mutants. Mutant larva displayed reduced locomotion and adults with neurally-reduced *pmm2* displayed severely impaired coordinated movement, with an inability to fly or even walk (Chapter 3). The adult movement loss was so severe that a new assay was needed for quantitative comparison ("ring locomotion" assay). There was a specific requirement for PMM2 within the nervous system, demonstrating that function in neurons is required to maintain coordinated movement and thus viability (Chapter 3).

Null *pmm2* mutants display severe reduction of glycoprotein glycosylation, with reduced N-linked glycosylation levels and diversity (Chapter 3). Consistently, the NMJ also showed

striking losses in synaptomatrix glycan composition with strong reduction of the HRP (bifucosylated N-glycan) and ECL (D-galactose) epitopes. Consistent with other glycosylation mutants (Dani et al., 2012, 2014; Jumbo-Lucioni et al., 2014; Parkinson et al., 2013), PMM2 loss caused striking NMJ overelaboration as well as strongly increased neurotransmission, supporting the conclusion that glycans primarily inhibit synaptic differentiation (Chapter 3). Loss of pmm2 on either side of the synapse resulted in overabundant NMJ structure. Interestingly, the elevated neurotransmission was only present with dual pre and postsynaptic *pmm2* knockdown; wild type expression of *pmm2* on either side of the synapse maintained control neurotransmission levels. This is an unusual result as mutations that alter neurotransmission strength typically have a primarly pre or postsynaptic requirement where loss on one side causes the primary phenotype; however, the pmm2 mutant phenotype requires dual loss on both sides of the synapse (Jumbo-Lucioni et al., 2014; Parkinson et al., 2013; Staples and Broadie, 2013). Aditionally, this provides an example of the separable nature of NMJ structure with function where increased structure seen with pre or post knockdown did not correlate to elevated neurotransmission strength.

During this study, it was revealed that *pmm2* mutants show striking tracheal defects, with consistently fragmented and melanized trachea in larvae (Fig. 21). This striking phenotype caused trachea to appear like dark, broken sticks, which gave a strikingly distinct appearance to mutant larvae when moving and crawling. Importantly, this phenotype has been associated with mutation of extracellular matrix metalloproteinases (MMPs), which also play critical roles shaping synapse structure and function (Dear et al., 2016; Kessenbrock et al., 2010; Page-McCaw et al., 2007; Sternlicht and Werb, 2001). Based on these observations, it was hypothesized that PMM2 loss could impair MMP glycosylation, or MMP ability to cleave improperly glycosylated substrates (Godenschwege et al., 2000; Llano et al., 2000; Llano et al., 2002; Pohar et al., 1999). To test this hypothesis, we assayed the two MMPs present in *Drosophila* (secreted MMP1 and GPI-anchored MMP2), as well as the single Tissue Inhibitor of MMPs (TIMP) (Dear et al., 2016; Kessenbrock et al., 2010; Page-McCaw et al., 2007). MMP2 was found to be highly glycosylated, whereas most MMP1 isoforms were not detectably glycosylated (Chapter 3). Importantly, loss of PMM2-dependent MMP2 glycosylation resulted in

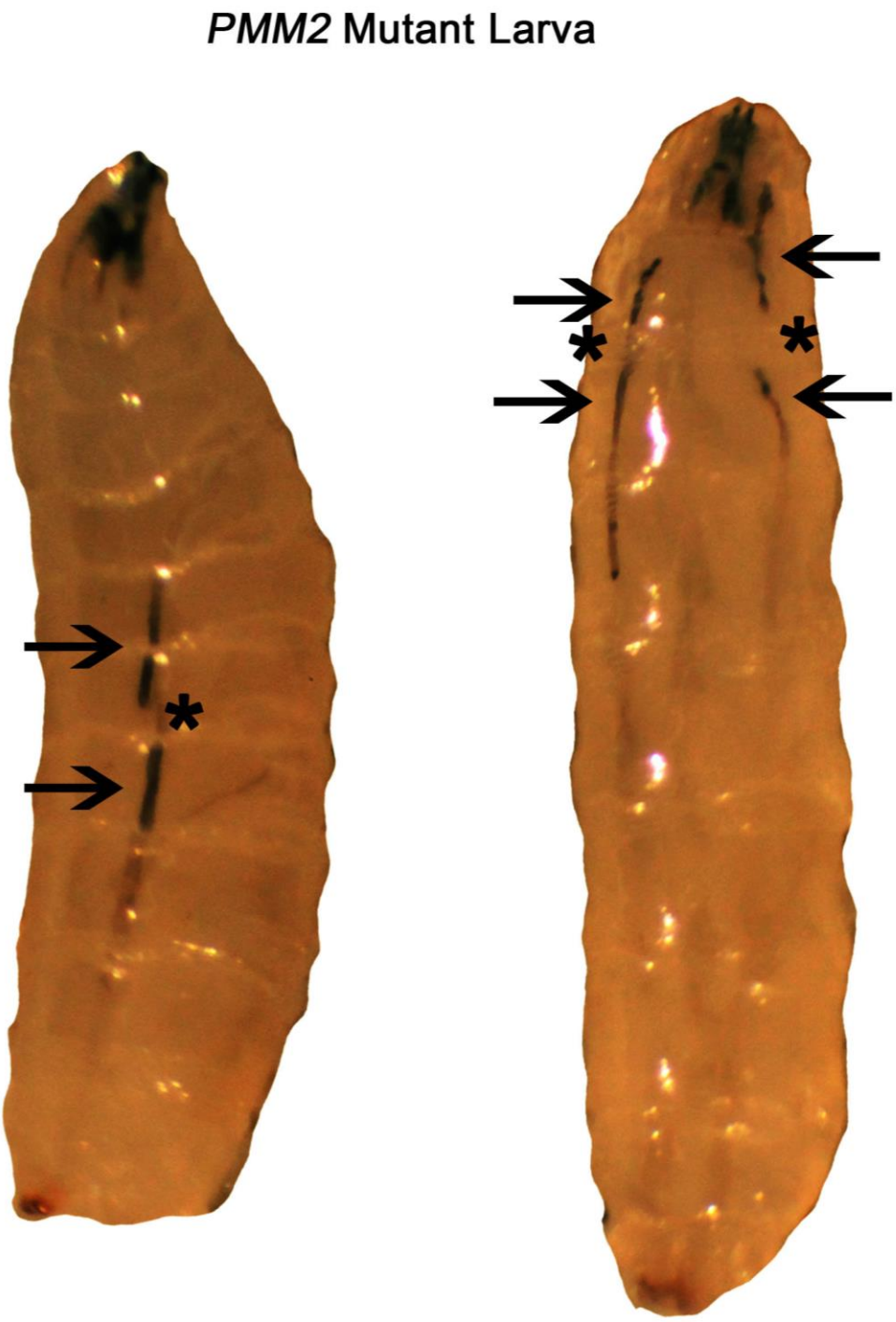

Figure 21

Figure 21: Tracheal Maintenance Requires pmm2 Activity

Trachea break, melanize and harden with the reduction of *pmm2*. Several breaks begin to form in the 2nd instar larva and in the 3rd instar trachea surrounding the breaks have begun to melanize and harden, giving the appearance of dark sticks underneath the cuticle. Arrows point at melanized trachea and breaks are shown with an "*".

reduced expression at the NMJ synapse, whereas MMP1 abundance was not significantly altered. The TIMP regulator is also reduced in abundance with removal of PMM2, which would be predicted to either help alleviate consequences of MMP2 loss or amplify the dysregulated MMP1/MMP2 ratio that is required to maintain synaptic development and function (Dear et al., 2016). We are unable to determine if the loss of TIMP is actively directed by the cell to limit its inhibition on the reduced levels of MMP2, or if the loss of TIMP is causative of the pmm2 reduction and only serves to amplify the unregulated MMP1/MMP2 ratio, but both possibilities are interesting to consider.

Recent work has shown that MMPs play critical roles regulating *Drosophila* NMJ structural and functional synaptogenesis via modulation of Wg *trans*-synaptic signaling (Dear et al., 2016). Consistently, *pmm2* RNAi knockdown suppresses Wg signaling at the developing NMJ synapse (Chapter 3). Importantly, MMPs were recently shown to cleave the HSPG Wg co-receptor Dally-like Protein (Dlp) to control Wg signaling in the *Drosophila* ovary (Wang and Page-McCaw, 2014). Consistently, *pmm2* RNAi knockdown strongly reduced synaptic levels of the Dlp Wg co-receptor as well as the Wg ligand (Chapter 3), and also strongly reduced downstream signaling through the Frizzled Nuclear Import (FNI) pathway (Speese et al., 2012). Impaired Wg signaling is a counter-intuitive result given the overelaborated structure and elevated function at the *pmm2* mutant NMJ (Chapter 3) because Wg loss has previously been associated with decreased NMJ structure and functional development (Ataman et al., 2008; Kerr et al., 2014; Packard et al., 2002). The reduced Wg signaling could be a result of several possibilities including MMP2 interactions, Wg and Fz2 receptor glycosylation requirements and Wg reduction to compensate for increased synaptic development. The last possibility is the most tempting, since it would best account for the decrease in Wg signaling that typically drives NMJ outgrowth and increased function (Ataman et al., 2008; Kerr et al., 2014; Packard et al., 2002). However, there is as yet no evidence to support this hypothesis. PMM2-dependent glycosylation at the NMJ synapse may reflect roles in multiple intersecting pathways, impacting a range of glycoproteins that jointly control synaptic growth, structural differentiation and neurotransmission strength (Koles et al., 2007; Scott and Panin, 2014). Future work will aim at deciphering individual glycan contributions, which are presumed to combinatorially result in

the structural and functional NMJ defects characterizing this new PMM2-CDG disease state model.

PMM2 Future Directions

Numerous research directions could be pursued to improve the *Drosophila* PMM2-CDG disease model. The first important avenue would be to produce rescue constructs to verify the specificity of *pmm2* mutant phenotypes. Although rescue constructs were made for this thesis, they were ineffectual in preventing the early lethality. The primary suspected reason is that an incorporated His tag in the rescue constructs prevented function, or even resulted in a dominant lethal form of *pmm2*. Future work should aim at redesigning the rescue construct, either without any tags or with the use of more conventional tags at different locations (Koles et al., 2015; Richier and Salecker, 2015). A second important avenue would be to generate human *pmm2* rescue constructs in order to test functional conservation, always a key priority in establishing a disease model. If human *pmm2* is able to rescue the *Drosophila* null mutant, then constructs with the most common human disease causing mutations should also be generated (Barone et al., 2014; Pagon et al., 2014). The most common human pmm2 mutation is R141H with L32R being the second most common. The R141H mutation is homozygous lethal with less than 3% enzymatic activity but the heterozygous condition is asymptomatic. The vast majority of PMM2-CDG patients have compound heterozygous mutations which results in a wide array of symptoms that include mental retardation, psychomotor disability and failure to thrive (Barone et al., 2014 a,b). These human PMM2-CDG lines would provide an excellent platform to study hypomorphic *pmm2* activity in a simplified system.

Another future direction stems from work in the zebrafish PMM2-CDG disease model, which suggests a role for increased mannose-6-phosphate in PMM2-CDG disease state phenotypes (Cline et al., 2012). Further work is needed to dissect the possible roles played by altered abundance of glycan precursors, particularly mannose-6-phosphate buildup, through examining genetic interactions that restore the relative abundance of these pools. Utilizing the *Drosophila* genetic toolkit, it would be relatively easy to knockdown PMM2 and phosphomannoisomerase (MPI or PMI) simultaneously (Sharma et al., 2014), thus reducing the

elevated levels of mannose-6-phosphate in *pmm2* mutants. This line of study would first involve tests of MPI mutant phenotypes, and then the effects of combined MPI and *pmm2* mutations in both behavioral and synaptic structure/function assays (Chapter 3). In parallel, simple over-expression MPI in a control background could be very informative for correlative comparisons of phenotypes, to decipher possible phenotypes caused by the loss of glycosylation verses mannose-6-phosphate accumulation (Cline et al., 2012; Sharma et al., 2014). Dependent on outcomes, potential treatments could be targeted approaches to reduce MPI activity with pharmacology. MPI can be inhibited with pharmaceutical inhibitors in the benzoisothiazolone series, which have been shown to promote mannose-1-phosphate production in PMM2-CDG patient fibroblasts and zebrafish embryos (Sharma et al., 2011). Although this possible future research avenue has a relatively strong foundation, even if reducing MPI activity in humans alleviated the symptoms from increased mannose-6-phosphate, the patients still have a reduction in glycosylation that will not be alleviated.

A primary aspiration for any disease model is to find effective treatments for a conserved disease state, and a goal for this new *Drosophila* MPP2-CDG model is to explore a range of pharmaceutical options. For example, drug avenues to increase PMM2 enzymatic activity have been hypothesized, but have not yet been systematically tested (Thiel and Korner, 2013). There are over 100 known different *pmm2* mutations that cause the PMM2-CDG disease state, and each mutation affects the enzymatic activity in a different manner (Freeze et al., 2014). This may significantly hamper the ability for any one drug intervention to aid all PMM2-CDG cases. However, future studies could focus particularly on drugs that act as chaperones that help PMM2 form the functional homodimer complex, as multiple mutations result specifically in the loss of dimer formation (Yuste-Checa et al., 2014). Another potential path forward would be to focus on other enzymes in the pathway with closely related functions. For example, PMM2 has a sibling enzyme phosphomannomutase type 1 (PMM1), which functions as a glucose-1,6-biphosphatase and is expressed strongly in the nervous system (Veiga-da-Cunha et al., 2008). PMM1 and PMM2 share structural and functional similarity, but have different *in vivo* substrates such that PMM1 does not compensate for PMM2 loss (Veiga-da-Cunha et al., 2008). Interestingly, however, PMM1 activity *in vitro* does convert mannose-6-

phosphate into mannose-1-phosphate, revealing the ability for PMM1 to perform the PMM2 enzymatic role (Pirard et al., 1999). A research avenue could focus on finding pharmaceutical reagents that drive PMM1 to function more like PMM2. Even weakly driving PMM1 towards PMM2 activity could greatly improve patient development, given the hypomorphic nature of the disease state and especially since PMM1 is strongly expressed in neural tissue. A large-scale, small molecule pharmaceutical screen using the new *Drosophila* PMM2-CDG model could prove very effective (Giacomotto and Segalat, 2010). Our hope and expectation is that future studies utilizing the powerful *Drosophila* genetic toolkit will further our understanding of the PMM2-CDG disease state and provide the means to produce as effective therapy.

References

Ataman, B., Ashley, J., Gorczyca, D., Gorczyca, M., Mathew, D., Wichmann, C., Sigrist, S.J. and Budnik, V. (2006). Nuclear trafficking of Drosophila Frizzled-2 during synapse development requires the PDZ protein dGRIP. Proc. Natl. Acad. Sci. USA. 103(20), 7841-6.

Ataman, B., Ashley, J., Gorczyca, M., Ramachandran, P., Fouquet, W., Sigrist, S.J. and Budnik, V. (2008). Rapid activity-dependent modifications in synaptic structure and function require bidirectional Wnt signaling. Neuron. 57(5), 705-18.

Baas, S., Sharrow, M., Kotu, V., Middleton, M., Nguyen, K., Flanagan-Steet, H., Aoki, K., Tiemeyer, M. (2011). Sugar-free frosting, a homolog of SAD kinase, drives neural-specific glycan expression in the Drosophila embryo. *Development.* 138(3), 553-63.

Barone, R., Carrozzi, M., Parini, R., Battini, R., Martinelli, D., Elia, M., Spada, M., Lilliu, F., Ciana, G., Burlina, A., Leuzzi, V., Leoni, M., Sturiale, L., Matthijs, G., Jaeken, J., Di Rocco, M., Garozzo, D., Fiumara, A. (2015). A nationwide survey of PMM2-CDG in Italy: high frequency of a mild neurological variant associated with the L32R mutation. *J Neurol.* 262(1), 154-64.

Barone, R., Fiumara, A., Jaeken, J. (2014). Congenital disorders of glycosylation with emphasis on cerebellar involvement. *Semin Neurol*. 34(3), 357-66.

Chen, K. and Featherstone, D.E. (2005). Discs-large (DLG) is clustered by presynaptic innervation and regulates postsynaptic glutamate receptor subunit composition in Drosophila. BMC Biol. 3:1.

Cline, A., Gao, N., Flanagan-Steet, H., Sharma, V., Rosa, S., Sonon, R., Azadi, P., Sadler, K.C., Freeze, H.H., Lehrman, M.A., Steet, R. (2012). A zebrafish model of PMM2-CDG reveals altered neurogenesis and a substrate-accumulation mechanism for N-linked glycosylation deficiency. *Mol Biol Cell*. 23(21), 4175-87.

Dani, N., Broadie, K. (2012). Glycosylated synaptomatrix regulation of trans-synaptic signaling. *Dev Neurobiol*. 72(1), 2-21.

Dani, N., Nahm, M., Lee, S., Broadie, K. (2012). A targeted glycan-related gene screen reveals heparan sulfate proteoglycan sulfation regulates WNT and BMP trans-synaptic signaling. *PLoS Genet*. 8(11), e1003031

Dani N., Zhu H., Broadie, K. (2014). Two protein N-acetylgalactosaminyl transferases regulate synaptic plasticity by activity-dependent regulation of integrin signaling. *J Neurosci*. 34(39), 13047-65.

Dear, M.L., Dani, N., Parkinson, W., Zhou, S., Broadie, K. (2016). Two matrix metalloproteinase classes reciprocally regulate synaptogenesis. *Development* 143(1), 75-87.

Desai, C.J., Popova, E. and Zinn, K. (1994). A Drosophila receptor tyrosine phosphatase expressed in the embryonic CNS and larval optic lobes is a member of the set of proteins bearing the "HRP" carbohydrate epitope. J. Neurosci. 14(12), 7272-83.

Enneking, E.M., Kudumala, S.R., Moreno, E., Stephan, R., Boerner, J., Godenschwege, T.A. and Pielage, J. (2013). Transsynaptic Coordination of Synaptic Growth, Function, and Stability by the L1-Type CAM Neuroglian. PLoS Biol. 11(4), e1001537.

Freeze, H.H., Chong, J.X., Bamshad, M.J., Ng, B.G. (2014). Solving glycosylation disorders: fundamental approaches reveal complicated pathways. *Am J Hum Genet*. 94(2), 161-75.

Geisler, C., Kotu, V., Sharrow, M., Rendić, D., Pöltl, G., Tiemeyer, M., Wilson, I.B., Jarvis, D.L. (2012). The Drosophila neurally altered carbohydrate mutant has a defective Golgi GDP-fucose transporter. *J Biol Chem*. 287(35), 29599-609.

Giacomotto, J., Ségalat, L. (2010). High-throughput screening and small animal models, where are we? *Br J Pharmacol*. 160(2), 204-16.

Godenschwege, T.A., Pohar, N., Buchner, S., Buchner, E. (2000). Inflated wings, tissue autolysis and early death in tissue inhibitor of metalloproteinases mutants of *Drosophila*. *Eur J Cell Biol*. 79(7), 495-501.

Del Grosso, F., De Mariano, M., Passoni, L., Luksch, R., Tonini, G.P. and Longo, L. (2011). Inhibition of N-linked glycosylation impairs ALK phosphorylation and disrupts pro-survival signaling in neuroblastoma cell lines. BMC Cancer. 11, 525.

Haines, N., Seabrooke, S. and Stewart, B.A. (2007). Dystroglycan and protein O-mannosyltransferases 1 and 2 are required to maintain integrity of Drosophila larval muscles. Mol. Biol. Cell. 18(12), 4721-30.

Jumbo-Lucioni P, Parkinson W, Broadie K. (2014). Overelaborated synaptic architecture and reduced synaptomatrix glycosylation in a *Drosophila* classic galactosemia disease model. *Dis Model Mech*. 7(12), 1365-78.

Kamimura, K., Ueno, K., Nakagawa, J., Hamada, R., Saitoe, M. and Maeda, N. (2013). Perlecan regulates bidirectional Wnt signaling at the Drosophila neuromuscular junction. J. Cell Biol. 200(2), 219-33.

Katz, F., Moats, W., Jan, Y.N. (1988). A carbohydrate epitope expressed uniquely on the cell surface of Drosophila neurons is altered in the mutant nac (neurally altered carbohydrate). *EMBO J*. 7(11), 3471-7.

Kerr, K.S., Fuentes-Medel, Y., Brewer, C., Barria, R., Ashley, J., Abruzzi, K.C., Sheehan, A., Tasdemir-Yilmaz, O.E., Freeman, M.R., Budnik, V. (2014). Glial wingless/Wnt regulates glutamate receptor clustering and synaptic physiology at the *Drosophila* neuromuscular junction. *J Neurosci*. 34(8), 2910-20.

Kessenbrock, K., Plaks, V., Werb, Z. (2010). Matrix metalloproteinases: regulators of the tumor microenvironment. *Cell*. 141(1), 52-67.

Koles, K., Lim, J.M., Aoki, K., Porterfield, M., Tiemeyer, M., Wells, L. and Panin, V. (2007). Identification of N-glycosylated proteins from the central nervous system of Drosophila melanogaster. Glycobiology. 17(12), 1388-403.

Koles, K., Nunnari, J., Korkut, C., Barria, R., Brewer, C., Li, Y., Leszyk, J., Zhang, B. and Budnik, V. (2012). Mechanism of evenness interrupted (Evi)-exosome release at synaptic boutons. J. Biol. Chem. 287(20), 16820-34.

Koles, K., Yeh, A.R., Rodal, A.A. (2015). Tissue-specific tagging of endogenous loci in Drosophila melanogaster. *Biol Open*. 5(1), 83-9.

Kurosaka, A., Yano, A., Itoh, N., Kuroda, Y., Nakagawa, T., Kawasaki, T. (1991). The structure of a neural specific carbohydrate epitope of horseradish peroxidase recognized by anti-horseradish peroxidase antiserum. *J Biol Chem.* 266(7), 4168-72.

Kurz, S., Aoki, K., Jin, C., Karlsson, N.G., Tiemeyer, M., Wilson, I.B., Paschinger, K. (2015). Targeted release and fractionation reveal glucuronylated and sulphated N- and O-glycans in larvae of dipteran insects. *J Proteomics*. 126, 172-88.

Lahey, T., Gorczyca, M., Jia, X.X. and Budnik, V. (1994). The Drosophila tumor suppressor gene dlg is required for normal synaptic bouton structure. Neuron. 13(4), 823-35.

Léonard, R., Rendic, D., Rabouille, C., Wilson, I.B., Préat, T. and Altmann, F. (2006). The Drosophila fused lobes gene encodes an N-acetylglucosaminidase involved in N-glycan processing. J. Biol. Chem. 281(8), 4867-75.

Llano, E., Adam, G., Pendás, A.M., Quesada, V., Sánchez, L.M., Santamariá, I., Noselli, S., López-Otín, C. (2002). Structural and enzymatic characterization of *Drosophila* Dm2-MMP, a membrane-bound matrix metalloproteinase with tissue-specific expression. *J Biol Chem*. 277(26), 23321-9.

Llano, E., Pendás, A.M., Aza-Blanc, P., Kornberg, T.B., López-Otín, C. (2000). Dm1-MMP, a matrix metalloproteinase from *Drosophila* with a potential role in extracellular matrix remodeling during neural development. *J Biol Chem*. 275(46), 35978-85.

Martin, P.T. (2003). Glycobiology of the neuromuscular junction. J. Neurocytol. 32(5-8), 915-29.

Müller, M. and Davis, G.W. (2012). Transsynaptic control of presynaptic Ca^{2+} influx achieves homeostatic potentiation of neurotransmitter release. Cur. Biol. 22(12),1102-8.

Nakamura N, Stalnaker SH, Lyalin D, Lavrova O, Wells L, Panin VM. (2010). Drosophila Dystroglycan is a target of O-mannosyltransferase activity of two protein O-mannosyltransferases, Rotated Abdomen and Twisted. Glycobiology. 20(3), 381-94.

Nilsson, J. (2016). Liquid chromatography-tandem mass spectrometry-based fragmentation analysis of glycopeptides. *Glycoconj J.* Epub

Packard, M., Koo, E.S., Gorczyca, M., Sharpe, J., Cumberledge, S., Budnik, V. (2002). The *Drosophila* Wnt, wingless, provides an essential signal for pre- and postsynaptic differentiation. *Cell*. 111(3), 319-30.

Page-McCaw, A., Ewald, A.J., Werb, Z. (2007). Matrix metalloproteinases and the regulation of tissue remodelling. *Nat Rev Mol Cell Biol*. 8(3), 221-33.

Pagon, R.A., Adam, M.P., Ardinger, H.H., Wallace, S.E., Amemiya, A., Bean, L.J.H., Bird, T.D., Fong, C.T., Mefford, H.C., Smith, R.J.H., Stephens, K., Sparks, S.E., Krasnewich, D.M. (2014). Congenital Disorders of N-linked Glycosylation Pathway Overview. *GeneReviews Internet.*

Parkinson, W., Dear, M.L., Rushton, E., Broadie, K. (2013). N-glycosylation requirements in neuromuscular synaptogenesis. *Development*. 2013 140(24), 4970-81.

Paschinger, K., Rendić, D. and Wilson, I.B. (2009). Revealing the anti-HRP epitope in Drosophila and Caenorhabditis. *Glycoconj. J*. 26(3), 385-95.

Pirard, M., Achouri, Y., Collet, J.F., Schollen, E., Matthijs, G., Van Schaftingen, E. (1999). Kinetic properties and tissular distribution of mammalian phosphomannomutase isozymes. *Biochem J*. 339 (Pt 1), 201-7.

Pohar, N., Godenschwege, T.A., Buchner, E. (1999). Invertebrate tissue inhibitor of metalloproteinase: structure and nested gene organization within the synapsin locus is conserved from Drosophila to human. *Genomics*. 57(2), 293-6.

Rendić, D., Sharrow, M., Katoh, T., Overcarsh, B., Nguyen, K., Kapurch, J., Aoki, K., Wilson, I.B. and Tiemeyer, M. (2010). Neural-specific α3-fucosylation of N-linked glycans in the Drosophila embryo requires fucosyltransferase A and influences developmental signaling associated with O-glycosylation. Glycobiology. 20(11),1353-65.

Richier, B., Salecker, I. (2015). Versatile genetic paintbrushes: Brainbow technologies. *Wiley Interdiscip Rev Dev Biol.* 4(2), 161-80.

Rohrbough, J. and Broadie, K. (2010). Anterograde Jelly belly ligand to Alk receptor signaling at developing synapses is regulated by Mind the gap. Development. 137(20), 3523-33.

Sarkar, M., Leventis, P.A., Silvescu, C.I., Reinhold, V.N., Schachter, H., and Boulianne, G.L. (2006). Null mutations in Drosophila N-acetylglucosaminyltransferase I produce defects in locomotion and a reduced life span. J. Biol. Chem. 281(18),12776-85

Schachter, H. and Boulianne, G. (2011). Life is sweet! A novel role for N-glycans in Drosophila lifespan. Fly (Austin). 5(1), 18-24.

Scott, H., Panin, V.M. (2014a). N-glycosylation in regulation of the nervous system. *Adv Neurobiol*. 9, 367-94.

Scott H, Panin VM. (2014b). The role of protein N-glycosylation in neural transmission. *Glycobiology*. 24(5), 407-17.

Seppo, A., Tiemeyer, M. (2000). Function and structure of Drosophila glycans. *Glycobiology*. 10(8), 751-60.

Sharma, V., Ichikawa, M., He, P., Scott, D.A., Bravo, Y., Dahl, R., Ng, B.G., Cosford, N.D., Freeze, H.H. (2011). Phosphomannose isomerase inhibitors improve N-glycosylation in selected phosphomannomutase-deficient fibroblasts. *J Biol Chem.* 286(45), 39431-8.

Sharma, V., Nayak, J., DeRossi, C., Charbono, A., Ichikawa, M., Ng, B.G., Grajales-Esquivel, E., Srivastava, A., Wang, L., He, P., Scott, D.A., Russell, J., Contreras, E., Guess, C.M., Krajewski, S., Del Rio-Tsonis, K., Freeze, H.H. (2014). Mannose supplements induce embryonic lethality and blindness in phosphomannose isomerase hypomorphic mice. *FASEB J.* 28(4), 1854-69.

Speese, S.D., Ashley, J., Jokhi, V., Nunnari, J., Barria, R., Li, Y., Ataman, B., Koon, A., Chang, Y.T., Li, Q., Moore, M.J., Budnik, V. (2012). Nuclear envelope budding enables large ribonucleoprotein particle export during synaptic Wnt signaling. *Cell.* 149(4), 832-46.

Staples, J. and Broadie, K. (2013). The cell polarity scaffold Lethal Giant Larvae regulates synapse morphology and function**.** J. Cell. Sci. (Epub ahead of print)

Sternlicht, M.D. and Werb, Z. (2001). How Matrix metalloproteinases regulate cell behavior. *Annu Rev Cell Biol*. 17, 463–516.

Tanaka, K., Kitagawa, Y. and Kadowaki, T. (2002). Drosophila segment polarity gene product porcupine stimulates the posttranslational N-glycosylation of wingless in the endoplasmic reticulum. J. Biol. Chem. 277(15), 12816-23.

Thiel, C., Körner, C. (2013). Therapies and therapeutic approaches in Congenital Disorders of Glycosylation. *Glycoconj J*. 30(1), 77-84.

Varki, A., Sharon, N. (2009). Historical background and overview. In: *Essentials of Glycobiology*. (ed. A. Varki, R.D. Cummings, J.D. Esko, H.H. Freeze, P. Stanley, C.R. Bertozzi, G.W. Hart, M.E. Etzler), pp. 1-22. Cold Spring Harbor (NY): Cold Spring Harbor Lab Press.

Veiga-da-Cunha, M., Vleugels, W., Maliekal, P., Matthijs, G., Van Schaftingen, E. (2008). Mammalian phosphomannomutase PMM1 is the brain IMP-sensitive glucose-1,6-bisphosphatase. *J Biol Chem*. 283(49), 33988-93.

Wang, X., Page-McCaw, A. (2014). A matrix metalloproteinase mediates long-distance attenuation of stem cell proliferation. *J Cell Biol*. 206(7), 923-36.

Whitlock, K.E. (1993). Development of Drosophila wing sensory neurons in mutants with missing or modified cell surface molecules. *Development*. 117(4), 1251-60.

Yan, D., Wu, Y., Feng, Y., Lin, S.C., Lin, X. (2009). The core protein of glypican Dally-like determines its biphasic activity in wingless morphogen signaling. Dev Cell. 17(4), 470-81.

Yuste-Checa, P., Gámez, A., Brasil, S., Desviat, L.R., Ugarte, M., Pérez-Cerdá, C., Pérez, B. (2015). The Effects of PMM2-CDG-Causing Mutations on the Folding, Activity, and Stability of the PMM2 Protein. *Hum Mutat*. 36(9), 851-60.